To the Graduate Council:

I am submitting herewith a thesis written by John Otis Walling entitled "Mathematical Modeling of Nitrogen Oxide Pollutant Concentrations within Depressed Highway Sections." I recommend that it be accepted in partial fulfillment of the requirements for the degree of Master of Science, with a major in Environmental Engineering.

Kenneth E. Noll

Kenneth E. Noll, Major Professor

We have read this thesis
and recommend its acceptance:

Dale A. Drew

J. Clement Burdick

Accepted for the Council:

Vice Chancellor
Graduate Studies and Research

MATHEMATICAL MODELING OF NITROGEN OXIDE POLLUTANT CONCENTRATIONS WITHIN DEPRESSED HIGHWAY SECTIONS

A Thesis

Presented to

the Graduate Council of

The University of Tennessee

In Partial Fulfillment

of the Requirements for the Degree

Master of Science

---

by

John Otis Walling

August 1974

ACKNOWLEDGMENTS

The author wishes to express his appreciation to the Bureau of Highways, Tennessee Transportation Department, for support on the research project entitled "Air Monitoring Program to Determine the Impact of Highways on Ambient Air Quality."

The author also extends his appreciation to Dr. Kenneth E. Noll, Terry L. Miller, and Jeffrey S. Gilbert for their assistance in this experiment.

1165789

ABSTRACT

The purpose of this report is to make use of field measured data to calibrate Stanford Research Institute's (SRI) Street Canyon Model for predicting total nitrogen oxide concentrations within a depressed highway section and to formulate a new model that provides an improved correlation with the measured data.

In this investigation, an air monitoring field program was employed to collect the total nitrogen oxide concentrations, meteorological, and traffic data required to calibrate and formulate a mathematical model. A monitoring site was chosen on I-40 East in Nashville, Tennessee. At this site, total nitrogen oxide concentrations were measured at various vertical heights within and above a depressed highway section.

The total collected monitoring data was reduced and used as input into a computer program. This program calibrated the geometric mean K calibration coefficient and determined the correlation of the data with the different models. This resulted in a calibrated SRI model which gave favorable predictive capabilities for total nitrogen oxide concentrations within the depressed highway section at the I-40 East monitoring site.

A new general model was formulated which made the dispersion term a function of a power factor. After the general model's power factor and calibration coefficient were determined, a new empirical model was determined that gave improved correlation with the data within the depressed section and also allowed for a reasonable prediction of the values measured above the depressed section.

In conclusion, by using the same general model and methodology used to determine the specific empirical model for the I-40 East site,

other statistical models can be developed which predict ambient pollutant levels for highway terrain configurations which are considerably different from the type of highway section investigated in this report.

TABLE OF CONTENTS

CHAPTER		PAGE
I.	INTRODUCTION	1
II.	SOURCE, DISPERSION, AND EFFECTS OF NITROGEN OXIDES	3
	Introduction	3
	Source of Highway Emissions	4
	Production of Nitrogen Oxides	4
	Variables that Affect Nitric Oxide Emissions	5
	The Type of Vehicles	5
	The Vehicle Age	6
	The Vehicular Modes of Operation	6
	The Transport of Dispersion of Nitrogen Oxide	8
	Transport	8
	Dispersion	8
	Nitrogen Dioxide Effects	9
	Biological Effects	11
	Phytotoxic Effects	11
	Coloration Effects	11
	Photochemical Smog Effects	12
III.	EXPERIMENTAL PROGRAM	13
	Introduction	13
	Monitoring Site Description	14
	The Bag Sampling Collection Network	17
	Types of Measurements Employed	19
	Traffic Measurements	19

CHAPTER PAGE

Heavy Duty Mix. 19
Average Vehicle Speed 20
Wind Data Measurements. 20
Temperature and Humidity. 21
Atmospheric Stability 21
The Oxides of Nitrogen Analyzer 21
The Analyzer's Calibration Procedure 23
Analysis of Measured Data. 27
Traffic Data Analysis 27
Traffic Density. 27
Heavy Duty Mix 27
Traffic Speed. 73
Meteorological Data Analysis. 73
Stability Analysis 73
The Wind Frequency Analysis. 76
Analysis of Measured Total Nitrogen Oxide Concentrations. 76
Diurnal Variations of Measured Concentration with Traffic Density and Inverse Wind Speeds 76
Vertical Profiles 80
IV. CALIBRATION OF SRI'S STREET CANYON MODEL FOR TOTAL NITROGEN OXIDE CONCENTRATIONS WITHIN A DEPRESSED HIGHWAY SECTION 89
Introduction 89
SRI Street Canyon Submodel 89

CHAPTER PAGE

Leeward Case 90
Windward Case. 93
Parallel Case. 93
The Use of Stanford Research Institute's Street Canyon Model for Total Nitrogen Oxide Concentration Within a Depressed Highway Section 93
AP-42 Emission Factor Determination for 1974 94
The Emission Rate Determination. 95
The Correlation of the Measured Data with SRI's Model . . 97
The Calibration of SRI's Model for Total Nitrogen Oxide Estimates within a Depressed Highway Section . . . 101
The Correlation of the Measured Total Nitrogen Oxide Concentrations with Various Parameters 106
V. A NEW DEPRESSED HIGHWAY MODEL. 109
Introduction. 109
Leeward Case. 111
The Determination of the Dispersion Term's Exponent. . . 111
The Determination of the Calibration Coefficient 120
The Comparison of the Models 120
Windward Case 124
The Determination of the Dispersion Term's Exponent. . . 124
The Determination of the Calibration Coefficient 128
The Comparison of the Models 128
The Predicted Nitrogen Oxide Concentrations above The Depressed Highway Section 128

CHAPTER PAGE

VI. CONCLUSIONS. 131

LIST OF REFERENCES 134

VITA 138

LIST OF TABLES

TABLE		PAGE
1.	NITROGEN OXIDE EMISSIONS FOR VEHICULAR MODES OF OPERATION. .	7
2.	ATMOSPHERIC STABILITIES CLASSES.	22
3.	SEPTEMBER 25 TOTAL NITROGEN OXIDE DATA	28
4.	SEPTEMBER 26 TOTAL NITROGEN OXIDE DATA	39
5.	SEPTEMBER 27 TOTAL NITROGEN OXIDE DATA	55
6.	TOTAL STABILITY CLASSES DURING THE INVESTIGATION	77
7.	LEEWARD DATA CORRELATIONS WITH DIFFERENT PARAMETERS.	107
8.	WINDWARD DATA CORRELATIONS WITH DIFFERENT PARAMETERS	108
9.	THE CORRELATION OF THE VARIOUS APPROACHES WITH THE LEEWARD DATA.	116
10.	LEEWARD SIDE EXPONENTS OF THE DISPERSION TERM.	119
11.	LEEWARD SIDE CALIBRATION COEFFICIENTS.	121
12.	THE CORRELATION OF THE VARIOUS APPROACHES WITH WINDWARD DATA.	126
13.	THE NEW MODEL'S PREDICTIVE CAPABILITIES ABOVE THE DEPRESSED HIGHWAY SECTION	130

LIST OF FIGURES

FIGURE		PAGE
1.	MECHANIC WIND DISPERSION FROM A CHANGE IN TOPOGRAPHY. . . .	10
2.	I-40 EAST MONITORING SITE	15
3.	I-40 EAST VERTICAL RECEPTOR LOCATIONS	16
4.	OXIDES OF NITROGEN ANALYZER FLOW DIAGRAM.	24
5.	DYNAMIC CALIBRATION SYSTEM.	26
6.	DIURNAL TRAFFIC DENSITY	72
7.	DIURNAL HEAVY DUTY MIX.	74
8.	DIURNAL TRAFFIC SPEEDS.	75
9.	TOTAL WIND ROSE DURING INVESTIGATION.	78
10.	INVERSE WIND SPEED, TRAFFIC VOLUME, AND RECEPTOR CONCENTRATION RELATIONSHIPS.	79
11.	DIURNAL LEEWARD RECEPTOR CONCENTRATION PROFILES	81
12.	DIURNAL WINDWARD RECEPTOR CONCENTRATION PROFILES.	82
13.	ARITHMETIC MEAN VERTICAL CONCENTRATIONS FOR CROSSWIND CONDITIONS	83
14.	ARITHMETIC MEAN VERTICAL CONCENTRATIONS FOR PARALLEL WIND CONDITIONS.	84
15.	NORMALIZED VERTICAL PROFILE FOR PARALLEL WIND CONDITIONS	86
16.	NORMALIZED VERTICAL PROFILE FOR CROSSWIND CONDITIONS. . . .	87
17.	SRI STREET CANYON DESCRIPTION	91
18.	AVERAGE SPEED CORRECTION FACTOR FOR ALL MODEL YEARS	96
19.	EXAMPLE CORRELATION	98

FIGURE PAGE

20. UNCALIBRATED SRI MODEL CORRELATION WITH WINDWARD MEASURED DATA. 99
21. UNCALIBRATED SRI MODEL CORRELATION WITH LEEWARD MEASURED DATA. 100
22. LEAST SQUARES FIT OF UNCALIBRATED SRI MODEL 102
23. CUMULATIVE FREQUENCY OF K VALUES FOR THE LEEWARD DATA . . . 104
24. CUMULATIVE FREQUENCY OF K VALUES FOR THE WINDWARD DATA. . . 105
25. COMPARISON OF WIND SPEED ABOVE AND WITHIN THE DEPRESSED SECTION. 112
26. WIND ANGLE RELATIONSHIP WITH THE LEEWARD SIDE OF THE -15 FOOT TO -25 FOOT MEASURED CONCENTRATION. 113
27. VARIOUS FITS OF CONCENTRATION RATIOS WITH RESPECT TO THE LEEWARD WIND ANGLES. 114
28. A COMPARISON OF THE NEW MODEL'S RATIO OF MEASURED CONCENTRATIONS WITH SRI MODEL'S. 117
29. LEEWARD SIDE CALIBRATION COEFFICIENTS WITH RESPECT TO THE WIND ANGLE 122
30. THE NEW MODEL'S CORRELATION WITH THE MEASURED LEEWARD DATA 123
31. VARIOUS FITS OF CONCENTRATION RATIOS WITH RESPECT TO THE WINDWARD WIND ANGLES 125
32. COMPARISON OF THE WINDWARD CONCENTRATION RATIO FOR SRI AND THE NEW MODEL. 127
33. CORRELATION OF NEW MODEL WITH WINDWARD DATA 129

CHAPTER I

INTRODUCTION

Within the last twenty years, the importance of controlling air pollution sources of nitrogen oxides has increased significantly. This emphasis has been due to the discovery of nitrogen oxides' detrimental biological, phytotoxic, coloration, and photochemical smog effects. Because of these effects, the Clean Air Act of 1970 included regulations on sources of nitrogen oxides.

Although the source of nitrogen oxide can be from any combustion process, a majority of these pollutants are produced from automobiles. This amounts to about 60 and 90 percent of the total nitrogen oxides produced in industrialized urban and non-urban areas, respectively.

Since the majority of the air pollutants (nitrogen oxides, hydrocarbons, and carbon monoxide) are emitted from automobiles, various research has been performed to determine methods of controlling the formation of the various pollutants in the engine, the amount of the automobile's emissions, the dispersion of the emitted pollutants, and the impact of these pollutants on the environment. From this research, several different line source and box model equations have been formulated for predicting pollutant concentrations along the highway corridor.

Because each of the predictive techniques differ, the Environmental Engineering Department of The University of Tennessee was contracted by the Federal Transportation Department to evaluate and improve upon existing mathematical models. This was accomplished by comparing the different predictive techniques with field measured pollutant concentra-

tions at various locations in Nashville, Tennessee. As part of this research, nitrogen oxide concentrations were measured at various vertical heights within a depressed highway section. After measuring the various highway traffic and meteorological conditions, a street canyon model was compared with the measured concentrations.

The objective of this report is to present the nitrogen oxide monitoring data collected as part of this research effort. This report makes use of the field measurements to (1) validate and calibrate the existing Stanford Research Institute (SRI) Street Canyon Model for predicting nitrogen oxide concentrations within a depressed highway section and (2) to formulate a new model that provides an improved correlation with the measured data.

This report presents this information in the following order:

(1) A review of variables that influence the impact of nitrogen oxide concentrations is presented in Chapter II.

(2) Chapter III presents the field measured data and how this data was obtained.

(3) Chapter IV presents the existing Stanford Research Institute's Model, the mean K calibration approach, and the statistical analysis used to determine the model's correlation with the measured data.

(4) In Chapter V, an empirical model was formulated based upon Stanford Research Institute's model and data obtained from field measurements.

(5) The results of this report are summarized in Chapter VI.

This overall research effort has provided a new empirical model for total nitrogen oxide dispersion within a depressed highway section, and present a methodology which can be used to develop new empirical models that provides improved correlations with the monitoring data.

CHAPTER II

SOURCE, DISPERSION, AND EFFECTS OF NITROGEN OXIDES

I. INTRODUCTION

The degree of emissions from air pollution sources and the degree of dispersion away from such sources are the major factors that contribute to the creation of pollution levels that can cause detrimental effects. The horizontal and vertical dispersion is dependent primarily on meteorological conditions, sometimes on geographic conditions, and is generally beyond man's sphere of control. In contrast, air pollution sources can emit pollutants in sufficient quantities to produce deleterious effects and are within man's sphere of control.

The vehicular emissions of certain pollutants and their lack of dispersion can produce severe effects along the highway corridor. The conditions that restrict the normal transport and dilution of contaminant emissions include a stable atmosphere which prevents diffusion upward, from the points of origin, and geographical terrain features which may cause the flow to follow certain patterns and to carry from one area to another whatever the air may contain. The sources that contribute to the contaminants along highways are from a combination of the local traffic emissions and background contaminants from the area's stationary sources.

This chapter addresses the interaction of these factors. This includes discussing chemical mechanisms of nitric oxide formation in internal combustion engine, general conditions that influence the dispersion

and transport of these pollutants, chemical transformation of nitric oxide to nitrogen dioxide in the atmosphere, and the levels of nitrogen that produce detrimental effects.

II. SOURCE OF HIGHWAY EMISSIONS

Production of Nitrogen Oxides

All of the various compounds of nitrogen oxides such as nitric oxide (NO), nitrogen tetroxide (N_2O_4), nitrogen dioxide (NO_2), nitrous oxide (N_2O), nitrogen trioxide (N_2O_3), and nitrogen pentoxide (N_2O_5), can be produced from gasoline and diesel engines.[1*] Because of the instability of most of the compounds, only nitric oxide (NO) and nitrogen dioxide (NO_2) are important as air contaminants. Of these, nitric oxide is the only pollutant formed from the engine in significant quantities.

Nitric oxide is formed through direct combination of nitrogen and oxygen from the air in the intense heat of any combustion process. This formation is thermodynamically controlled, and it is explained by the following free radical chain reaction mechanism.[2,3]

$$O_2 \longrightarrow 2O^{\cdot}$$

$$O^{\cdot} + N_2 \longrightarrow NO + N^{\cdot}$$

$$N^{\cdot} + O_2 \longrightarrow NO + O^{\cdot}$$

---

*Superscript numbers refer to those entries in the List of References.

If this chemical equilibrium prevailed during the engine cycle, one would expect that the nitric oxide concentration would drop during the expansion stroke, due to the decreased gas temperature. However, instead of nitric oxide decomposition being thermodynamically controlled, it is kinetically controlled, and the formed nitric oxide concentration remains constant.[4]

Variables That Affect Nitric Oxide Emissions

Federal test procedures have been established to measure vehicular emissions over a 7.5 mile chassis dynamometer driving cycle. Based on the test procedures, several variables that affect the quantity of exhausted nitric oxide were determined.[5,6] The variables consisted of the vehicle type, vehicle age, and vehicular mode of operation. By knowing the relative magnitude of how each variable affects nitric oxide emission, an emission factor, in units of grams per vehicle mile, was determined. Then the emission factor can be multiplied by the number of vehicles per hour, to mathematically estimate the pollutant emissions.

The Type of Vehicles. Because different types of vehicles emit different amounts of nitric oxide concentrations, the number of each different type of vehicles is an important factor in determining the total amount of emissions. The different vehicular types of vehicles can generally be divided into classes by type of engine (diesel or gasoline powered) and by vehicle size (light duty vehicle less than two axles and heavy duty vehicle greater than two axles). For instance, a heavy duty diesel powered vehicle emits approximately three times as much nitric oxide as the respective gasoline powered heavy and light

duty vehicles which emit approximately nine times as much for the same conditions.[7] Because of this, the percent of these vehicular types must be known, in order to realistically estimate the emission factor and the total amount of emissions.

The Vehicle Age. The vehicle age is a very important factor that affects the amount of vehicular emissions. For instance, the nitric oxide emissions from the 1973 model vehicles were lower than the previous year's models due to the installation of exhaust gas recirculation control systems.[8] Because the exhaust gas recirculation system will deteriorate with time, a deterioration rate factor is needed. Therefore, the deterioration rate factor of each model's control device and the percent of each year's vehicular model in operation can affect the total amount of pollutants appreciably.

The Vehicular Modes of Operation. The amount of vehicular nitric oxide emissions varies with the different modes of engine operation (idle, acceleration, cruise, and deceleration). The reason nitric oxide emissions vary during different modes of operation is due to their variations in peak engine temperature and pressure. Since an increase of peak engine temperature and pressure produced greater nitric oxide emissions, the acceleration and cruise modes of operation substantially increase the amount of nitric oxide emissions emitted. Table 1 gives the variation of nitric oxide emissions with each of these modes.[9,10] Because of the variation of these emissions, the percent of time that a vehicle travels in each mode of operation can influence the total amount of nitric oxides emitted along the highway corridor.

TABLE 1. NITROGEN OXIDE EMISSIONS FOR VEHICULAR MODES OF OPERATION.

Mode of Operation	Nitrogen Oxides (ppm)
Idle	30
Cruise	1500
Acceleration	3000
Deceleration	60

III. THE TRANSPORT AND DISPERSION OF NITROGEN OXIDE

The severity of nitrogen oxide levels at any receptor along the highway is dependent not only on the amount of vehicular emitted pollutants, but also on the extent of which the pollutants are horizontally and vertically dispersed. The extent of this mixing is directly related to the amount of the nitric oxide dilution, from the exhaust to the receptor. Therefore, the greater the horizontal and vertical mixing, the greater the pollutant is dissipated. This section will discuss some of the factors that influence the mixing.

Transport

The degree transport of emitted nitric oxide concentrations is dependent upon the local surface wind speed and topography. The valley winds are the most important of the topographic winds in air pollution analysis.[11]

Valley circulations are caused by heating and cooling. The winds blow up slope (perpendicular to the axis of the valley) in the forenoon and down slope in the late evening. Along the axis of the valley, the winds blow up valley in the late afternoon and down valley in the early morning or late at night. Valleys can also cause channeling of the cross-winds that strike obliquely and change their direction so that they travel along the axis of the valley.

Dispersion

The extent of vertical dispersion of the pollutants is determined by the stability of the atmosphere, that is the degree of the turbulent

mixing in the air mass. This in turn depends on the temperature gradient in the lowest layer of the atmosphere. If the temperature decreases with altitude at a rate greater than 5.4°C per 1000 feet (the dry adiabatic lapse rate), the atmosphere is unstable and turbulent mixing occurs. If the temperature decreases less than 5.4°C per 1000 feet or increases with height, the atmosphere is stable. With the exchange of air between the surface and the upper levels suppressed, vertical mixing is inhibited.[12]

Vertical dispersion can also be influenced by mechanical turbulence. This type of mixing is caused by air motion over the rough surface of the earth or by sudden changes in topography. Figure 1 illustrates the helical circulation mixing caused by a topographic depression in the terrain. If a highway was located in the depression, the vertical mixing from vehicular traffic would be greater on the leeward side (right side) than on the windward side (left side) due to the sudden change in topography.[13]

Horizontal dispersion is mainly influenced by wind speed and the degree of fluctuations in wind direction. The greater the fluctuations in wind direction, the greater the horizontal dispersion.[14]

IV. NITROGEN DIOXIDE EFFECTS

After the nitric oxide (NO) emissions have been dispersed in the atmosphere, nitric oxide reacts with oxygen (O_2) or ozone (O_3) to form nitrogen dioxide (NO_2) by one of the following reactions.[15]

$$2NO + O_2 \longrightarrow NO_2$$

$$NO + O_3 \longrightarrow NO_2 + O_2$$

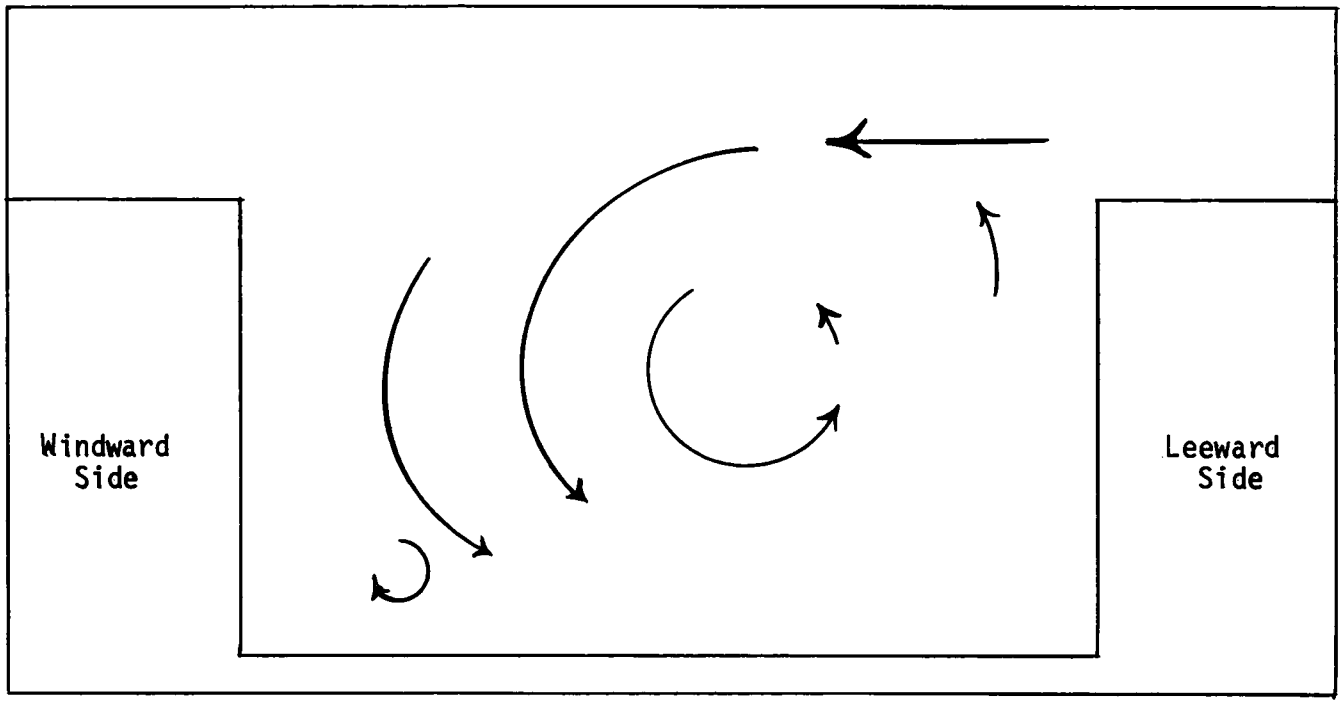

FIGURE 1. MECHANIC WIND DISPERSION FROM A CHANGE IN TOPOGRAPHY

After this partial conversion, both nitric oxide and nitrogen dioxide are present in varying amounts in the atmosphere. However, only ambient levels of nitrogen dioxide concentrations can produce detrimental effects. If the nitrogen dioxide levels are large enough, they can cause biological, phytotoxic, coloration, and the production of photochemical smog effects. The levels of nitrogen dioxide concentrations required to cause these various effects are as follows.

Biological Effects

Nitrogen levels of approximately five parts per million can produce lung injury and edema, and in greater concentrations fatal lung damage.[11]

Phytotoxic Effects

Data on phytotoxic effects indicate that exposures of nitrogen dioxide levels less than one part per million affects plant growth and greater than two to three parts per million cause a bleaching effect on plant leaves.[16]

Coloration Effects

Nitrogen dioxide absorbs light in both the ultraviolet and visible spectrum. At levels of 0.25 parts per million and above, nitrogen dioxide imparts a yellow-brown color to the horizon sky and distant white objects. It has been estimated that a level of 0.25 parts per million produces a color effect that impairs visibility so much that objects 10 miles away seem 20 miles. This amount of visibility reduction is objectionable to the public.[15]

Photochemical Smog Effects

Research has demonstrated that nitrogen dioxide in the presence of sunlight undergoes a number of complicated reactions with various organic compounds to produce the effects associated with photochemical smog.[17] Exhaust emissions from vehicular traffic contribute significantly to the production of compounds that form photochemical smog. Because of the important role nitrogen oxide emissions play in the formation of photochemical smog, the Clean Air Act of 1970 contained regulations on the amount of nitrogen oxide emissions that can be emitted from vehicles in 1976.

Nitrogen dioxide is heavily indicated as an undesirable pollutant of the atmosphere, regardless of the air pollution problem under consideration. Nevertheless, since every mole of nitric oxide emitted to the atmosphere has the potential to produce a mole of nitrogen dioxide, one may not be considered one without the other.[18]

CHAPTER III

EXPERIMENTAL PROGRAM

I. INTRODUCTION

Having identified the variables influencing nitrogen oxide concentrations along the highway corridor, it was decided to make on-site measurements of such variables and actual concentrations. This was done in order to validate and calibrate the existing predictive model and to formulate a new improved model. Regardless of the soundness of theory on which a depressed highway model is based, field measurements are required to determine a dimensionless coefficient, in order for the model to conclusively predict the true concentration. This empirical coefficient can be derived by relating the actual field measured concentration for the monitoring site with the model's predicted values. The reason this determination must be performed is due to the lack of thorough understanding of the true relationship of such variables as wind speed, wind direction, stability, traffic density (volume/time), emission factors, and terrain effects.

For this work, the values for the different variables are not only essential for determining an empirical coefficient, but also in validating the existing Stanford Research Institute's Submodel and in formulating a new improved model. The existing model requires the input of traffic speed, traffic density, wind speed, heavy duty mix, wind direction, plus various highway measurements, and receptor distances. All these parameters were measured either continuously or intermittently during the air monitoring program at Interstate-40 East in Nashville, Tennessee.

This chapter describes the experimental program, including monitoring site description, sample collection procedure, instruments used, analyzer calibration procedure, and analysis of measured data.

II. MONITORING SITE DESCRIPTION

During the period of September 24 through September 27, a field air monitoring program was established in Nashville, Tennessee. This monitoring program was to measure pollutant concentrations of carbon monoxide, hydrocarbons, and total nitrogen oxides within and above a depressed highway section. A 30 foot depressed highway section was selected four miles East of downtown Nashville on Interstate-40 East. Since this interstate contained two out-bound lanes from Nashville, the peak traffic conditions occurred in the mid-afternoon to early evening.

The first day was utilized installing the air monitoring equipment and setting up a sampling network. The relative positions of the monitoring equipment are shown in Figure 2. The analyzers were located at one central location that was above the depressed section on the North side of Interstate-40 East. A canvas shelter was installed to protect these analyzers from inclement weather and from solar radiation. Other instruments now shown in the Figure 2 are the traffic counter's position 1/8 mile on I-40 prior to reaching the monitoring site, the permanent 30 foot weather station located 1/4 mile Southwest of the monitoring site, and a temporary weather station located within the depressed section.

The dimensions of the depressed section and the location of the receptors are shown in Figure 3. The depressed section contained a total width of 64 feet, two shoulders 10 feet wide, and two traffic lanes 12

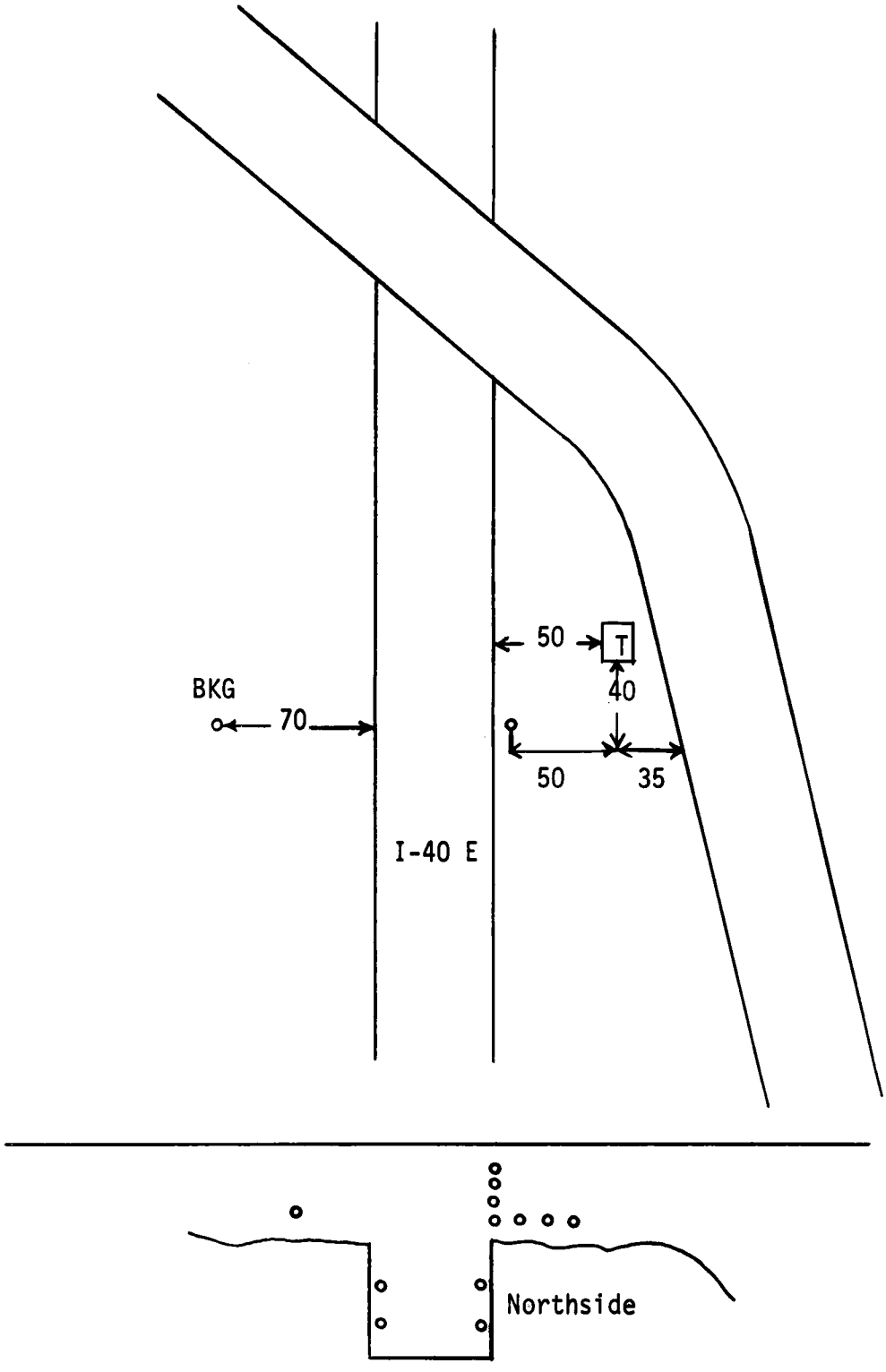

NOTE: All measurements are in feet.

FIGURE 2. I-40 EAST MONITORING SITE

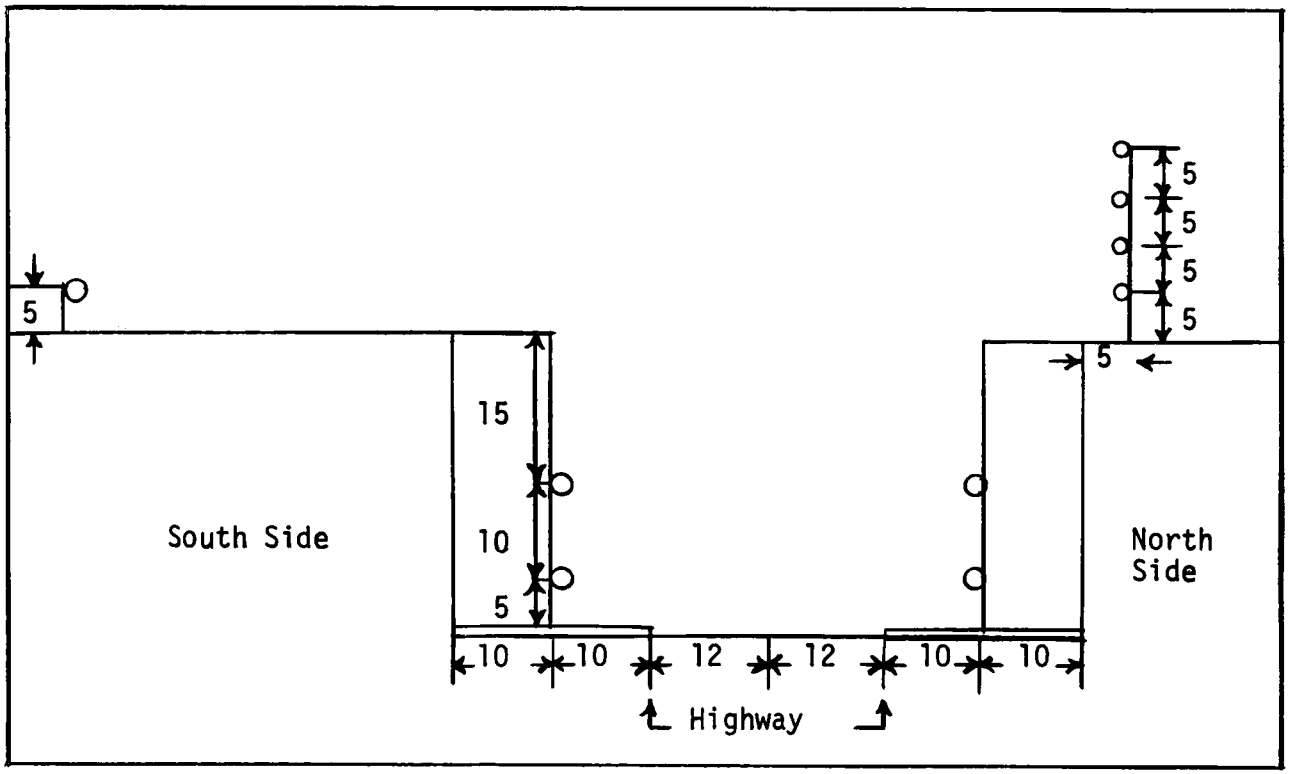

FIGURE 3. I-40 EAST VERTICAL RECEPTOR LOCATIONS

feet wide. The receptors within the depressed section on both North (windward) and South (leeward) side were located vertically -25 feet, and -15 feet below the top of the 30 foot section and horizontally 10 feet from the edge of the highway. Besides these receptors within the depressed section, the North side of I-40 contained receptors with a vertical profile of 5, 10, 15, and 20 feet above the section and a horizontal 25 feet from the road's edge. The remaining receptor was located upwind on the South side, five feet above the section and 80 feet from the road's edge. This receptor was used as a background station for monitoring the total nitrogen oxide concentrations from the area sources.

III. THE BAG SAMPLING COLLECTION NETWORK

A bag sampling network was utilized to collect pollutant concentrations at the vertical receptor heights and locations in and above the depressed section. This type of network allowed greater flexibility, maximum data collection, and minimum cost requirements.

The sampling network consisted of six liter Scotchpak bags, vacuum pumps, restrictors, and 1/4 inch I.D. x 1/2 inch O.D. tygon tubing. Vacuum pumps were used to draw the receptors sample back through the tubing to central locations, where the Scotchpak bag was filled. The flows from the vacuum pumps were restricted in order to obtain a four liter bag sample in a 15 minute sampling period. Thus, as many as nine probes were operated at the I-40 East site during the same time period. This allowed the determination of vertical concentration profiles within and above the cut section.

Another advantage of utilizing this method of gathering samples was the ability to measure not only oxides of nitrogen from the bag samples, but also carbon monoxide and total hydrocarbons from the sample bags. This allowed the comparison of the most inert pollutant concentrations, carbon monoxide, with the oxides of nitrogen and thus determining its reactivity in the atmosphere.

One disadvantage with a bag collection network was that bag samples will, with time, slowly decay toward a zero concentration.[19] Because of the uncertainties of the longevity on reactivity of oxides of nitrogen with the Scotchpak sampling bags, a field experiment was performed. This experiment consisted of filling a sample bag with span gas, allowing it to remain in the bag for 24 hours, and determining the decay of the oxide of nitrogen concentration. This experiment resulted in an average of a six percent decay over a 24 hour time period. Since all oxides of nitrogen concentrations were sampled within two hours of filling the bag, the decay would be negligible within this short time period. Since the sampling bag's interferences were eliminated, the only other interferences in the measured concentrations could occur in the line from the receptor to the sampling bag. Earlier experiments had shown that the tygon tubing interfered with measured carbon monoxide due to solar radiation.[20] This was corrected by covering the tubing with aluminum foil. The experiment for testing any interference between the probe and sampling bag consisted of injecting the calibration gas at the probe and also running an identical sample directly into the analyzer. This experiment resulted in no decrease or increase in the oxides of nitrogen concentration of the gas injected at the probe relative to that introduced directly at the instrument.

By conducting such experiments, a greater amount of confidence was gained in using the bag sampling network for total nitrogen oxides.

IV. TYPES OF MEASUREMENTS EMPLOYED

Various types of measurement techniques and equipment were employed to obtain the required input data needed to formulate or to revise the existing street canyon submodel for oxides of nitrogen. The techniques and equipment used to determine each of these parameters are outlined below.

Traffic Measurements

All traffic counts were obtained from mechanical (pneumatic) counters provided by the State Highway Commission. This type of counter consists of a flexible rubber tube fastened to the pavement and perpendicular to the path of the vehicle travel and a counter.[21] As a vehicle crosses the tube, the air inside the tube is compressed, actuating a pressure counter switch. The counter continuously accumulates the total number of double axles, and the cumulative total hourly number of vehicles are printed at 15 minute intervals. Thus, this allowed the determination of 15 minute traffic count.

Heavy Duty Mix

Heavy duty vehicle counts were made manually using the standard classification of trucks according to the number of axles.[22] Thus, such trucks as light duty delivery and pick-up trucks were counted the same as car counts. The heavy duty vehicle counts indicated that the truck

mix was about evenly divided between diesel and non-diesel heavy duty vehicles. This factor is utilized in Chapter IV when the emission factors are calculated.

Average Vehicle Speed

The average vehicle speed was determined periodically using a stop watch method. This method involves the use of transverse pavement markings which are located at the end of the course, and an observer to start and stop the watch as the vehicle passes the markings. Since the distance had been determined previously, so that the average speed could be ascertained by dividing the distance of the course by the time of the vehicle travel. During a fifteen minute interval, several measurements were determined and the average of these values was used as the fifteen minute average speed value.

Wind Data Measurements

The wind speed and wind direction were measured continuously at each site location with a Meteorology Research Incorporation (MRI) Mechanical Weather Station Model 1071.[23] This weather station utilized a cup-type anemometer and a wind vane to measure the wind speed and wind direction. The weather station also contained a battery operated strip chart for a permanent record of the weather data.

The site location of the one permanent MRI location was at the highest point near the sampling sites. This MRI instrument was located 30 feet high on a telescopic pole. The height of the station allowed the measuring of the wind speed without the local terrain affecting the

measured values. It also allowed the option of calibrating the monitoring site's wind data with the airport weather data, similar to the work by Schnelle.[24]

Besides this permanent weather station, an MRI package was placed on a 10 foot mast and located within the depressed highway section close to the 30 foot wind instrument to obtain the correlation between the speeds and directions for the two locations.

Temperature and Humidity

A Bendix Corporation model 590 hygro-thermograph was used to continuously record the atmospheric temperature and the relative humidity throughout the monitoring day. Because the hygro-thermograph ran mechanically, it required no power supply for it's daily operation.

Atmospheric Stability

Atmospheric stabilities were based on the six Pasquill Stability classes of A to F which range from extremely unstable to extremely stable vertical stability. Stabilities were determined every 15 minute period using Table 2. The determination of the stability class was based on the following field recorded parameters: the wind speed (at the 30 foot MRI wind station), the temperature reading, the insolation, the season, percent of cloud cover, and the time of the day. The stabilities were first determined by one person and then checked by another to minimize errors in judgement.

The Oxides of Nitrogen Analyzer

The type of ambient air monitoring instrument utilized for measuring concentrations of oxides of nitrogen was a Bendix Model 8101-B.[25]

TABLE 2. ATMOSPHERIC STABILITIES CLASSES.

Surface Wind Speed (at 10 m) (m/sec.)	Insolation			Night	
	Strong	Moderate	Slight	Thinly Overcast or ≥ 4/8 Low Cloud	≤ 3/8 Cloud
< 2	A	A-B	B	--	--
2-3	A-B	B	C	E	F
3-5	B	B-C	C	D	E
5-6	C	C-D	D	D	D
< 6	C	D	D	D	D

*The neutral category D, should be assumed for overcast conditions during day or night.

Figure 4 shows a flow diagram of this type analyzer. The analyzer employs the principle of photometric detection of the chemiluminescence resulting from the flameless gas phase reaction of nitric oxide (NO) and ozone.

Since the flameless gas reaction only occurs between nitric oxide (NO) and ozone, it is necessary to convert the nitrogen dioxide (NO_2) into nitric oxide (NO) to obtain a total oxides of nitrogen measurements. A catalytic converter is utilized to change nitrogen dioxide (NO_2) into nitric oxide (NO), with no effect on incoming nitric oxide. This is the input for the total oxide of nitrogen measurement ($NO + NO_2 = NOx$).

The reaction chamber of the detector cell provides the proper environment to assure that the flameless gas phase reaction produces light energy. This light passes through the optical filter to the photomultiplier tube, where it is converted into electrical energy and amplified. The degree of gas phase reaction is directly proportional to the amount of nitrogen oxides present in the air sample, thus producing a proportional amount of light, and providing an accurate measurement medium.

The output from the photomultiplier tube is coupled into an electrometer amplifier. This is electronically converted so that the analyzer registers a part per million measured reading on its meter.

V. THE ANALYZER'S CALIBRATION PROCEDURE

Before going to the field with the nitrogen oxide analyzer, laboratory tests were performed to check the analyzer's linearity and to verify the certified 1.1 part per million nitric oxide span gas to be used in

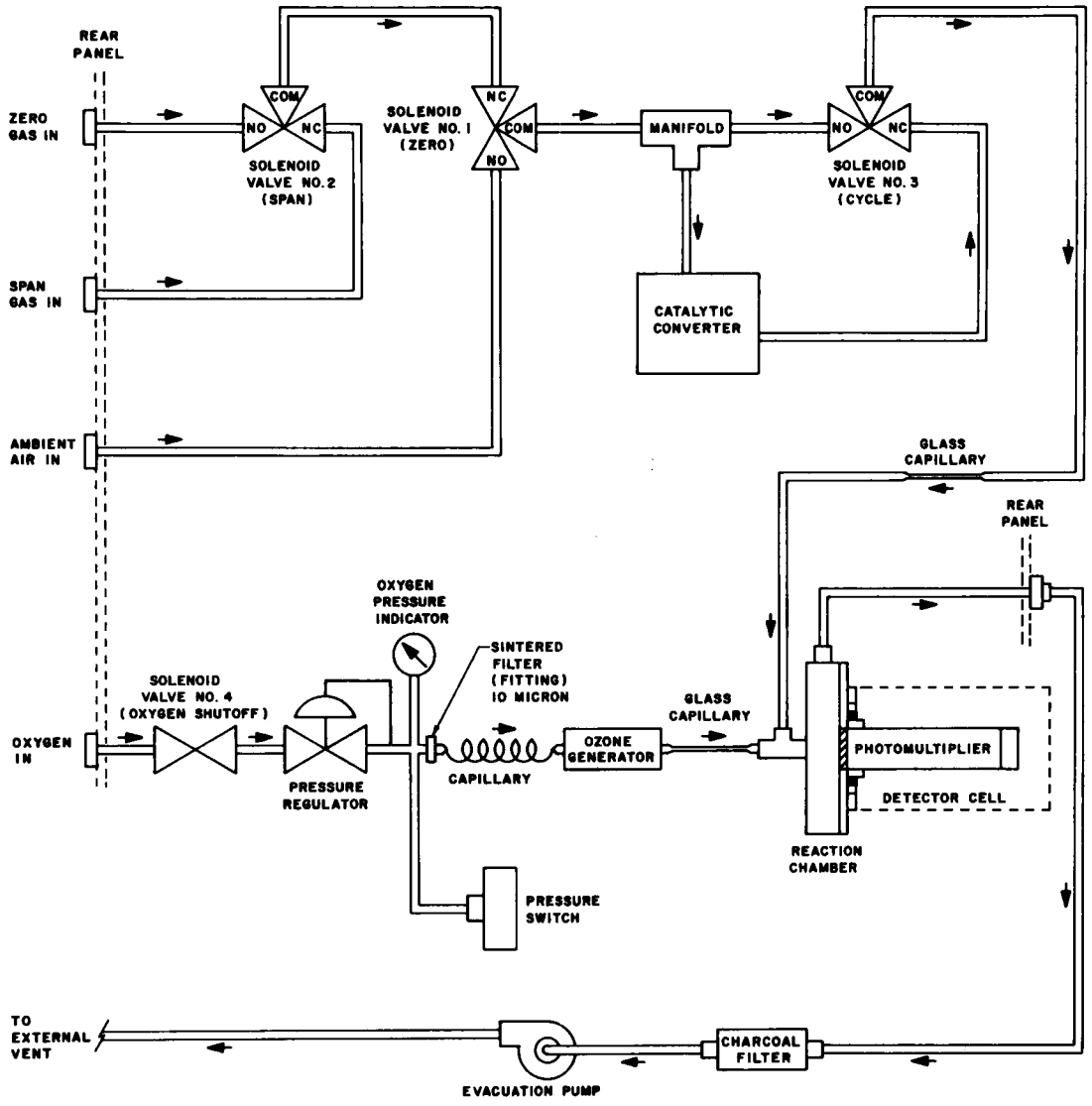

FIGURE 4. OXIDES OF NITROGEN ANALYZER FLOW DIAGRAM

the field. For both of these tests, the dilution method shown in Figure 5 was used. With this method, a certified bottle of span gas was diluted to the desired concentration by regulation of the diluent gas, nitrogen, added.[26] For the analyzer linearity test, the analyzer was calibrated throughout its measurement range by changing the amount of diluent. This test established the analyzer's linearity throughout its range. For validation of the 1.1 part per million span gas, a bottle of 10 parts per million nitric oxide was diluted with nitrogen to obtain 1.1 part per million. Since both gave the same instrument deflection, the field span gas bottle could now be used in the field calibrations with a greater degree of confidence.

When monitoring with the nitrogen oxides analyzer at I-40 East, the analyzer was warmed up over an hour each morning to reaching electronic stability. After this time, the analyzer was calibrated using a two point zero gas and upscale span gas calibration procedure. A pressurized steel cylinder of ultra pure dry nitrogen was used as a zero gas and cylinder containing the 1.1 part per million nitric oxide was used as the 100 percent deflection point. The calibration was performed several times a day. Initially, the calibration was executed every 15 minutes until complete certainty was established in the analyzer's electronic stability.

After this was determined, the analyzer was calibrated every one or two hours in order to adjust for drifts due to changes of temperature throughout the monitoring day.

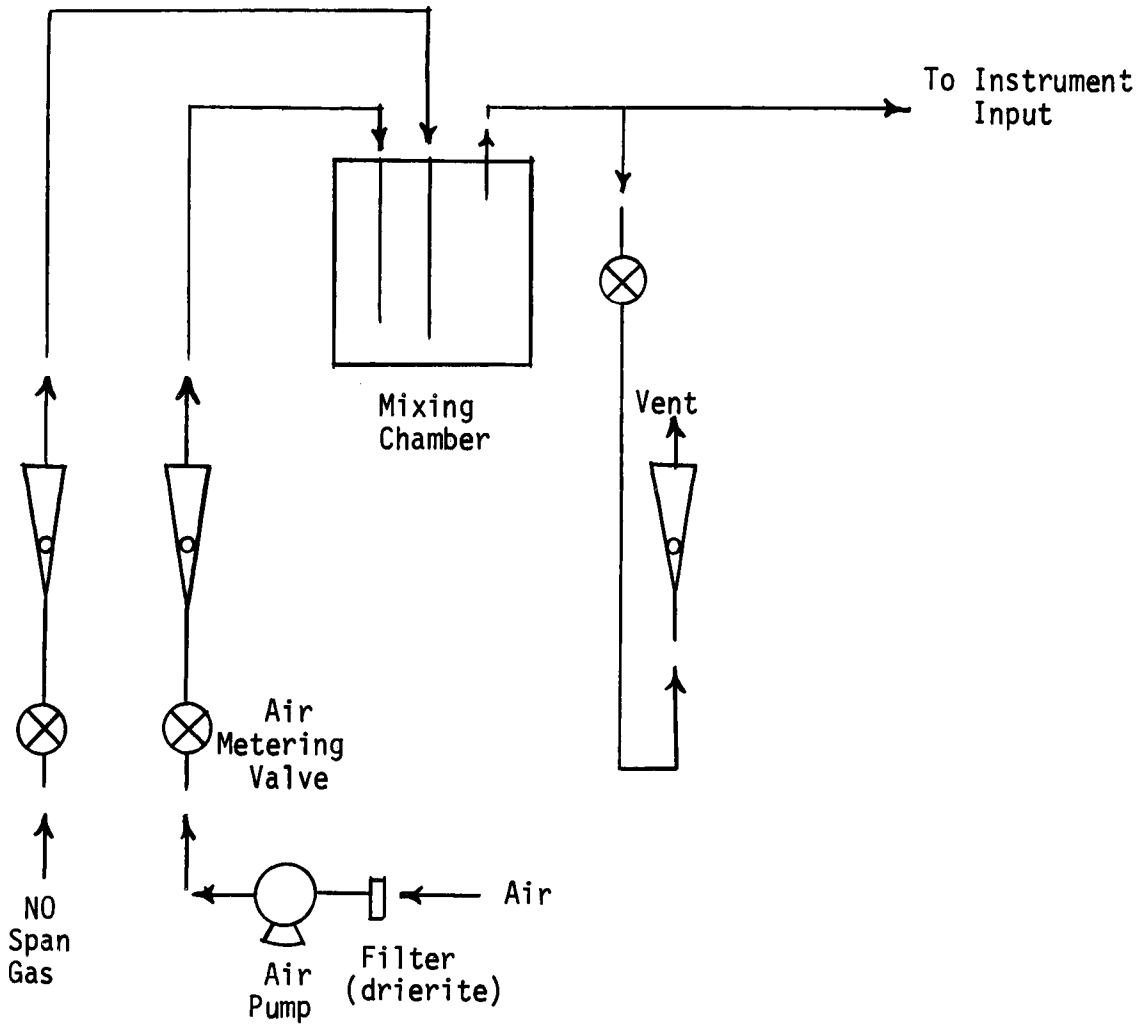

FIGURE 5. DYNAMIC CALIBRATION SYSTEM

VI. ANALYSIS OF MEASURED DATA

After all traffic, meteorological, and measured total nitrogen oxide concentration data were reduced into 15 minute intervals and adjusted for calibration, the data were ready to be analyzed and used as input into a statistical computer program. Tables 3, 4, and 5 list this reduced data for September 25, 26, and 27. These tables list measured traffic, meteorological, and nitrogen oxide concentration data for time of day; side of road leeward (L), windward (W), or background (BG); and for each vertical receptor position within a depressed highway section.

This section discusses the traffic, meteorological, and measured nitrogen oxide concentration data collected during the monitoring period.

Traffic Data Analysis

Traffic Density. Figure 6 gives a diurnal plot of the total traffic volume per hour for each 15 minutes of monitoring. From 8:00 a.m. until 2:00 p.m. each day, the traffic remained relatively constant at around 700 vehicles per hour. After 2:00 p.m., the traffic volume increased until reaching peak hours from 3:15 p.m. until 5:45 p.m. This evening peak hourly traffic was double the volume of morning traffic. Since I-40 East contains two outbound lanes from Nashville, this increased evening traffic was apparently due to people going home from work.

Heavy Duty Mix. Heavy duty vehicle (gasoline and diesel powered truck) counts remained relatively constant at around 16 per 15 minutes throughout the monitoring day. Of these total 15 minute counts, the number of gasoline and diesel powered trucks were about evenly divided.

TABLE 3. SEPTEMBER 25 TOTAL NITROGEN OXIDE DATA.

Time	Side	Probe Height (feet)	Conc. (ppm)	Traffic Volume (veh./hr.)	Heavy Duty Mix	Emission Factor (gm/veh. mile)	Stability	Wind Speed (m/sec.)	Wind Dir. (Degrees) @ Road ϕ
8^{15}	W	-25	0.19	696	4	8.57	E	1.12	80
	W	-15	0.14						
	W	5	0.09						
	BG		0.03						
8^{30}	W	-25	0.19	444	8	7.51	E	1.56	45
	W	-15	0.14						
	W	5	0.10						
	BG		0.03						
8^{45}	W	-25	0.13	540	20	9.65	E	2.01	50
	W	-15	0.11						
	W	5	0.07						
	BG		0.03						
9^{00}	W	-25	0.12	560	22	10.07	E	2.14	45
	W	-15	0.11						
	W	5	0.07						
	BG		0.03						
11^{00}	L	-25	0.10	688	12	8.25	D	4.69	90
	L	-25	0.06						
	BG		0.03						
11^{15}	L	-25	0.09	732	12	8.26	D	4.47	95
	L	-15	0.05						
	BG		0.03						
11^{30}	L	-25	0.10	796	12	8.29	D	4.47	90
	L	-15	0.07						

TABLE 3 (CONTINUED).

Time	Side	Probe Height (feet)	Conc. (ppm)	Traffic Volume (veh./hr.)	Heavy Duty Mix	Emission Factor (gm/veh. mile)	Stability	Wind Speed (m/sec.)	Wind Dir. (Degrees) @ Road ϕ
11^{35}_{45}	BG		0.03						
11	L	-25	0.10	788	13	8.43	C	3.58	85
	L	-15	0.06						
	BG		0.03						
12^{00}	W	-25	0.06	684	13	8.53	C	3.26	90
	W	-15	0.05						
	W	5	0.03						
	W	10	0.04						
	W	15	0.04						
	W	20	0.03						
	L	-25	0.11						
	L	-15	0.06						
	BG		0.03						
12^{15}	W	-25	0.09	788	13	8.67	B	3.26	90
	W	-15	0.09						
	W	5	0.05						
	W	10	0.04						
	W	15	0.04						
	W	20	0.03						
	L	-25	0.15						
	L	-15	0.07						
	BG		0.03						
12^{30}	W	-25	0.04	560	14	8.80	B	2.91	95
	W	-15	0.04						

TABLE 3 (CONTINUED).

Time	Side	Probe Height (feet)	Conc. (ppm)	Traffic Volume (veh./hr.)	Heavy Duty Mix	Emission Factor (gm/veh. mile)	Stability	Wind Speed (m/sec.)	Wind Dir. (Degrees) @ Road ϕ
12^{30}	W	5	0.04						
	W	10	0.03						
	W	15	0.03						
	W	20	0.02						
	L	-25	0.09						
	L	-15	0.05						
	BG		0.03						
12^{45}	W	-25	0.04	760	13	8.70	B	2.68	80
	W	-15	0.03						
	W	5	0.03						
	W	10	0.02						
	W	15	0.01						
	W	20	0.02						
	L	-25	0.08						
	L	-15	0.05						
	BG		0.01						
13^{00}	W	-25	0.05	616	12	8.55	B	2.91	100
	W	-15	0.05						
	W	5	0.04						
	W	10	0.03						
	W	15	0.02						
	W	20	0.03						
	BG		0.02						

TABLE 3 (CONTINUED).

Time	Side	Probe Height (feet)	Conc. (ppm)	Traffic Volume (veh./hr.)	Heavy Duty Mix	Emission Factor (gm/veh. mile)	Stability	Wind Speed (m/sec.)	Wind Dir. (Degrees) @ Road ϕ
13^{00}_{15}	BG								
13	W	-25	0.05	784	12	8.4	B	2.24	135
	W	-15	0.05						
	W	5	0.03						
	W	10	0.03						
	W	15	0.02						
	W	20	0.02						
	BG		0.02						
13^{30}	L	-25	0.10	556	11	8.25	B	2.24	90
	L	-15	0.06						
	BG		0.02						
13^{45}	W	-25	0.10	860	10	8.15	B	2.24	90
	W	15	0.08						
	W	5	0.05						
	W	10	0.05						
	W	15	0.03						
	W	20	0.03						
	L	-25	0.12						
	L	-15	0.06						
	BG		0.03						
14^{00}	W	-25	0.06	756	11	8.2	B	2.24	75
	W	15	0.05						
	W	5	0.02						
	W	10	0.02						

TABLE 3 (CONTINUED).

Time	Side	Probe Height (feet)	Conc. (ppm)	Traffic Volume (veh./hr.)	Heavy Duty Mix	Emission Factor (gm/veh. mile)	Stability	Wind Speed (m/sec.)	Wind Dir. (Degrees) @ Road ϕ
14^{00}	W	15	0.02						
	W	20	0.01						
	L	-25	0.10						
	L	-15	0.05						
	BG		0.02						
14^{15}	W	-25	0.06	996	8	7.82	B	2.68	80
	W	-15	0.06						
	W	5	0.04						
	W	10	0.03						
	W	15	0.03						
	W	20	0.02						
	L	-25	0.13						
	L	-15	0.06						
	BG		0.02						
14^{30}	W	-25	0.05	880	11	8.09	B	3.13	50
	W	-15	0.05						
	W	5	0.02						
	W	10	0.03						
	W	15	0.02						
	W	20	0.02						
	L	-25	0.12						
	L	-15	0.06						
	BG		0.02						
14^{45}	W	-25	0.06	964	8	7.74	B	3.13	60

TABLE 3 (CONTINUED).

Time	Side	Probe Height (feet)	Conc. (ppm)	Traffic Volume (veh./hr.)	Heavy Duty Mix	Emission Factor (gm/veh. mile)	Stability	Wind Speed (m/sec.)	Wind Dir. (Degrees) @ Road ϕ
14^{45}	W	-15	0.06						
	W	5	0.04						
	W	10	0.03						
	W	15	0.03						
	W	20	0.02						
	L	-25	0.14						
	L	-15	0.08						
	BG		0.02						
15^{00}	W	-25	0.11	956	8	7.66	B	2.58	45
	W	-15	0.08						
	W	5	0.04						
	W	10	0.03						
	W	15	0.03						
	W	20	0.02						
	L	-25	0.13						
	L	-15	0.07						
	BG		0.01						
15^{15}	W	-25	0.11	1332	7	7.55	B	2.9	30
	W	-15	0.08						
	W	5	0.04						
	W	10	0.03						
	W	15	0.03						
	W	20	0.03						
	L	-25	0.11						

TABLE 3 (CONTINUED).

Time	Side	Probe Height (feet)	Conc. (ppm)	Traffic Volume (veh./hr.)	Heavy Duty Mix	Emission Factor (gm/veh. mile)	Stability	Wind Speed (m/sec.)	Wind Dir. (Degrees) @ Road ϕ
15^{15}	L	-15	0.07						
	BG		0.01						
15^{30}	W	-25	0.15	1244	6	7.46	B	3.35	30
	W	-15	0.11						
	W	5	0.04						
	W	10	0.04						
	W	15	0.03						
	W	20	0.03						
	L	-25	0.16						
	L	-15	0.10						
	BG		0.01						
15^{45}	W	-25	0.10	1364	5	7.17	C	3.35	45
	W	-15	0.06						
	W	5	0.04						
	W	10	0.04						
	W	15	0.03						
	W	20	0.03						
	L	-25	0.08						
	L	-15	0.08						
	BG		0.01						
16^{00}	W	-25	0.11	1096	6	7.37	C	2.68	70
	W	-15	0.08						
	W	5	0.05						
	W	10	0.06						

TABLE 3 (CONTINUED).

Time	Side	Probe Height (feet)	Conc. (ppm)	Traffic Volume (veh./hr.)	Heavy Duty Mix	Emission Factor (gm/veh. mile)	Stability	Wind Speed (m/sec.)	Wind Dir. (Degrees) @ Road ϕ
16^{00}	W	15	0.04						
	W	20	0.04						
	L	-25	0.13						
	L	-15	0.07						
	BG		0.02						
16^{15}	W	-25	0.09	1504	5	7.24	C	3.35	60
	W	-15	0.07						
	W	10	0.04						
	W	15	0.03						
	W	20	0.03						
	L	-25	0.15						
	L	-15	0.07						
	BG	5	0.02						
16^{30}	W	-25	0.09	1380	8	7.80	C	3.35	60
	W	-15	0.08						
	W	5	0.04						
	W	10	0.04						
	W	15	0.04						
	W	20	0.04						
	L	-25	0.12						
	L	-15	0.08						
	BG		0.02						
16^{45}	W	-25	0.09	1596	5	7.30	C	3.35	60
	W	-15	0.08						

TABLE 3 (CONTINUED).

Time	Side	Probe Height (feet)	Conc. (ppm)	Traffic Volume (veh./hr.)	Heavy Duty Mix	Emission Factor (gm/veh. mile)	Stability	Wind Speed (m/sec.)	Wind Dir. (Degrees) @ Road ϕ
16^{45}	W	5	0.04						
	W	10	0.04						
	W	15	0.04						
	W	20	0.03						
	L	-25	0.13						
	L	-15	0.07						
	BG		0.02						
17^{00}	W	-25	0.10	1464	7	7.59	C	3.58	50
	W	-15	0.09						
	W	5	0.05						
	W	10	0.04						
	W	15	0.03						
	W	20	0.03						
	L	-25	0.16						
	L	-15	0.09						
	BG		0.03						
17^{15}	L	-25	0.14	1392	4	6.95	C	3.40	55
	L	-15	0.08						
	BG		0.03						
17^{30}	W	-25	0.09	1132	5	7.19	C	3.35	55
	W	-15	0.07						
	W	5	0.04						
	W	10	0.04						
	W	15	0.03						

TABLE 3 (CONTINUED).

Time	Side	Probe Height (feet)	Conc. (ppm)	Traffic Volume (veh./hr.)	Heavy Duty Mix	Emission Factor (gm/veh. mile)	Stability	Wind Speed (m/sec.)	Wind Dir. (Degrees) @ Road ϕ
17^{30}	W	20	0.03						
	L	-25	0.13						
	L	-15	0.07						
	BG		0.03						
17^{45}	W	-25	0.08	1076	5	7.12	C	3.35	45
	W	-15	0.07						
	W	5	0.04						
	W	10	0.04						
	W	15	0.03						
	W	20	0.04						
	L	-25	0.12						
	L	-15	0.07						
	BG		0.03						
18^{00}	W	-25	0.18	872	5	7.11	C	3.8	45
	W	-15	0.13						
	W	10	0.07						
	W	15	0.07						
	W	20	0.06						
	L	-25	0.18						
	L	-15	0.09						
	BG		0.03						
18^{15}	W	-25	0.16	880	5	7.06	C	3.49	45
	W	-15	0.13						

TABLE 3 (CONTINUED).

Time	Side	Probe Height (feet)	Conc. (ppm)	Traffic Volume (veh./hr.)	Heavy Duty Mix	Emission Factor (gm/veh. mile)	Stability	Wind Speed (m/sec.)	Wind Dir. (Degrees) @ Road ϕ
18^{15}	W	5	0.06						
	W	10	0.06						
	W	15	0.05						
	W	20	0.04						
	L	-25	0.17						
	L	-15	0.09						
	BG		0.03						
18^{30}	W	-25	0.17	680	5	7.06	C	3.04	50
	W	-15	0.16						
	W	5	0.08						
	W	10	0.08						
	W	15	0.07						
	W	20	0.06						
	L	-25	0.15						
	L	-15	0.08						
	BG		0.03						
18^{45}	W	-25	0.16	667		7.06	C	3.26	45
	W	-15	0.12						
	W	5	0.06						
	W	10	0.06						
	W	15	0.05						
	W	20	0.04						
	L	-25	0.15						
	L	-15	0.09						
	BG		0.03						

TABLE 4. SEPTEMBER 26 TOTAL NITROGEN OXIDE DATA.

Time	Side	Probe Height (feet)	Conc. (ppm)	Traffic Volume (veh./hr.)	Heavy Duty Mix	Emission Factor (gm/veh. mile)	Stability	Wind Speed (m/sec.)	Wind Dir. (Degrees) @ Road ϕ
8^{00}	W	-25	0.19	604	14	8.52	E	2.46	35
	W	-15	0.15						
	W	10	0.11						
	W	15	0.08						
	W	20	0.08						
8^{15}	BG		0.01						
	W	-25	0.10	756	14	8.54	D	3.35	30
	W	-15	0.08						
	W	5	0.04						
	W	10	0.04						
	W	15	0.03						
	W	20	0.02						
8^{45}	BG		0.01						
	W	-25	0.07	696	14	8.56	D	3.58	40
	W	-15	0.06						
	W	5	0.03						
	W	10	0.02						
	W	15	0.02						
	W	20	0.01						
9^{00}	BG		0.01						
	W	-25	0.11	632	14	8.57	D	4.02	40
	W	-15	0.08						
	W	5	0.04						
	W	10	0.04						

TABLE 4 (CONTINUED).

Time	Side	Probe Height (feet)	Conc. (ppm)	Traffic Volume (veh./hr.)	Heavy Duty Mix	Emission Factor (gm/veh. mile)	Stability	Wind Speed (m/sec.)	Wind Dir. (Degrees) @ Road ϕ
9^{00}	W	15	0.02						
	W	20	0.03						
	L	-25	0.16						
	L	-15	0.08						
	BG		0.01						
9^{15}	L	-25	0.10	656	14	8.6	D	3.8	35
	L	-15	0.05						
	BG		0.01						
9^{30}	L	-25	0.07	500	14	8.62	D	5.36	35
	L	-15	0.03						
	BG		0.01						
9^{45}	L	-25	0.08	680	13	8.56	D	5.36	45
	L	-15	0.05						
	BG		0.01						
10^{15}	L	-25	0.08	740	13	8.33	D	4.69	30
	L	-15	0.04						
	BG		0.01						
10^{30}	L	-25	0.09	624	12	8.27	D	5.14	30
	L	-15	0.05						
	BG		0.01						
10^{45}	L	-25	0.09	796	12	8.23	D	4.38	40
	L	-15	0.05						
	BG		0.01						
11^{00}	L	-25	0.05	648	12	8.25	D	5.59	45

TABLE 4 (CONTINUED).

Time	Side	Probe Height (feet)	Conc. (ppm)	Traffic Volume (veh./hr.)	Heavy Duty Mix	Emission Factor (gm/veh. mile)	Stability	Wind Speed (m/sec.)	Wind Dir. (Degrees) @ Road ϕ
11^{00}	L	-15	0.02						
	BG		0.01						
11^{15}	W	-25	0.03	836	12	8.26	D	7.15	50
	W	-15	0.03						
	W	5	0.02						
	W	10	0.02						
	W	15	0.02						
	W	20	0.01						
	L	-25	0.08						
	L	-15	0.03						
	BG		0.01						
11^{30}	W	-25	0.05	740	12	8.29	D	5.81	45
	W	-15	0.05						
	W	5	0.03						
	W	10	0.03						
	W	15	0.02						
	W	20	0.02						
	L	-25	0.12						
	L	-15	0.06						
	BG		0.01						
11^{45}	W	-25	0.03	884	12	8.43	D	5.36	70
	W	-15	0.03						
	W	5	0.03						
	W	10	0.02						

TABLE 4 (CONTINUED).

Time	Side	Probe Height (feet)	Conc. (ppm)	Traffic Volume (veh./hr.)	Heavy Duty Mix	Emission Factor (gm/veh. mile)	Stability	Wind Speed (m/sec.)	Wind Dir. (Degrees) @ Road ϕ
11^{45}	W	15	0.02						
	W	20	0.02						
	L	-25	0.09						
	L	-15	0.03						
	BG		0.01						
12^{00}	W	-25	0.04	776		8.53	C	4.69	40
	W	-15	0.03						
	W	5	0.03						
	W	10	0.01						
	W	15	0.01						
	W	20	0.01						
	L	-25	0.09						
	L	-15	0.04						
	BG		0.01						
12^{15}	W	-25	0.07	756		8.67	C	4.47	60
	W	-15	0.05						
	W	5	0.05						
	W	10	0.02						
	W	15	0.02						
	W	20	0.02						
	L	-25	0.12						
	L	-15	0.05						
	BG		0.01						
12^{30}	W	-25	0.05	612		8.80	C	4.12	55

TABLE 4 (CONTINUED).

Time	Side	Probe Height (feet)	Conc. (ppm)	Traffic Volume (veh./hr.)	Heavy Duty Mix	Emission Factor (gm/veh. mile)	Stability	Wind Speed (m/sec.)	Wind Dir. (Degrees) @ Road ϕ
12^{30}	W	-15	0.04						
	W	5	0.03						
	W	10	0.02						
	W	15	0.02						
	W	20	0.01						
	L	-25	0.07						
	L	-15	0.04						
	BG		0.01						
12^{45}	W	-25	0.07	784	13	8.7	C	4.25	45
	W	-15	0.06						
	W	5	0.04						
	W	10	0.03						
	W	15	0.03						
	L	-25	0.14						
	L	-15	0.06						
	BG		0.01						
13^{00}	L	-25	0.12	768	12	8.56	C	4.47	70
	L	-15	0.05						
	BG		0.01						
13^{15}	L	-25	0.09	764	12	8.4	C	4.92	65
	L	-15	0.04						
	BG		0.01						
13^{30}	L	-25	0.09	648	11	8.25	C	5.36	45

TABLE 4 (CONTINUED).

Time	Side	Probe Height (feet)	Conc. (ppm)	Traffic Volume (veh./hr.)	Heavy Duty Mix	Emission Factor (gm/veh. mile)	Stability	Wind Speed (m/sec.)	Wind Dir. (Degrees) @ Road ϕ
13^{30}	L	-15	0.05						
	BG		0.01						
13^{45}	W	-25	0.04	760	10	8.16	C	5.36	55
	W	-15	0.04						
	W	5	0.03						
	W	10	0.03						
	W	15	0.02						
	W	20	0.02						
	L	-25	0.11						
	L	-15	0.05						
	BG		0.01						
14^{00}	W	-25	0.06	716	10	8.05	C	4.92	50
	W	-15	0.05						
	W	5	0.03						
	W	10	0.03						
	W	15	0.03						
	W	20	0.02						
	L	-25	0.09						
	L	-15	0.05						
	BG		0.01						
14^{15}	L	-25	0.13						
	L	-15	0.06	1024	9	7.96	C	4.02	60
	BG		0.01						
14^{30}	W	-25	0.05	880	9	7.85	C	5.36	50

TABLE 4 (CONTINUED).

Time	Side	Probe Height (feet)	Conc. (ppm)	Traffic Volume (veh./hr.)	Heavy Duty Mix	Emission Factor (gm/veh. mile)	Stability	Wind Speed (m/sec.)	Wind Dir. (Degrees) @ Road ϕ
14^{30}	W	-15	0.04						
	W	5	0.03						
	W	10	0.03						
	W	15	0.02						
	W	20	0.01						
	L	-25	0.11						
	L	-15	0.05						
	BG		0.01						
14^{45}	L	-25	0.12	1144	8	7.74	C	4.92	70
	L	-15	0.06						
	BG		0.02						
15^{00}	W	-25	0.06	1004	8	7.66	C	4.69	70
	W	-15	0.05						
	W	5	0.04						
	W	10	0.04						
	W	15	0.03						
	W	20	0.02						
	L	-25	0.12						
	L	-15	0.06						
	BG		0.02						
15^{15}	W	-25	0.06	1456	7	7.55	C	4.92	60
	W	-15	0.05						
	W	5	0.03						
	W	10	0.04						

TABLE 4 (CONTINUED).

Time	Side	Probe Height (feet)	Conc. (ppm)	Traffic Volume (veh./hr.)	Heavy Duty Mix	Emission Factor (gm/veh. mile)	Stability	Wind Speed (m/sec.)	Wind Dir. (Degrees) @ Road ϕ
15^{15}	W	15	0.03						
	W	20	0.02						
	L	-25	0.15						
	L	-15	0.07						
	BG		0.01						
15^{30}	L	-25	0.15	1240	6	7.46	C	4.47	60
	L	-15	0.07						
	BG		0.01						
15^{45}	W	-25	0.04	1296	6	7.43	D	5.36	50
	W	-15	0.04						
	W	5	0.02						
	W	10	0.02						
	W	15	0.02						
	W	20	0.02						
	BG		0.01						
16^{00}	W	-25	0.06	1284	6	7.41	D	5.36	50
	W	-15	0.04						
	W	5	0.02						
	W	10	0.02						
	W	15	0.02						
	W	20	0.01						
	L	-25	0.10						
	L	-15	0.04						
	BG		0.02						

TABLE 4 (CONTINUED).

Time	Side	Probe Height (feet)	Conc. (ppm)	Traffic Volume (veh./hr.)	Heavy Duty Mix	Emission Factor (gm/veh. mile)	Stability	Wind Speed (m/sec.)	Wind Dir. (Degrees) @ Road ϕ
16^{15}	W	-25	0.08	1612	6	7.38	D	4.47	40
	W	-15	0.05						
	W	5	0.03						
	W	10	0.02						
	W	15	0.02						
	W	20	0.01						
	L	-25	0.12						
	L	-15	0.05						
	BG		0.01						
16^{30}	W	-25	0.05	1436	6	7.36	D	5.36	35
	W	-15	0.04						
	W	5	0.03						
	W	10	0.02						
	W	15	0.02						
	W	20	0.01						
	L	-25	0.10						
	L	-15	0.05						
	BG		0.01						
16^{45}	W	-25	0.08	1564	6	7.34	D	4.47	45
	W	-15	0.07						
	W	5	0.04						
	W	10	0.03						
	W	15	0.02						
	W	20	0.02						

TABLE 4 (CONTINUED).

Time	Side	Probe Height (feet)	Conc. (ppm)	Traffic Volume (veh./hr.)	Heavy Duty Mix	Emission Factor (gm/veh. mile)	Stability	Wind Speed (m/sec.)	Wind Dir. (Degrees) @ Road ϕ
16^{45}	L	-25	0.13						
	L	-15	0.05						
	BG		0.01						
17^{00}	L	-25	0.15	1356	5	7.29	D	4.25	30
	L	-15	0.06						
	BG		0.01						
17^{15}	W	-25	0.13	1652	5	7.23	D	3.58	20
	W	-15	0.10						
	W	5	0.04						
	W	10	0.04						
	W	15	0.03						
	W	20	0.02						
	L	-25	0.13						
	L	-15	0.05						
	BG		0.01						
17^{30}	W	-25	0.16	1196	5	7.19	D	4.02	15
	W	-15	0.11						
	W	5	0.04						
	W	10	0.04						
	W	15	0.03						
	W	20	0.02						
	L	-25	0.14						
	L	-15	0.06						
	BG		0.01						

TABLE 4 (CONTINUED).

Time	Side	Probe Height (feet)	Conc. (ppm)	Traffic Volume (veh./hr.)	Heavy Duty Mix	Emission Factor (gm/veh. mile)	Stability	Wind Speed (m/sec.)	Wind Dir. (Degrees) @ Road ϕ
17^{45}	W	-25	0.14	1264	5	7.12	D	3.13	10
	W	-15	0.1						
	W	5	0.04						
	W	10	0.04						
	W	15	0.03						
	W	20	0.02						
	L	-25	0.18						
	L	-15	0.07						
	BG		0.01						
18^{00}	W	-25	0.17	776	5	7.07	E	2.59	10
	W	-15	0.11						
	W	5	0.06						
	W	10	0.05						
	W	15	0.04						
	W	20	0.04						
	L	-25	0.13						
	L	-15	0.06						
	BG		0.01						
18^{15}	W	-25	0.19	912	5	7.0	E	2.01	0
	W	-15	0.17						
	W	5	0.08						
	W	10	0.07						
	W	15	0.06						
	W	20	0.05						

TABLE 4 (CONTINUED).

Time	Side	Probe Height (feet)	Conc. (ppm)	Traffic Volume (veh./hr.)	Heavy Duty Mix	Emission Factor (gm/veh. mile)	Stability	Wind Speed (m/sec.)	Wind Dir. (Degrees) @ Road ϕ
18^{15}	L	-25	0.17						
	L	-15	0.07						
	BG		0.01						
18^{30}	W	-25	0.19	660	12	8.21	E	2.91	10
	W	-15	0.13						
	W	5	0.05						
	W	10	0.05						
	W	15	0.04						
	W	20	0.03						
	L	-25	0.18						
	L	-15	0.07						
	BG		0.01						
18^{45}	L	-25	0.18	720	11	8.04	E	2.46	20
	L	-15	0.07						
	BG		0.01						
19^{00}	L	-25	0.13	632	12	8.32	E	3.13	30
	L	-15	0.04						
	BG		0.01						
19^{15}	W	-25	0.12	548	14	8.7	E	2.91	30
	W	-15	0.09						
	W	5	0.03						
	W	10	0.02						
	W	15	0.02						
	W	20	0.01						

TABLE 4 (CONTINUED).

Time	Side	Probe Height (feet)	Conc. (ppm)	Traffic Volume (veh./hr.)	Heavy Duty Mix	Emission Factor (gm/veh. mile)	Stability	Wind Speed (m/sec.)	Wind Dir. (Degrees) @ Road ϕ
19^{15}	L	-25	0.12						
	L	-15	0.04						
	BG		0.01						
19^{30}	W	-25	0.15	508	16	8.92	E	2.46	25
	W	-15	0.11						
	W	5	0.04						
	W	10	0.04						
	W	15	0.03						
	W	20	0.02						
	L	-25	0.20						
	L	-15	0.06						
	BG		0.01						
19^{45}	W	-25	0.13	576	14	8.64	E	2.46	10
	W	-15	0.02						
	W	5	0.02						
	W	10	0.02						
	W	15	0.02						
	W	20	0.01						
	L	-25	0.10						
	L	-15	0.04						
	BG		0.01						
20^{00}	W	-25	0.11	424	19	9.49	E	2.68	10
	W	-15	0.08						
	W	5	0.03						

TABLE 4 (CONTINUED).

Time	Side	Probe Height (feet)	Conc. (ppm)	Traffic Volume (veh./hr.)	Heavy Duty Mix	Emission Factor (gm/veh. mile)	Stability	Wind Speed (m/sec.)	Wind Dir. (Degrees) @ Road ϕ
20^{00}	W	10	0.03						
	W	15	0.02						
	W	20	0.02						
	L	-25	0.17						
	L	-15	0.06						
	BG		0.01						
20^{15}	W	-25	0.11	532	15	8.83	E	3.13	20
	W	-15	0.08						
	W	5	0.03						
	W	10	0.02						
	W	15	0.02						
	W	20	0.01						
	L	-25	0.13						
	L	-15	0.04						
	BG		0.01						
20^{30}	W	-25	0.06	368	22	9.98	E	3.8	10
	W	-15	0.04						
	W	5	0.03						
	W	10	0.02						
	W	15	0.01						
	W	20	0.01						
	L	-25	0.07						
	L	-15	0.03						
	BG		0.01						

TABLE 4 (CONTINUED).

Time	Side	Probe Height (feet)	Conc. (ppm)	Traffic Volume (veh./hr.)	Heavy Duty Mix	Emission Factor (gm/veh. mile)	Stability	Wind Speed (m/sec.)	Wind Dir. (Degrees) @ Road ϕ
20^{45}	W	-25	0.11	560	14	8.71	E	3.58	15
	W	-15	0.09						
	W	5	0.04						
	W	10	0.04						
	W	15	0.02						
	W	20	0.01						
	L	-25	0.10						
	L	-15	0.04						
	BG		0.01						
21^{00}	W	-25	0.10	456	17	9.27	E	3.86	20
	W	-15	0.04						
	W	5	0.03						
	W	10	0.03						
	W	15	0.03						
	W	20	0.02						
	L	-25	0.10						
	L	-15	0.04						
	BG		0.01						
21^{15}	W	-25	0.10	576	14	8.64	E	3.35	15
	W	-15	0.08						
	W	5	0.03						
	W	10	0.03						
	W	15	0.02						

TABLE 4 (CONTINUED).

Time	Side	Probe Height (feet)	Conc. (ppm)	Traffic Volume (veh./hr.)	Heavy Duty Mix	Emission Factor (gm/veh. mile)	Stability	Wind Speed (m/sec.)	Wind Dir. (Degrees) @ Road ϕ
21^{15}	W	20	0.02						
	L	-25	0.13						
	L	-15	0.05						
	BG		0.01						

TABLE 5. SEPTEMBER 27 TOTAL NITROGEN OXIDE DATA.

Time	Side	Probe Height (feet)	Conc. (ppm)	Traffic Volume (veh./hr.)	Heavy Duty Mix	Emission Factor (gm/veh. mile)	Stability	Wind Speed (m/sec.)	Wind Dir. (Degrees) @ Road ϕ
7^{45}	W	-25	0.39	680	14	8.52	E	1.12	15
	W	-15	0.36						
	W	5	0.24						
	W	10	0.23						
	W	15	0.21						
	W	20	0.21						
	L	-25	0.37						
	L	-15	0.28						
	BG		0.22						
8^{00}	W	-25	0.20	644	14	8.52	E	2.68	25
	W	-15	0.16						
	W	5	0.11						
	W	10	0.11						
	W	15	0.11						
	W	20	0.10						
	L	-25	0.21						
	L	-15	0.13						
	BG		0.08						
8^{15}	W	-25	0.21	840	14	8.54	E	2.24	40
	W	-15	0.21						
	W	5	0.13						
	W	10	0.13						
	W	15	0.13						
	W	20	0.11						

TABLE 5 (CONTINUED).

Time	Side	Probe Height (feet)	Conc. (ppm)	Traffic Volume (veh./hr.)	Heavy Duty Mix	Emission Factor (gm/veh. mile)	Stability	Wind Speed (m/sec.)	Wind Dir. (Degrees) @ Road ϕ
8^{15}	L	-25	0.23						
	L	-15	0.15						
	BG		0.06						
8^{30}	W	-25	0.21	596	14	8.56	E	2.01	30
	W	-15	0.15						
	W	5	0.07						
	W	10	0.04						
	W	15	0.03						
	W	20	0.02						
	L	-25	0.19						
	L	-15	0.10						
	BG		0.01						
8^{45}	W	-25	0.10	664	14	8.56	E	2.24	25
	W	-15	0.13						
	W	5	0.06						
	W	10	0.04						
	W	15	0.04						
	W	20	0.02						
	L	-25	0.17						
	L	-15	0.08						
	BG		0.01						
9^{00}	W	-25	0.14	536	14	8.57	E	2.46	25
	W	-15	0.09						
	W	5	0.05						

TABLE 5 (CONTINUED).

Time	Side	Probe Height (feet)	Conc. (ppm)	Traffic Volume (veh./hr.)	Heavy Duty Mix	Emission Factor (gm/veh. mile)	Stability	Wind Speed (m/sec.)	Wind Dir. (Degrees) @ Road ϕ
9^{00}	W	10	0.05						
	W	15	0.05						
	W	20	0.04						
	L	-25	0.13						
	L	-15	0.08						
	BG		0.01						
9^{15}	W	-25	0.09	652	14	8.6	D	3.13	40
	W	-15	0.06						
	W	5	0.05						
	W	10	0.04						
	W	15	0.04						
	W	20	0.03						
	L	-25	0.16						
	L	-15	0.08						
	BG		0.01						
9^{30}	W	-25	0.06	484	14	8.62	D	3.71	55
	W	-15	0.05						
	W	5	0.04						
	W	10	0.03						
	W	15	0.03						
	W	20	0.03						
	L	-25	0.11						
	L	-15	0.06						

TABLE 5 (CONTINUED).

Time	Side	Probe Height (feet)	Conc. (ppm)	Traffic Volume (veh./hr.)	Heavy Duty Mix	Emission Factor (gm/veh. mile)	Stability	Wind Speed (m/sec.)	Wind Dir. (Degrees) @ Road ϕ
9^{45}	W	-25	0.08	536	14	8.65	C	2.4	65
	W	-15	0.07						
	W	5	0.05						
	W	10	0.04						
	W	15	0.03						
	W	20	0.03						
	L	-25	0.09						
	L	-15	0.04						
	BG		0.01						
10^{00}	W	-25	0.08	628	13	8.45	C	2.68	45
	W	-15	0.07						
	W	5	0.03						
	W	10	0.03						
	W	15	0.03						
	W	20	0.01						
	L	-25	0.13						
	L	-15	0.07						
	BG		0.01						
10^{15}	W	-25	0.07	740	13	8.39	C	2.68	40
	W	-15	0.05						
	W	5	0.03						
	W	10	0.03						
	W	15	0.03						
	W	20	0.01						

TABLE 5 (CONTINUED).

Time	Side	Probe Height (feet)	Conc. (ppm)	Traffic Volume (veh./hr.)	Heavy Duty Mix	Emission Factor (gm/veh. mile)	Stability	Wind Speed (m/sec.)	Wind Dir. (Degrees) @ Road ϕ
10^{15}	L	-25	0.12						
	L	-15	0.06						
	BG		0.01						
10^{30}	W	-25	0.03	648	12	8.23	C	3.58	50
	W	-15	0.03						
	W	5	0.01						
	W	10	0.01						
	W	15	0.01						
	W	20	0.01						
	L	-25	0.07						
	L	-15	0.03						
	BG		0.01						
10^{45}	W	-25	0.04	752	12	8.06	C	4.47	45
	W	-15	0.02						
	W	5	0.02						
	W	10	0.02						
	W	15	0.01						
	W	20	0.01						
	L	-25	0.07						
	L	-15	0.03						
	BG		0.01						
11^{00}	W	-25	0.05	620	12	8.25	C	3.8	70
	W	-15	0.05						
	W	5	0.02						

TABLE 5 (CONTINUED).

Time	Side	Probe Height (feet)	Conc. (ppm)	Traffic Volume (veh./hr.)	Heavy Duty Mix	Emission Factor (gm/veh. mile)	Stability	Wind Speed (m/sec.)	Wind Dir. (Degrees) @ Road ϕ
11^{00}	W	10	0.02						
	W	15	0.02						
	W	20	0.02						
	L	-25	0.11						
	L	-15	0.06						
	BG		0.01						
11^{15}	W	-25	0.03	640	12	8.26	D	4.92	60
	W	-15	0.03						
	W	5	0.02						
	W	10	0.02						
	W	15	0.01						
	W	20	0.01						
	L	-25	0.09						
	L	-15	0.04						
	BG		0.01						
11^{30}	W	-25	0.05	672	12	8.29	D	4.47	55
	W	-15	0.04						
	W	5	0.02						
	W	10	0.02						
	W	15	0.01						
	W	20	0.01						
	L	-25	0.08						
	L	-15	0.04						
	BG		0.01						

TABLE 5 (CONTINUED).

Time	Side	Probe Height (feet)	Conc. (ppm)	Traffic Volume (veh./hr.)	Heavy Duty Mix	Emission Factor (gm/veh. mile)	Stability	Wind Speed (m/sec.)	Wind Dir. (Degrees) @ Road ϕ
11^{42}	L	-25	0.06	660	12	8.56	D	5.36	25
	L	-15	0.03						
	BG		0.01						
12^{00}	W	-25	0.06	788	13	8.71	D	5.81	30
	W	-15	0.04						
	W	5	0.02						
	W	10	0.02						
	W	15	0.02						
	W	20	0.01						
	L	-25	0.11						
	L	-15	0.05						
	BG		0.01						
12^{15}	W	-25	0.04	772	8	7.87	D	4.69	30
	W	-15	0.02						
	W	5	0.02						
	W	10	0.01						
	W	15	0.01						
	W	20	0.01						
	L	-25	0.07						
	L	-15	0.03						
	BG		0.01						
12^{30}	W	-25	0.03	640	21	10.0	D	4.92	30
	W	-15	0.03						
	W	5	0.02						

TABLE 5 (CONTINUED).

Time	Side	Probe Height (feet)	Conc. (ppm)	Traffic Volume (veh./hr.)	Heavy Duty Mix	Emission Factor (gm/veh. mile)	Stability	Wind Speed (m/sec.)	Wind Dir. (Degrees) @ Road ϕ
12^{30}	W	10	0.01						
	W	15	0.01						
	W	20	0.01						
	L	-25	0.09						
	L	-15	0.05						
	BG		0.01						
12^{45}	W	-25	0.07	748	12	8.52	D	5.36	45
	W	-15	0.05						
	W	5	0.02						
	W	10	0.02						
	W	15	0.01						
	W	20	0.01						
	L	-25	0.10						
	L	-15	0.05						
	BG		0.01						
13^{00}	W	-25	0.08	704	12	8.56	D	4.47	45
	W	-15	0.05						
	W	5	0.03						
	W	10	0.03						
	W	15	0.03						
	W	20	0.02						
	L	-25	0.12						
	L	-15	0.06						
	BG		0.01						

TABLE 5 (CONTINUED).

Time	Side	Probe Height (feet)	Conc. (ppm)	Traffic Volume (veh./hr.)	Heavy Duty Mix	Emission Factor (gm/veh. mile)	Stability	Wind Speed (m/sec.)	Wind Dir. (Degrees) @ Road ϕ
13^{15}	W	-25	0.07	724	11	8.36	D	3.35	15
	W	-15	0.07						
	W	5	0.03						
	W	10	0.02						
	W	15	0.02						
	W	20	0.02						
	L	-25	0.11						
	L	-15	0.05						
	BG		0.01						
13^{30}	W	-25	0.05	612	12	8.46	C	4.02	65
	W	-15	0.03						
	W	5	0.02						
	W	10	0.02						
	W	15	0.02						
	W	20	0.02						
	L	-25	0.09						
	L	-15	0.05						
	BG		0.01						
13^{45}	W	-25	0.05	832	9	7.98	C	4.69	50
	W	-15	0.04						
	W	5	0.03						
	W	10	0.03						
	W	15	0.02						
	W	20	0.02						

TABLE 5 (CONTINUED).

Time	Side	Probe Height (feet)	Conc. (ppm)	Traffic Volume (veh./hr.)	Heavy Duty Mix	Emission Factor (gm/veh. mile)	Stability	Wind Speed (m/sec.)	Wind Dir. (Degrees) @ Road ϕ
13^{45}	L	-25	0.10						
	L	-15	0.04						
	BG		0.01						
14^{00}	W	-25	0.05	724	10	8.02	C	4.92	50
	W	-15	0.03						
	W	5	0.03						
	W	10	0.03						
	W	15	0.03						
	W	20	0.02						
	L	-25	0.10						
	L	-15	0.05						
	BG		0.01						
14^{15}	W	-25	0.06	996	9	7.96	C	4.92	45
	W	-15	0.06						
	W	5	0.03						
	W	10	0.03						
	W	15	0.03						
	W	20	0.03						
	L	-25	0.14						
	L	-15	0.07						
	BG		0.01						
14^{30}	W	-25	0.06	916	7	7.57	C	5.36	40
	W	-15	0.05						
	W	5	0.03						

TABLE 5 (CONTINUED).

Time	Side	Probe Height (feet)	Conc. (ppm)	Traffic Volume (veh./hr.)	Heavy Duty Mix	Emission Factor (gm/veh. mile)	Stability	Wind Speed (m/sec.)	Wind Dir. (Degrees) @ Road ϕ
14^{30}	W	10	0.03						
	W	15	0.03						
	W	20	0.02						
	L	-25	0.09						
	L	-15	0.05						
	BG		0.01						
14^{45}	W	-25	0.05	1028	7	7.58	C	4.47	50
	W	-15	0.04						
	W	5	0.03						
	W	10	0.03						
	W	15	0.02						
	W	20	0.02						
	L	-25	0.10						
	L	-15	0.05						
	BG		0.01						
15^{00}	W	-25	0.05	940	8	7.66	C	4.47	50
	W	-15	0.05						
	W	5	0.03						
	W	10	0.02						
	W	15	0.02						
	W	20	0.02						
	L	-25	0.10						
	L	-15	0.04						
	BG		0.02						

TABLE 5 (CONTINUED).

Time	Side	Probe Height (feet)	Conc. (ppm)	Traffic Volume (veh./hr.)	Heavy Duty Mix	Emission Factor (gm/veh. mile)	Stability	Wind Speed (m/sec.)	Wind Dir. (Degrees) @ Road ϕ
15^{15}	W	-25	0.05	1360	7	7.55	C	4.92	45
	W	-15	0.05						
	W	5	0.03						
	W	10	0.03						
	W	15	0.02						
	W	20	0.02						
	L	-25	0.11						
	L	-15	0.05						
	BG		0.01						
15^{30}	W	-25	0.07	1224	6	7.41	C	4.25	45
	W	-15	0.05						
	W	5	0.04						
	W	10	0.03						
	W	15	0.02						
	W	20	0.02						
	L	-25	0.11						
	L	-15	0.05						
	BG		0.01						
15^{45}	W	-25	0.07	1316	8	7.72	C	4.92	45
	W	-15	0.05						
	W	5	0.04						
	W	10	0.03						
	W	15	0.03						
	W	20	0.02						

TABLE 5 (CONTINUED).

Time	Side	Probe Height (feet)	Conc. (ppm)	Traffic Volume (veh./hr.)	Heavy Duty Mix	Emission Factor (gm/veh. mile)	Stability	Wind Speed (m/sec.)	Wind Dir. (Degrees) @ Road ϕ
15^{45}	L	-25	0.09						
	L	-15	0.05						
	BG		0.01						
16^{00}	W	-25	0.06	1064	6	7.40	C	4.92	60
	W	-15	0.06						
	W	5	0.04						
	W	10	0.03						
	W	15	0.02						
	W	20	0.02						
	L	-25	0.12						
	L	-15	0.05						
	BG		0.02						
16^{15}	W	-25	0.05	1308	6	7.38	C	4.47	40
	W	-15	0.05						
	W	5	0.04						
	W	10	0.03						
	W	15	0.02						
	W	20	0.02						
	L	-25	0.12						
	L	-15	0.06						
	BG		0.01						
16^{30}	W	-25	0.06	1256	4	7.09	C	4.47	55
	W	-15	0.05						
	W	5	0.03						

TABLE 5 (CONTINUED).

Time	Side	Probe Height (feet)	Conc. (ppm)	Traffic Volume (veh./hr.)	Heavy Duty Mix	Emission Factor (gm/veh. mile)	Stability	Wind Speed (m/sec.)	Wind Dir. (Degrees) @ Road ϕ
16^{30}	W	10	0.03						
	W	15	0.02						
	W	20	0.02						
	L	-25	0.14						
	L	-15	0.07						
	BG		0.01						
16^{45}	W	-25	0.09	1552	6	7.44	C	4.38	40
	W	-15	0.06						
	W	5	0.03						
	W	10	0.03						
	W	15	0.02						
	W	20	0.02						
	L	-25	0.13						
	L	-15	0.07						
	BG		0.01						
17^{00}	W	-25	0.09	1452	5	7.29	D	4.92	45
	W	-15	0.06						
	W	5	0.03						
	W	10	0.03						
	W	15	0.02						
	W	20	0.02						
	L	-25	0.11						
	L	-15	0.05						
	BG		0.01						

TABLE 5 (CONTINUED).

Time	Side	Probe Height (feet)	Conc. (ppm)	Traffic Volume (veh./hr.)	Heavy Duty Mix	Emission Factor (gm/veh. mile)	Stability	Wind Speed (m/sec.)	Wind Dir. (Degrees) @ Road ϕ
17^{15}	W	-25	0.09	1592	5	7.23	D	5.36	35
	W	-15	0.06						
	W	5	0.03						
	W	10	0.03						
	W	15	0.03						
	W	20	0.02						
	L	-25	0.14						
	L	-15	0.08						
	BG		0.01						
17^{30}	W	-25	0.11	1368	5	7.23	D	4.47	40
	W	-15	0.09						
	W	5	0.04						
	W	10	0.04						
	W	15	0.03						
	W	20	0.03						
	L	-25	0.16						
	L	-15	0.08						
	BG		0.01						
17^{45}	W	-25	0.07	1292	5	7.23	D	4.47	40
	W	-15	0.05						
	W	5	0.03						
	W	10	0.03						
	W	15	0.02						
	W	20	0.02						

TABLE 5 (CONTINUED).

Time	Side	Probe Height (feet)	Conc. (ppm)	Traffic Volume (veh./hr.)	Heavy Duty Mix	Emission Factor (gm/veh. mile)	Stability	Wind Speed (m/sec.)	Wind Dir. (Degrees) @ Road ϕ
17^{45}	L	-25	0.11						
	L	-15	0.05						
	BG		0.01						
18^{00}	W	-25	0.06	876	5	7.07	D	4.47	45
	W	-15	0.04						
	W	5	0.02						
	W	10	0.02						
	W	15	0.02						
	W	20	0.01						
	L	-25	0.10						
	L	-15	0.05						
	BG		0.01						
18^{15}	W	-25	0.08	1036	5	7.00	D	4.47	45
	W	-15	0.07						
	W	5	0.03						
	W	10	0.03						
	W	15	0.03						
	W	20	0.02						
	L	-25	0.12						
	L	-15	0.06						
	BG		0.01						
18^{30}	W	-25	0.10	668	5	6.99	D	3.35	45
	W	-15	0.08						
	W	6	0.04						

TABLE 5 (CONTINUED).

Time	Side	Probe Height (feet)	Conc. (ppm)	Traffic Volume (veh./hr.)	Heavy Duty Mix	Emission Factor (gm/veh. mile)	Stability	Wind Speed (m/sec.)	Wind Dir. (Degrees) @ Road ϕ
18^{30}	W	10	0.04						
	W	15	0.03						
	W	20	0.02						
	L	-25	0.12						
	L	-15	0.06						
	BG		0.01						
18^{45}	W	-25	0.11	732	5	6.99	D	2.9	45
	W	-15	0.09						
	W	5	0.03						
	W	10	0.03						
	W	15	0.03						
	W	20	0.03						
	L	-25	0.13						
	L	-15	0.06						
	BG		0.01						

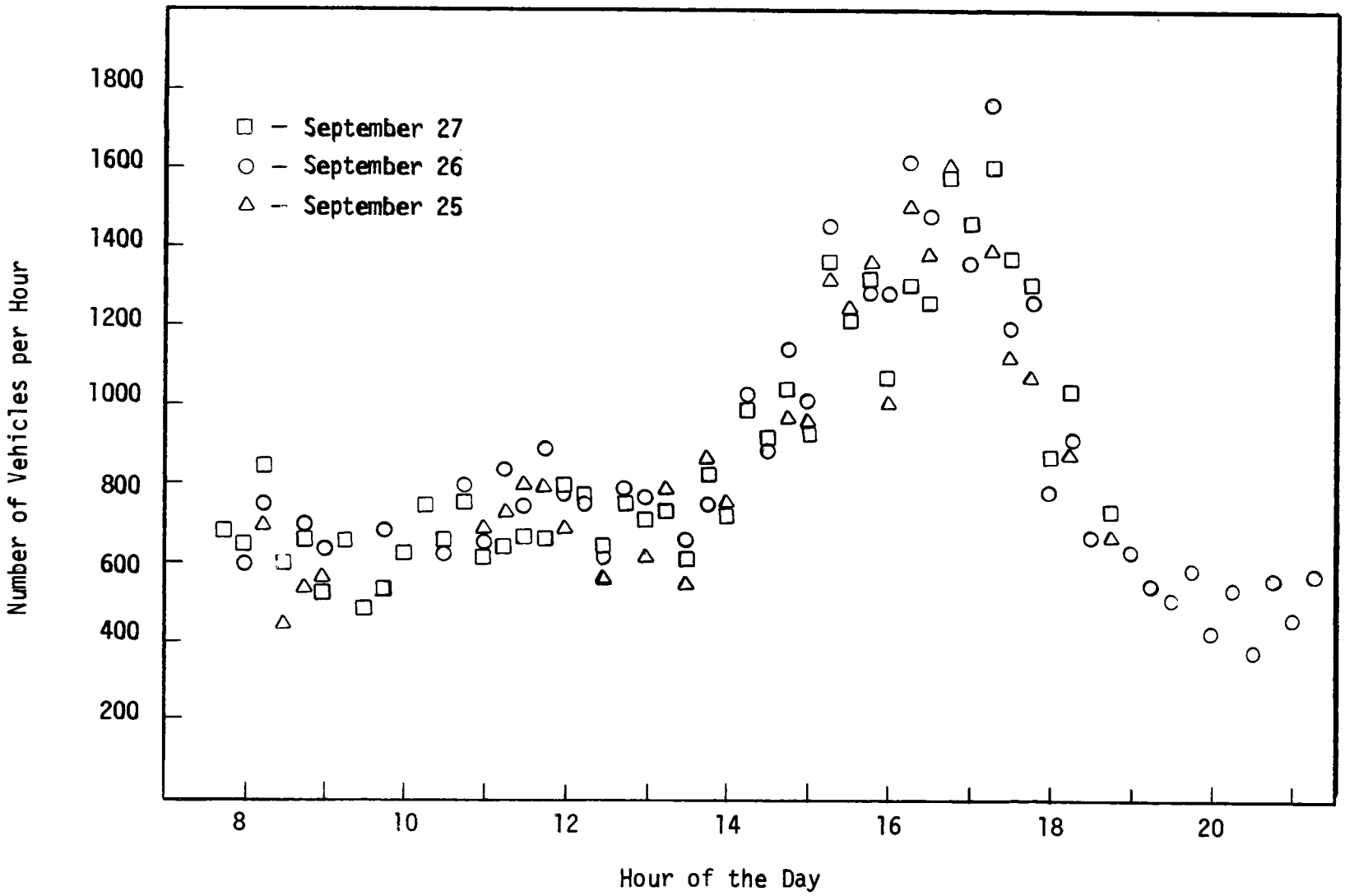

FIGURE 6. DIURNAL TRAFFIC DENSITY

Figure 7 illustrates the diurnal fluctuation of total heavy duty percent. Since heavy duty truck counts were relatively constant, the percent of heavy duty mix was dependent on total vehicle counts. For this reason, the percent heavy duty mix was relatively constant until noon, and afternoon due to increased total vehicle counts, the percent heavy duty mix decreased. The daily average heavy duty mix was about 10 percent.

Traffic Speed. Traffic speeds were constant throughout the monitoring day. Figure 8 illustrates a diurnal plot of the total traffic speed data. The traffic speeds ranged from 53 to 64 miles an hour. The average speed was approximately 60 miles per hour. The reason for the steady traffic speed was due to a lack of traffic congestion.

Meteorological Data Analysis

Stability Analysis. Atmospheric stability classes were determined by using Pasquill's stability classes as discussed in Section IV. Stability class determinations during the I-40 East monitoring are presented below.

During the morning of each day, a stability class E was observed due to low wind speeds and slight solar radiation. The duration of E stability usually lasted from 8:00 a.m. until 9:00 a.m., except for September 26 when a D stability was observed due to wind speeds ranging from three to six meters per second.

During the late morning, the solar insolation was always slight, and stability class varied from either C or D depending upon the wind speed. Stability C was also observed the afternoons of September 26 and 27 due to moderate wind speeds and solar radiation. Stability D, considered

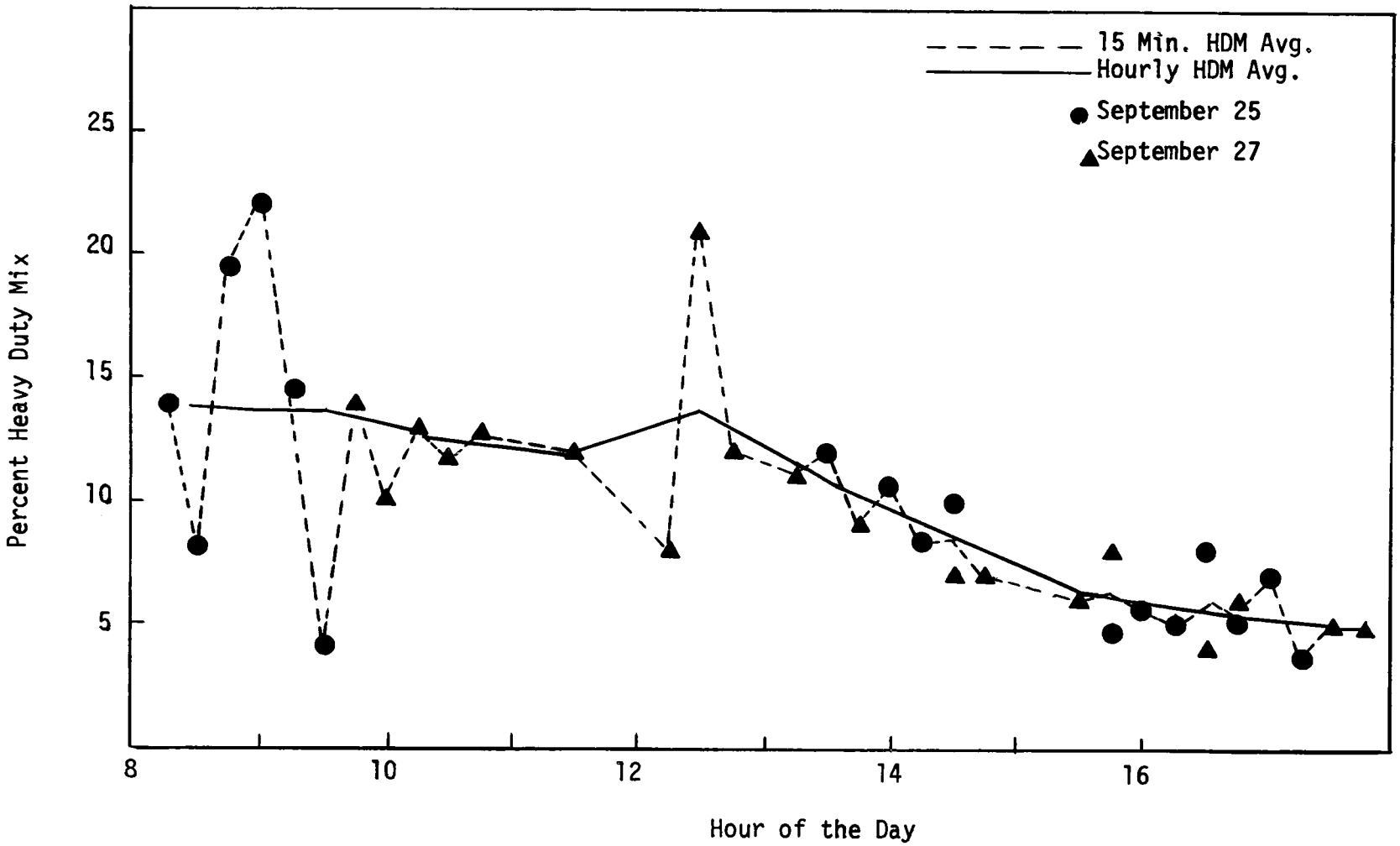

FIGURE 7. DIURNAL HEAVY DUTY MIX

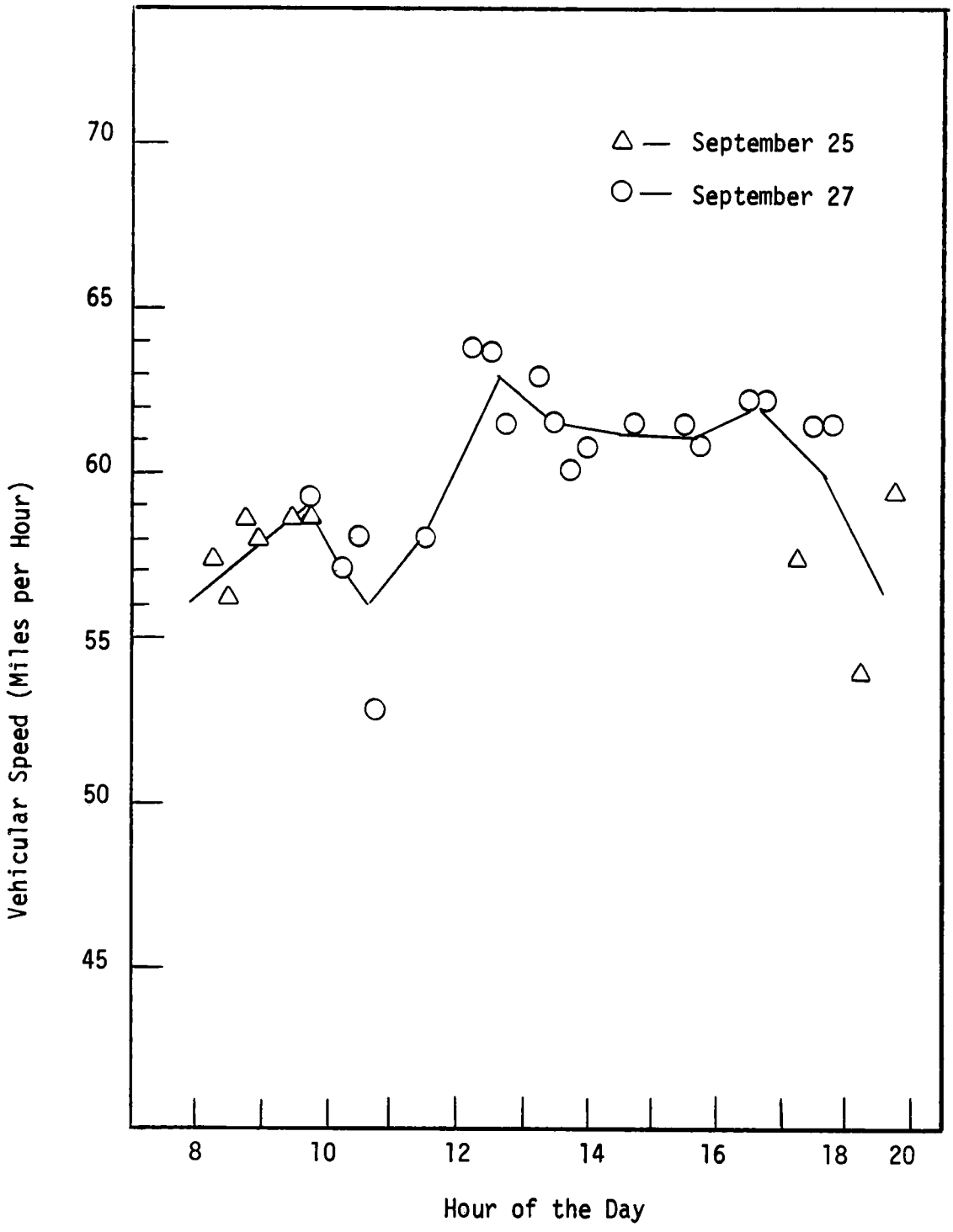

FIGURE 8. DIURNAL TRAFFIC SPEEDS

neutral, and Stability C, considered slightly unstable, occurred most of the time during monitoring.

Stability B was observed during 12:15 to 5:30 p.m. on September 25. This was due to a strong solar intensity and low wind speed during that afternoon. Stability B described a moderately unstable air mass, resulting in a fairly high degree of vertical mixing.

Table 6 summarizes the stability classes observed during each day and 15 minute period of monitoring.

The Wind Frequency Analysis. Wind speeds were moderate during the monitoring at I-40 East. The wind speed ranged consistently between 6 to 10 miles per hour each day. Wind directions were predominately from the Southeast. The frequency of each wind direction is illustrated in the wind rose of Figure 9. Figure 9 also gives the cumulative frequency for a five wind speed in each wind direction. Since the wind frequency was predominately from the South to the Southeast and the road angle was due East, only 25 percent of the monitoring was performed during parallel wind directions.

Analysis of Measured Total Nitrogen Oxide Concentrations

Diurnal Variations of Measured Concentration with Traffic Density and Inverse Wind Speeds. Since the fluctuation of measured total nitrogen oxide concentrations varies directly with the traffic density and inverse wind speed, Figure 10 was plotted to determine how these variables affected the measured concentration during days of investigation. This plot gives a diurnal plot of the average concentration, traffic volume, and inverse wind speed for each 15 minutes of monitoring.

TABLE 6. TOTAL STABILITY CLASSES DURING THE INVESTIGATION.

Date	Time	Stability Class
8/25/73	8:15 a.m. - 9:00 a.m.	E
	11:00 a.m. - 11:30 a.m.	D
	11:45 a.m. - 12:00 noon	C
	12:15 p.m. - 3:30 p.m.	D
	3:45 p.m. - 5:45 p.m.	C
8/26/73	8:00 a.m.	E
	8:15 a.m. - 11:45 a.m.	D
	12:00 noon - 3:30 p.m.	C
	3:45 p.m. - 5:45 p.m.	D
	6:00 p.m. - 9:15 p.m.	E
8/27/73	8:00 a.m. - 9:00 a.m.	E
	9:15 a.m. - 9:30 a.m.	D
	9:45 a.m. - 11:00 a.m.	C
	11:45 a.m. - 1:15 p.m.	D
	1:30 p.m. - 4:45 p.m.	C
	5:00 p.m. - 6:45 p.m.	D

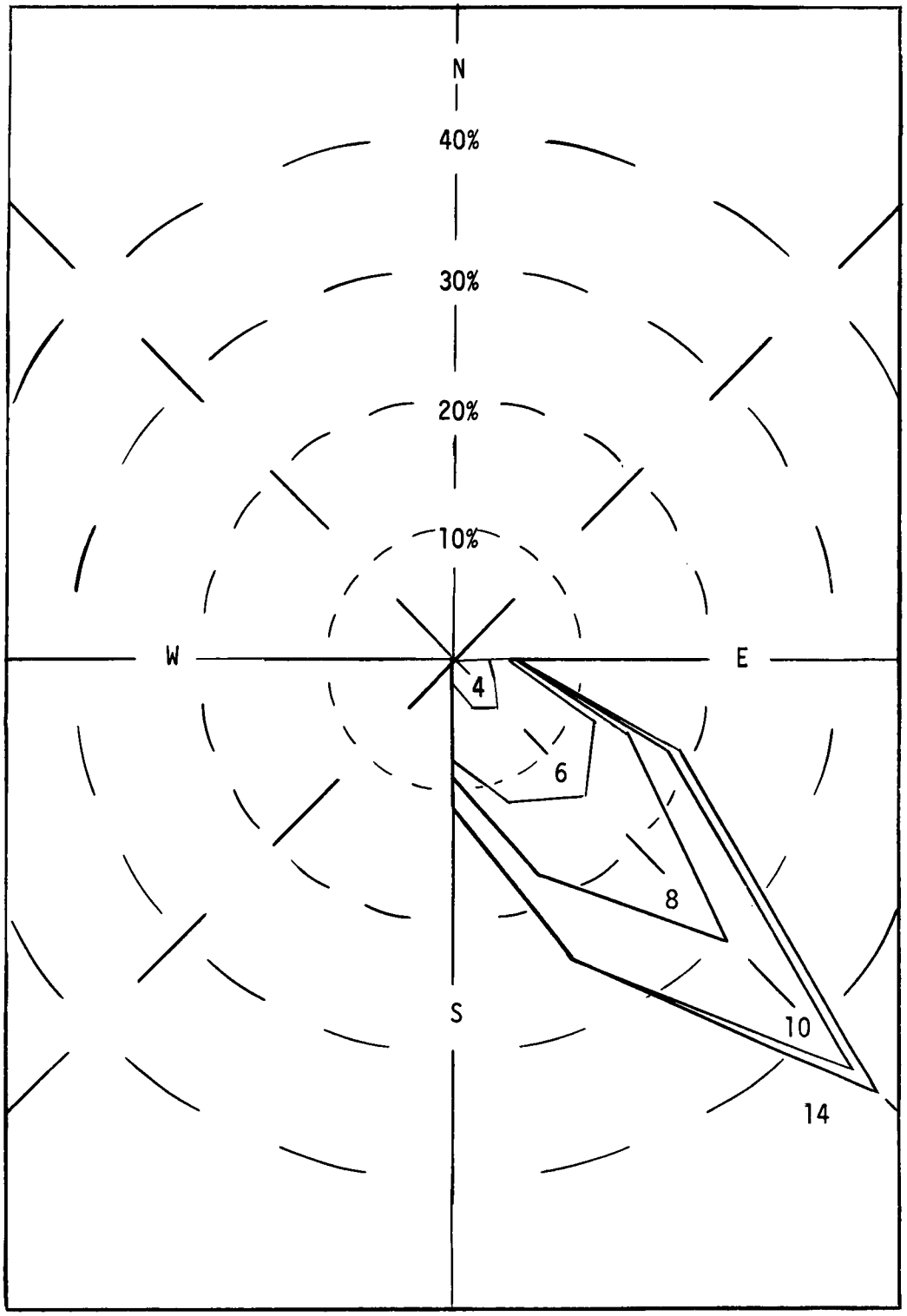

FIGURE 9. TOTAL WIND ROSE DURING INVESTIGATION

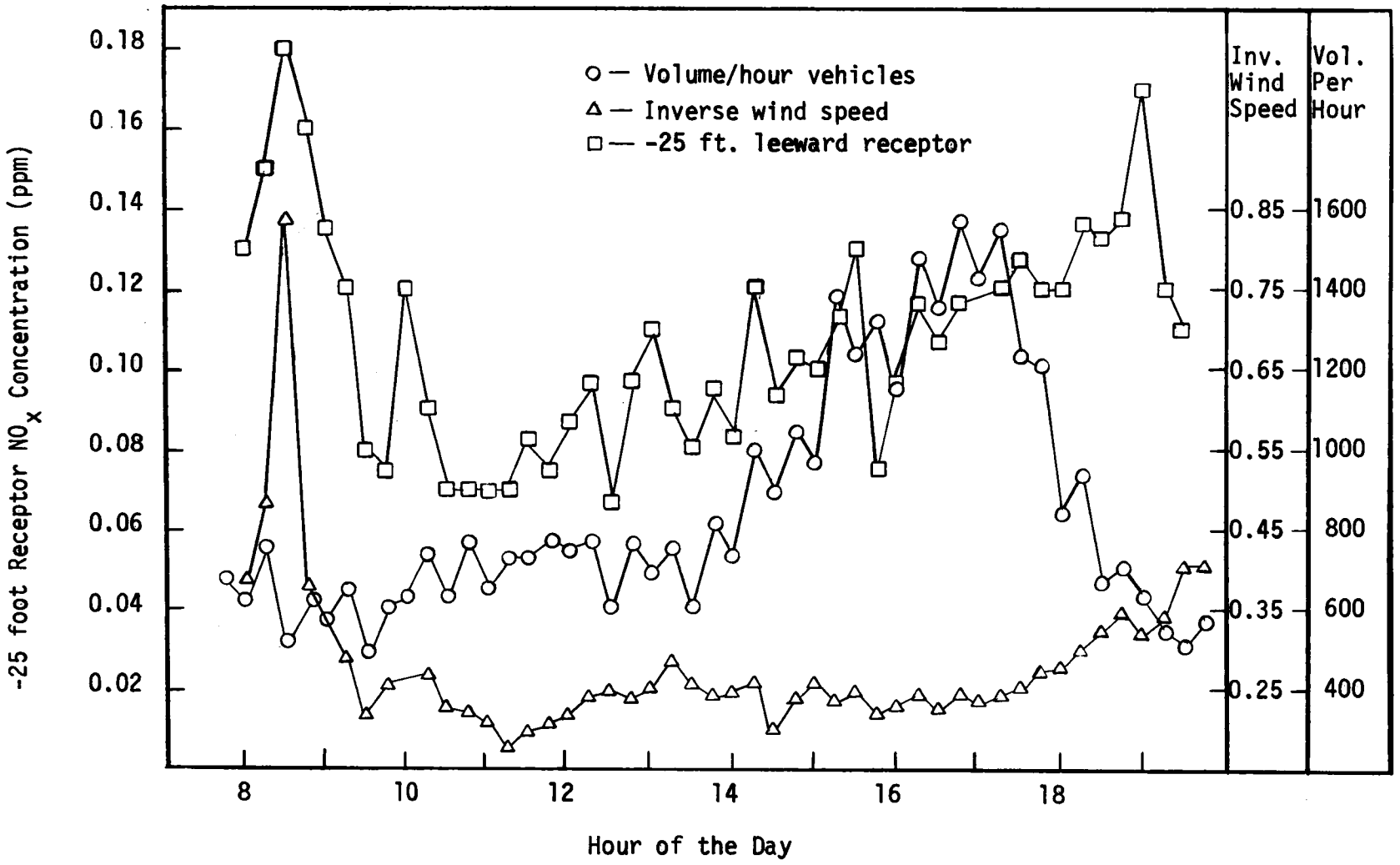

FIGURE 10. INVERSE WIND SPEED, TRAFFIC VOLUME, AND RECEPTOR CONCENTRATION RELATIONSHIPS

During the early morning and evening, the measured total nitrogen oxide concentrations fluctuations are attributed mainly to low wind speeds. In both cases, the traffic volumes are relatively low. However, because of the low wind speeds, the measured total nitrogen oxides have reached peak levels during these time periods.

From 10:00 a.m. until 3:00 p.m., the fluctuations in the total nitrogen oxide levels seem to be attributed to both the traffic volume and wind speeds. After 3:00 p.m. until 5:30 p.m., the measured total nitrogen oxide trace is dominated by the high traffic volumes. During this time, the wind speeds remained relatively constant, but the total nitrogen oxide levels increased due to the traffic volume.

Vertical Profiles. Figure 11 gives a diurnal plot of total nitrogen oxide concentration profiles for the leeward side -25 foot and -15 foot receptors. The -15 foot receptor trace seems to follow the -25 foot trace as would be expected. It should be noted that the ratio of the two concentration levels seem to be relatively constant throughout the day.

Figure 12 gives the same diurnal plot for the windward side -25 and -15 foot receptors. Although like the leeward, both -25 and -15 foot receptor concentrations vary in the same manner, the relative difference in concentrations for the windward profile -25 and -15 receptors is quite less. This can be attributed to the air pollutants reaching the windward side being more evenly mixed in the vertical as compared to the leeward side.

Figure 13 and Figure 14 illustrates the arithmetic mean for all measured concentrations at each receptor separated according to crosswind

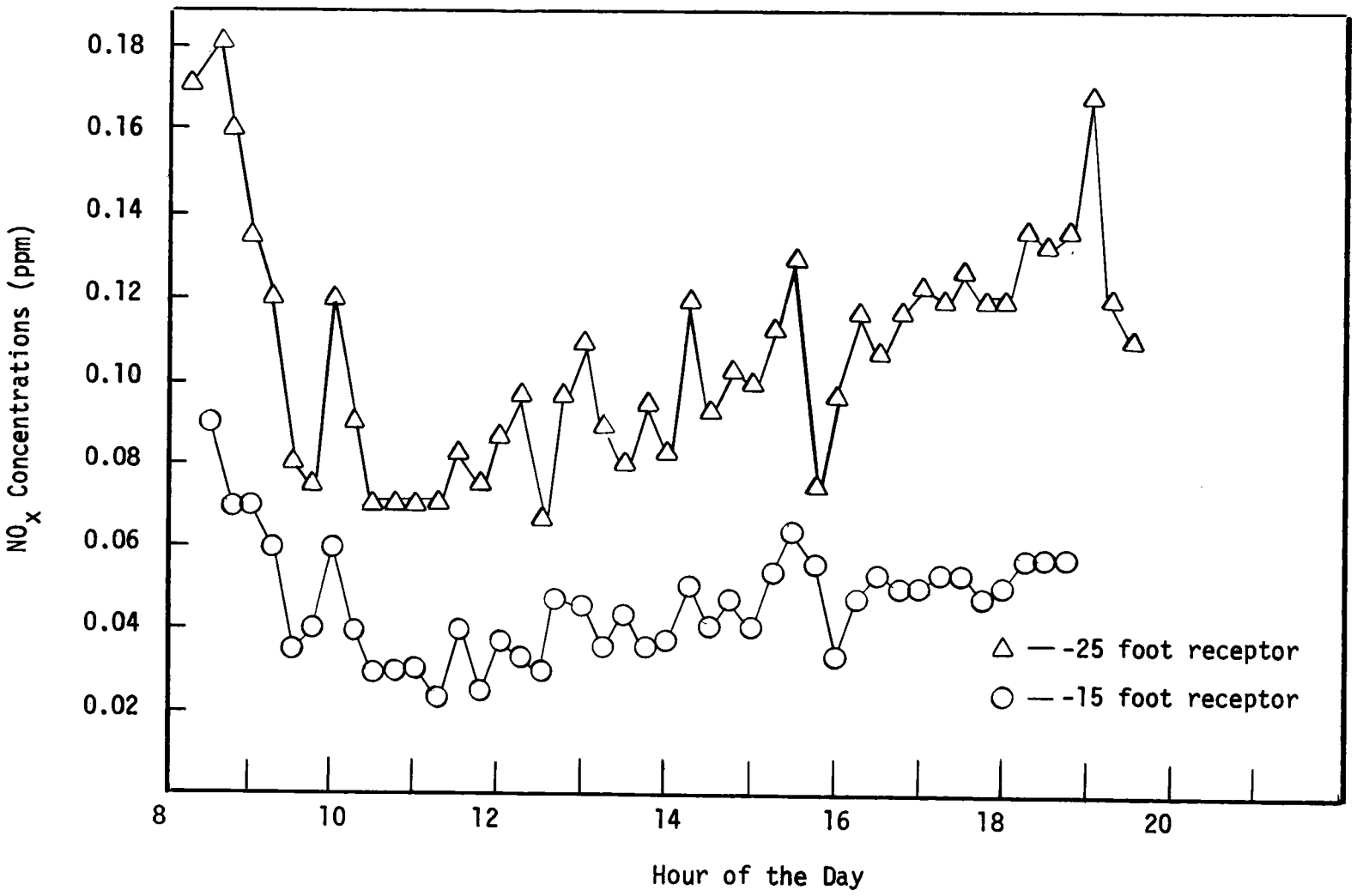

FIGURE 11. DIURNAL LEEWARD RECEPTOR CONCENTRATION PROFILES

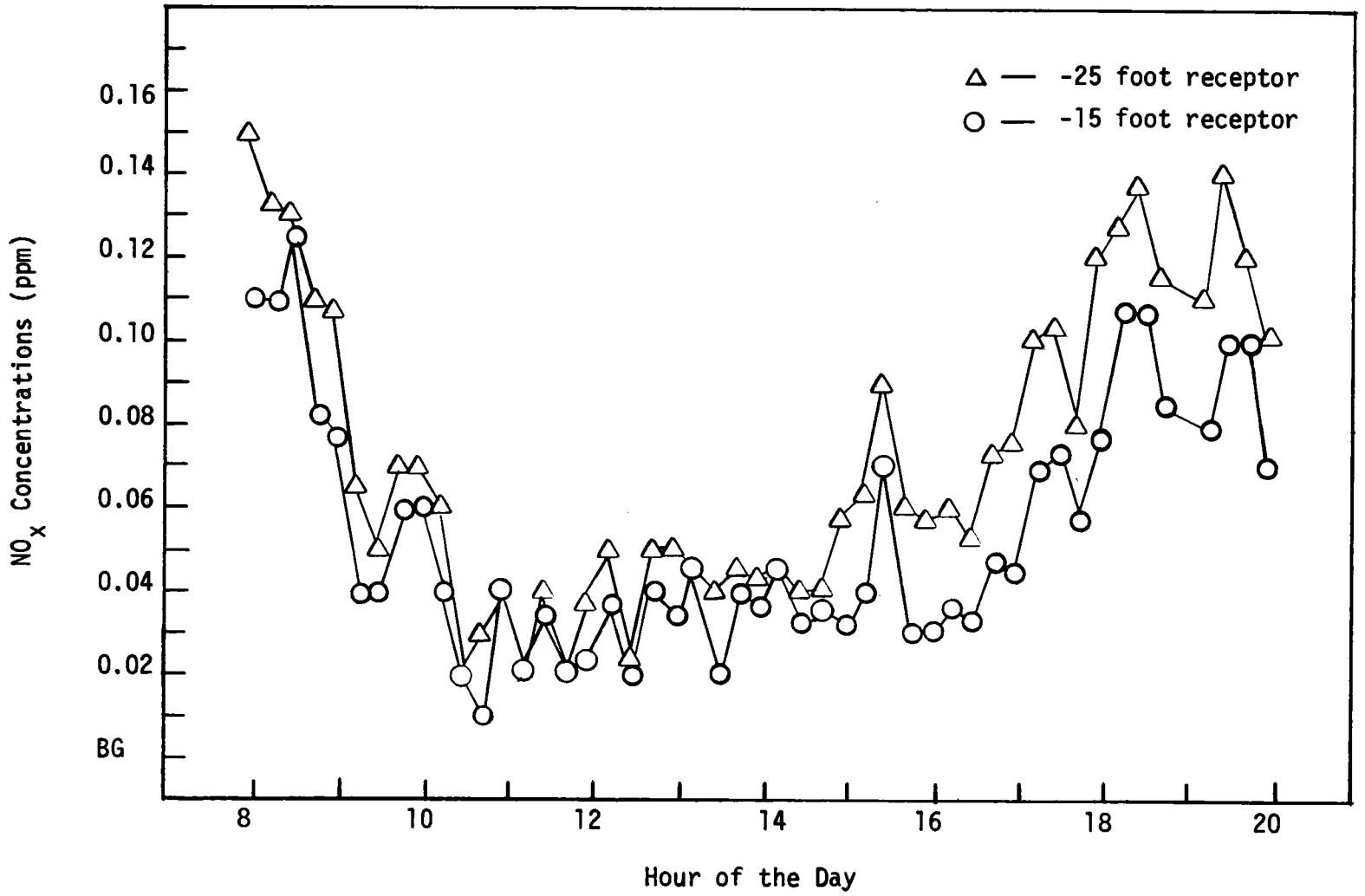

FIGURE 12. DIURNAL WINDWARD RECEPTOR CONCENTRATION PROFILES

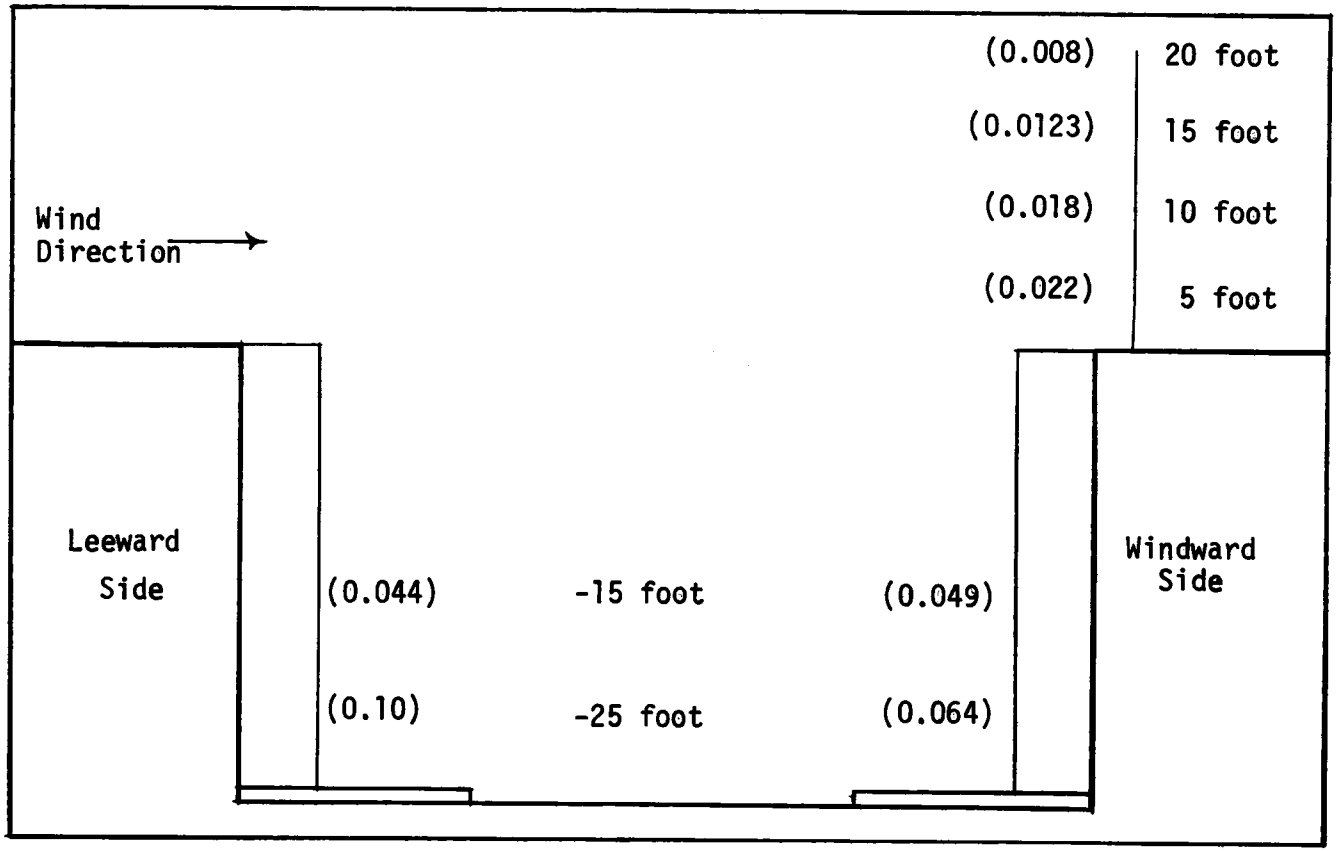

*Note: NO_x concentrations in parts per million.

FIGURE 13. ARITHMETIC MEAN VERTICAL CONCENTRATIONS FOR CROSSWIND CONDITIONS

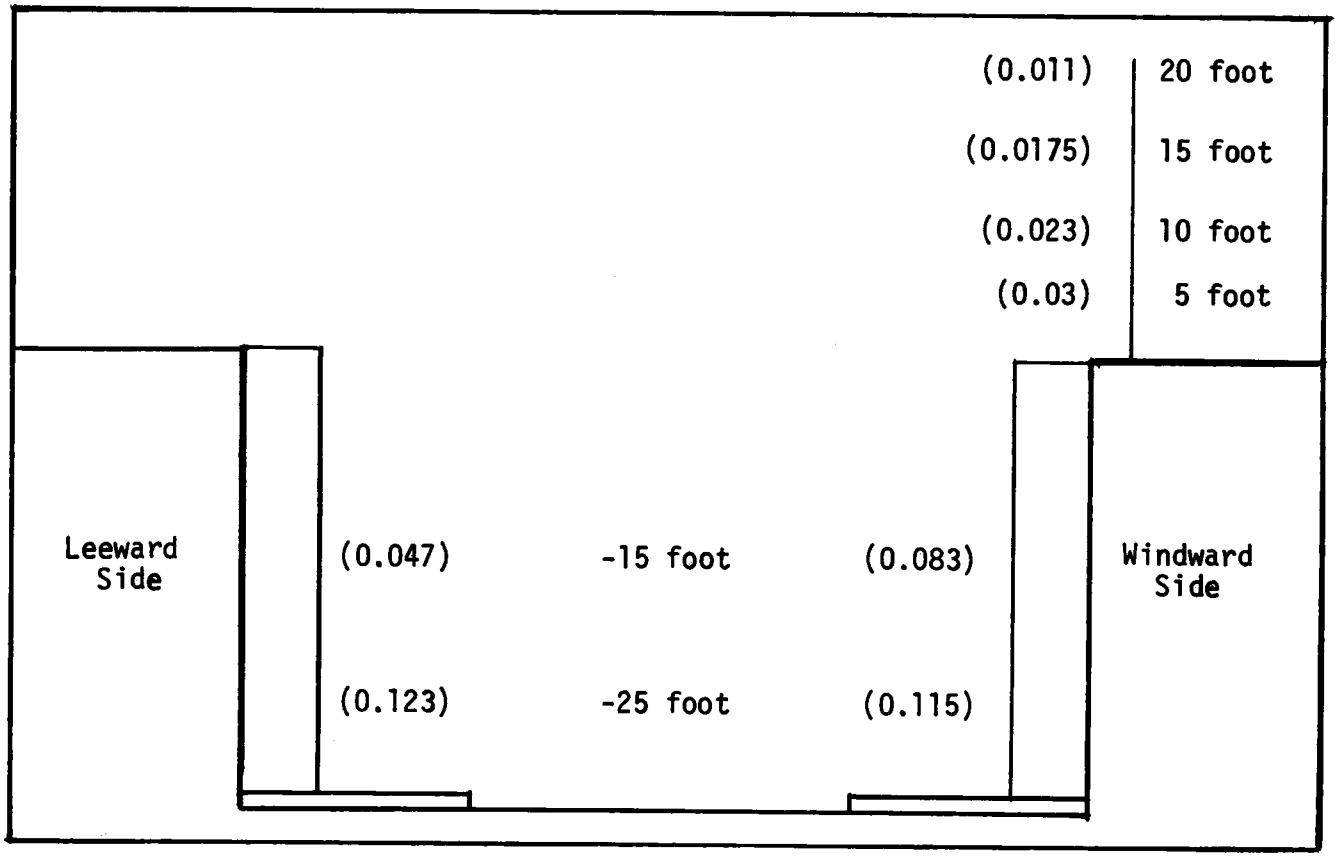

*Note: NO_x concentrations in parts per million.

FIGURE 14. ARITHMETIC MEAN VERTICAL CONCENTRATIONS FOR PARALLEL WIND CONDITIONS

and parallel wind conditions. The -25 foot leeward side receptor concentration has a greater concentration than the windward side in both the parallel and crosswind case.

Due to the single helical air motion within the depressed highway section for the crosswind case, the difference in the -25 foot receptor concentrations is very pronounced in the crosswind case. In the parallel wind case, due to the lack of this air motion, both the leeward and windward receptor concentrations remain about the same.

From Figures 13 and 14, the concentration on both the windward and leeward side decrease with increased vertical height. This is due to the greater amount of vertical mixing as the pollutant emission reaches each receptor.

The variations between the vertical profile for the leeward and windward side parallel and crosswind cases were analyzed. Because of different traffic density and wind speeds during the crosswind and parallel wind conditions, the vertical height concentrations were each non-dimensionalized to the nitrogen oxide concentration measured at the -15 foot receptor within the depressed highway section. A plot of the arithmetic mean for all measured concentration for parallel and crosswind data for each receptor normalized to -15 foot probe is illustrated in Figures 15 and 16.

For the windward side's crosswind and parallel case wind directions, the rate of concentration decrease was linear from -25 foot receptor concentration to the +5 foot receptor concentration. For the crosswind case, this linearity of the concentration decrease with height is constant at about 3.1 percent per foot for all receptor heights. However, in the

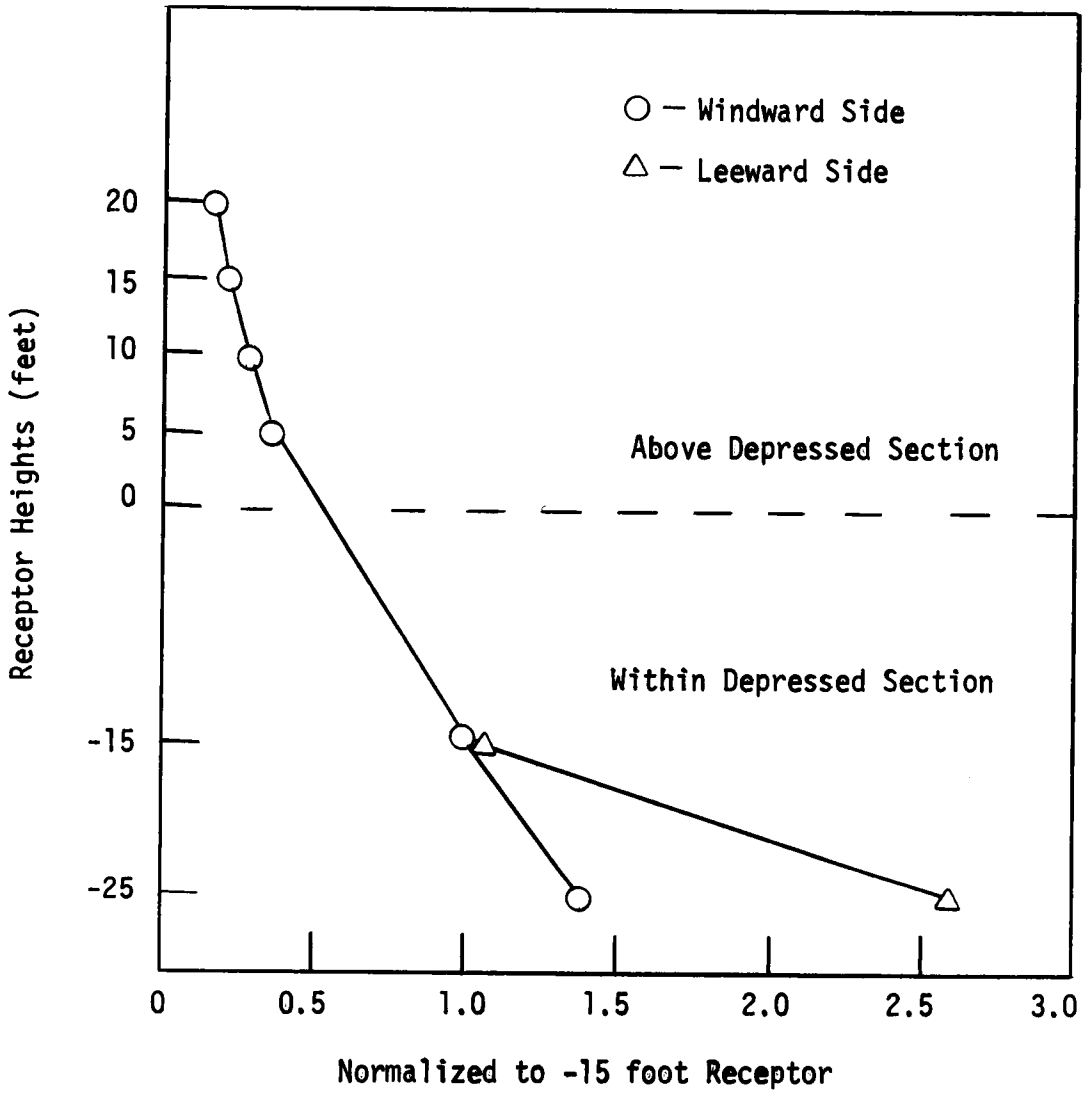

FIGURE 15. NORMALIZED VERTICAL PROFILE FOR PARALLEL WIND CONDITIONS

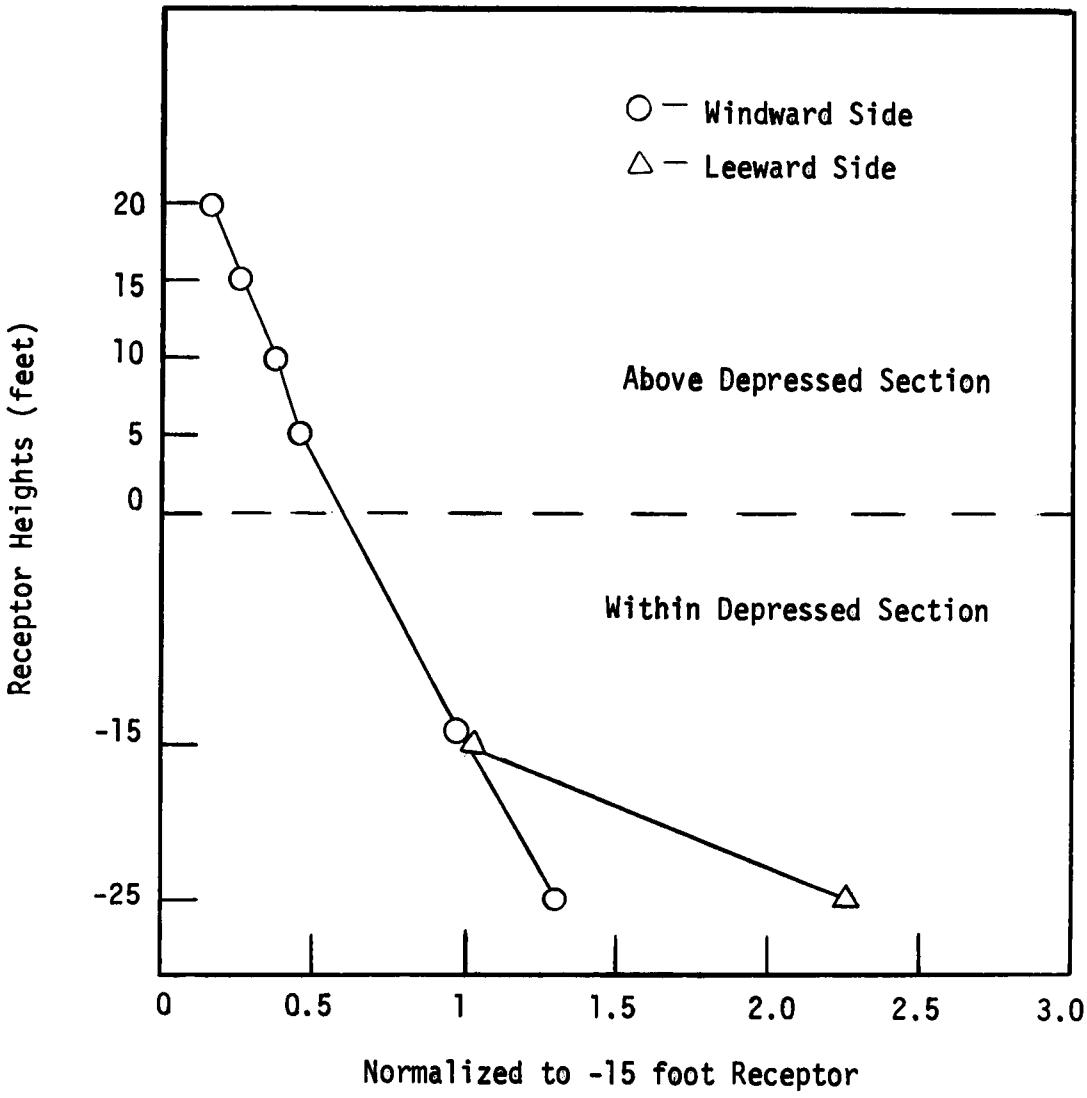

FIGURE 16. NORMALIZED VERTICAL PROFILE FOR CROSSWIND CONDITIONS

parallel case, the rate of decrease was 3.6 percent per foot from -15 foot probe to the +5 foot probe, but unlike the crosswind case, the rate of decrease changes significantly from the +5 foot receptor to the +20 foot receptor. This change is from a rate of decrease of 3.6 percent per foot to approximately 0.3 percent per foot with respect to the -15 foot receptor.

The leeward side parallel case gives a greater concentration fall off with vertical height than the crosswind case. The parallel case decreases at a rate of 16 percent per foot while the leeward case decreased at a rate of 12.5 percent per foot.

CHAPTER IV

CALIBRATION OF SRI'S STREET CANYON MODEL FOR TOTAL NITROGEN OXIDE CONCENTRATIONS WITHIN A DEPRESSED HIGHWAY SECTION

I. INTRODUCTION

After reducing the data into a final form for each 15 minutes of monitoring, the data were used as input parameters into a statistical analysis program. This statistical program determined correlations between the measured total nitrogen oxide (NO_x) concentrations and the predicted concentrations from a modified Stanford Research Street Canyon Submodel. Besides this correlation, other correlations were performed in order to determine if combinations of such parameters as emission factors, traffic volumes, and inverse wind speeds gave better results.

This chapter describes the existing Stanford Research Institute's (SRI) model, the variations of this model for total nitrogen oxide predictions, the calibration and correlation analysis, the validation, and calibration of SRI's model, and the correlation of various parameters with measured total nitrogen oxide concentrations.

II. SRI STREET CANYON SUBMODEL

Stanford Research Institute's (SRI) Street Canyon Submodel was determined from the San Jose experiment [27] to estimate the dispersion of vehicular carbon monoxide emissions within a city street canyon. Since the depressed highway section at I-40 East had straight vertical walls and resembled a street canyon, this report attempted to extend the

recommended usage of SRI's model for predicting total nitrogen oxide concentrations within the depressed section.

The basic rationale behind SRI's model is based on Georgii's[28] work and the San Jose experiment. For these works, air motion within the canyon was believed to be a single-helical circulation. As shown in Figure 17, this helical air circulation gives substantially higher concentrations to receptors on the leeward side (right side of Figure 17) than on the windward side (left side of the Figure) because of the reverse flow component across the street, near the surface. This model assumes that the measured concentration, C, at the receptor is derived from two components. One component is contributed from a background concentration, C_{bk}, in the air entering the canyon from above, and the other concentration component, ΔC, is supplied from locally generated vehicular pollutant emissions, Q, in the street.[29] Hence, we have

$$C = C_{bk} + \Delta C \qquad (1)$$

This model calculates the concentration component from the vehicular emissions at a given receptor location by three different equations. Different equations are used depending on whether the wind directions are parallel or crosswind with respect to the road angle and whether receptor locations are on the leeward or windward side of a canyon.

Leeward Case

A leeward case equation is employed to calculate concentrations, ΔC, from local vehicular emission for crosswinds (wind directions greater than 30° with respect to the road) and the receptor side of the highway

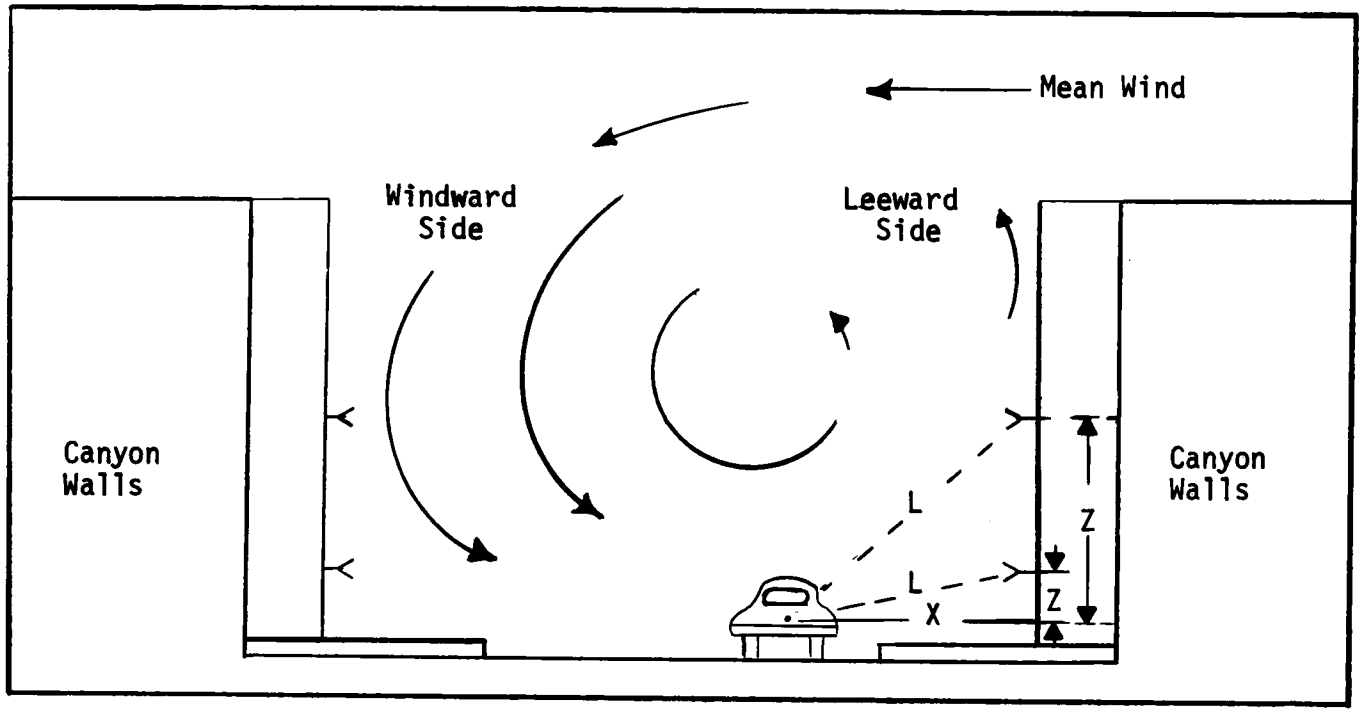

FIGURE 17. SRI STREET CANYON DESCRIPTION

where reverse air movements within the canyon transports vehicular emissions directly to the receptor. This equation can be represented by a simple box model form.

$$\Delta C_L = Q/U_s \; Y \qquad (2)$$

Where: ΔC_L = concentration component from the vehicular emissions for a receptor on the leeward side of the highway.

Q = rate of vehicular pollutant emissions.

U_s = mean wind speed near the street.

Y = depth of mixing volume.

The leeward case model was then determined by SRI to be as follows:

$$\Delta C_L = \frac{K \times Q}{(U + 0.5) \times ((X^2 + Z^2)^{\frac{1}{2}} + L_o)} \qquad (3)$$

Where: Q = rate of vehicular pollutant emissions in the street (gm/ (m·sec)).

U = rooftop wind speed (m/sec.), 0.5 m/sec. is due to the influence of the vehicles' forward motion. Therefore, U_s of the box model = $k_1(U + .5)$.

X = horizontal distance from the receptor to the center of the nearest lane (m).

Z = vertical distance from the road to the receptor (m).

L_o = two meters, the dimension where vehicular emission was assumed completely mixed. Therefore, the depth of mixing volume (Y) from a box model = $k_2((X^2 + Z^2)^{\frac{1}{2}} + L_o)$.

K = empirical non-dimensional constant ($K = 1/k_1 \; k_2$), $K \approx 7$ for carbon monoxide concentrations).

Windward Case

A windward case equation is for crosswind directions and for receptors located on the windward side. Similar to the previous leeward case, a box model concept was also used for formulation of this equation, where the depth of mixing volume is considered to be constrained by the canyon's size.

$$\Delta C_W = \frac{K \times Q}{W \times (U + .5)} \times \frac{(H - Z)}{H} \qquad (4)$$

Where: ΔC_W = vehicular emissions concentration component for receptors on the highway's windward side.

W = width of canyon (m).

H = average building height or depth of depressed highway (m).

Parallel Case

A parallel case equation was determined for wind directions within $\pm 30^{o}$ of the highway angle and for prediction of concentrations at receptor locations on either highway side. This equation predicts parallel wind concentrations by taking an average of the leeward and windward equation.

$$\Delta C_I = \tfrac{1}{2} (\Delta C_L + \Delta C_W) \qquad (5)$$

Where: ΔC_I = the parallel wind concentration component from the vehicular emissions.

III. THE USE OF STANFORD RESEARCH INSTITUTE'S STREET CANYON MODEL FOR TOTAL NITROGEN OXIDE CONCENTRATION WITHIN A DEPRESSED HIGHWAY SECTION

In SRI's model, the emission rate, Q, is determined from a special emission factor equation for carbon monoxide and the traffic volume.

Since the emission factor equation can only be utilized for carbon monoxide, total nitrogen oxide emission factors had to be determined. These determinations are complicated by such variables as the vehicular type (light duty gasoline, heavy duty gasoline, and heavy duty diesel engines), deterioration rate, age, and speed. Each of these variables can change the amounts of pollutants emitted. Two different documents give methods of determining the emission factors for nitrogen oxides. These documents are Study of the Emission from Light Duty Vehicles in Six Cities[30] and Compilation of Air Pollution Emission Factors, AP-42.[7] The six city study determined the pollutant emissions for different model years, different modes of vehicular operation, different vehicular speeds, and for only light duty vehicles. In the AP-42 study, a method is given to determine nitrogen oxide emission factors for different model years, route speeds, and types of vehicles. Since heavy duty vehicles add appreciably to the total nitrogen oxide concentration within the depressed highway section, the Environmental Protection Agency publication AP-42 was used to determine the emission factors for the total nitrogen oxides in SRI's model.

AP-42 Emission Factor Determination for 1974

Based on the 1974 model mix year, total emission factors were determined by the following equation.

$$E = (A \times (1-HDM)) + B \times (HDM/2) \times SP + C \times (HDM/2) \qquad (6)$$

Where: E = total emission factor (gm/(veh·mile)).

HDM = heavy duty mix which was evenly divided between gasoline and diesel powered engines.

SP = speed correction factor.

A = emission factor for light duty gasoline powered engines (gm/(veh·mile)).

B = emission factor for heavy duty gasoline powered engines (gm/(veh·mile)).

C = emission factor for heavy duty diesel engines (gm/(veh·mile)).

The individual emission factors for the different types of vehicles are determined from the national average percent of each model on the nation's highways and the deterioration rates of the vehicular control devices. From AP-42, the individual emission factors were equal to 4.2, 9.2, and 23 for the respective light duty gasoline, heavy duty gasoline, and heavy duty diesel engines. The speed correction factor was determined for total nitrogen oxides from Figure 18.

The Emission Rate Determination

Rates of vehicular emissions were approximated at I-40 East using the field measured traffic volume and by calculating the emission factor from measured heavy duty mix and traffic. The following equation was used to calculate the emission rate.

$$Q = 1.73 \times 10^{-7} \times N \times E \times 10^{6} \qquad (7)$$

Where: Q = rates of emission of nitrogen oxide.

N = number of vehicles per hour.

E = emission factor (grams/vehicle mile).

10^6 = conversion term from gram to micrograms

1.73×10^{-7} = conversion term from grams per mile hour to gm/m sec.

This determination for the emission rate was substituted into the leeward and windward side parallel and crosswind case to give a predictive model for total nitrogen oxide concentrations within a depressed highway section.

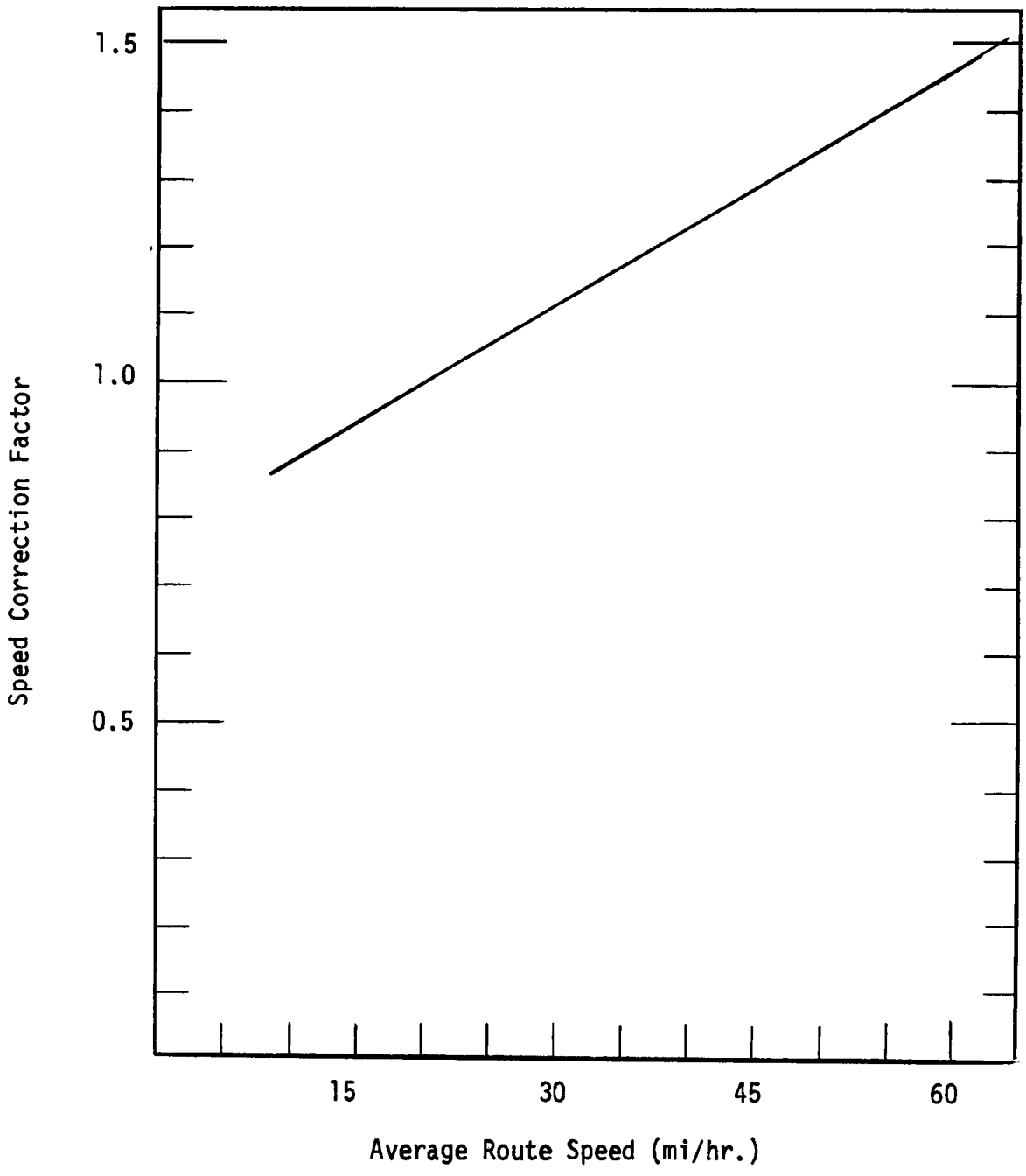

FIGURE 18. AVERAGE SPEED CORRECTION FACTOR FOR ALL MODEL YEARS

IV. THE CORRELATION OF THE MEASURED DATA WITH SRI'S MODEL

Using a suggested calibration coefficient of seven and emission factors determined from AP-42, the estimated total nitrogen oxide concentrations were correlated with the field measured concentrations. Figure 19 gives a random sample of some of the 200 leeward data comparisons.

The best relationship between SRI model's estimates and field measured data would be a uniform variance about a slope of one passing through the origin. Because of this fact, the slope of one was used to evaluate the correlation between the estimated and the measured concentrations. This says if the data is skewed above or below this slope, the model needs to be calibrated. As can be seen in Figure 19, the data for the leeward side is skewed above this slope. However, the concentrations estimated using SRI's model can still be correlated with field measured concentrations. This is accomplished as shown in Figure 19 by enveloping the slope and ascertaining the number of data points within a specified percent of the slope. For example, in Figure 19 approximately 37 percent of the data present is within $\pm$20 percent of the slope of one. Using this program, SRI's model correlations were determined and the results plotted on log probability paper as cumulative percent error versus the percent data within this error.[31] Figures 20 and 21 give the cumulative plots of the SRI's model correlation for the total windward and leeward data. This indicates that 50 percent of the windward data and leeward data are within $\pm$30 percent and $\pm$78 percent of the slope of one, respectively. From this data, it can be established that in order for

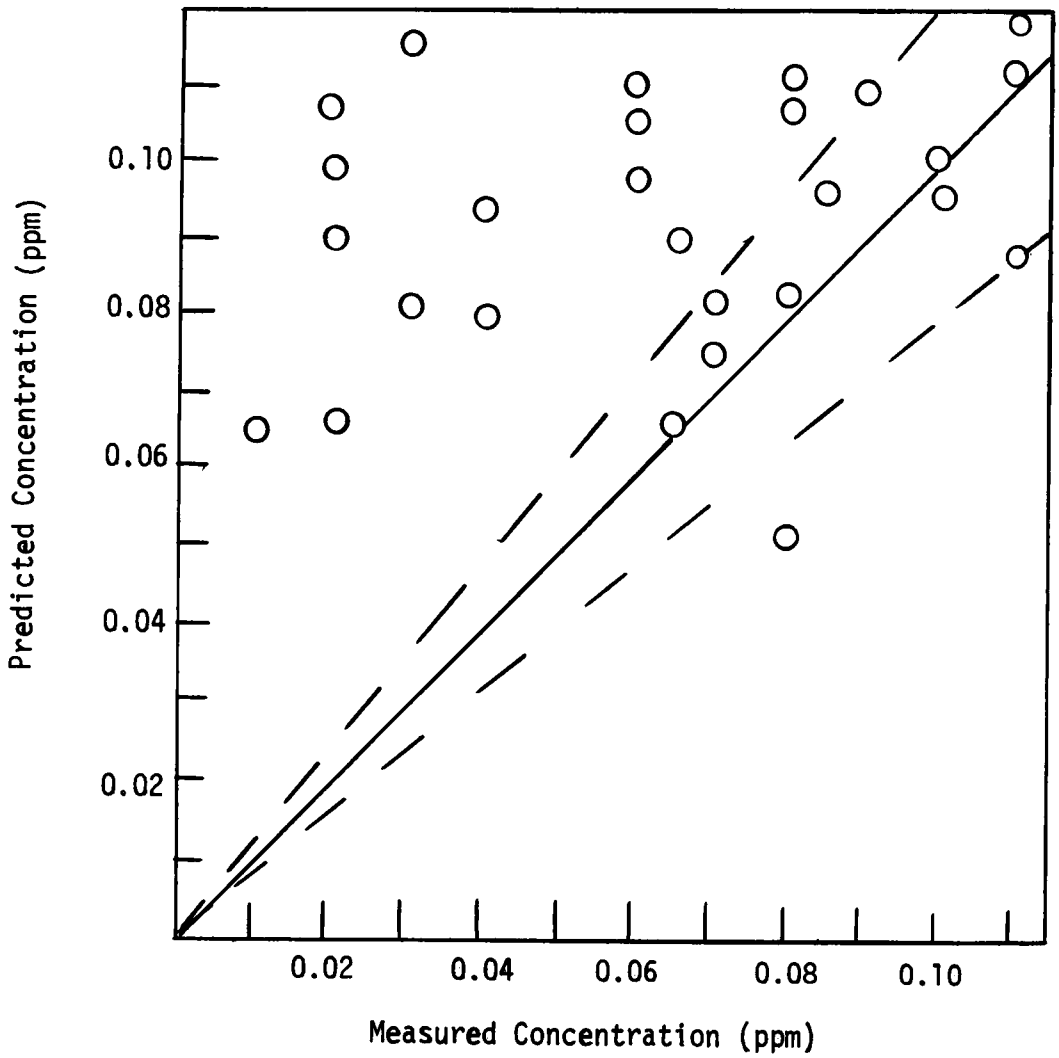

FIGURE 19. EXAMPLE CORRELATION

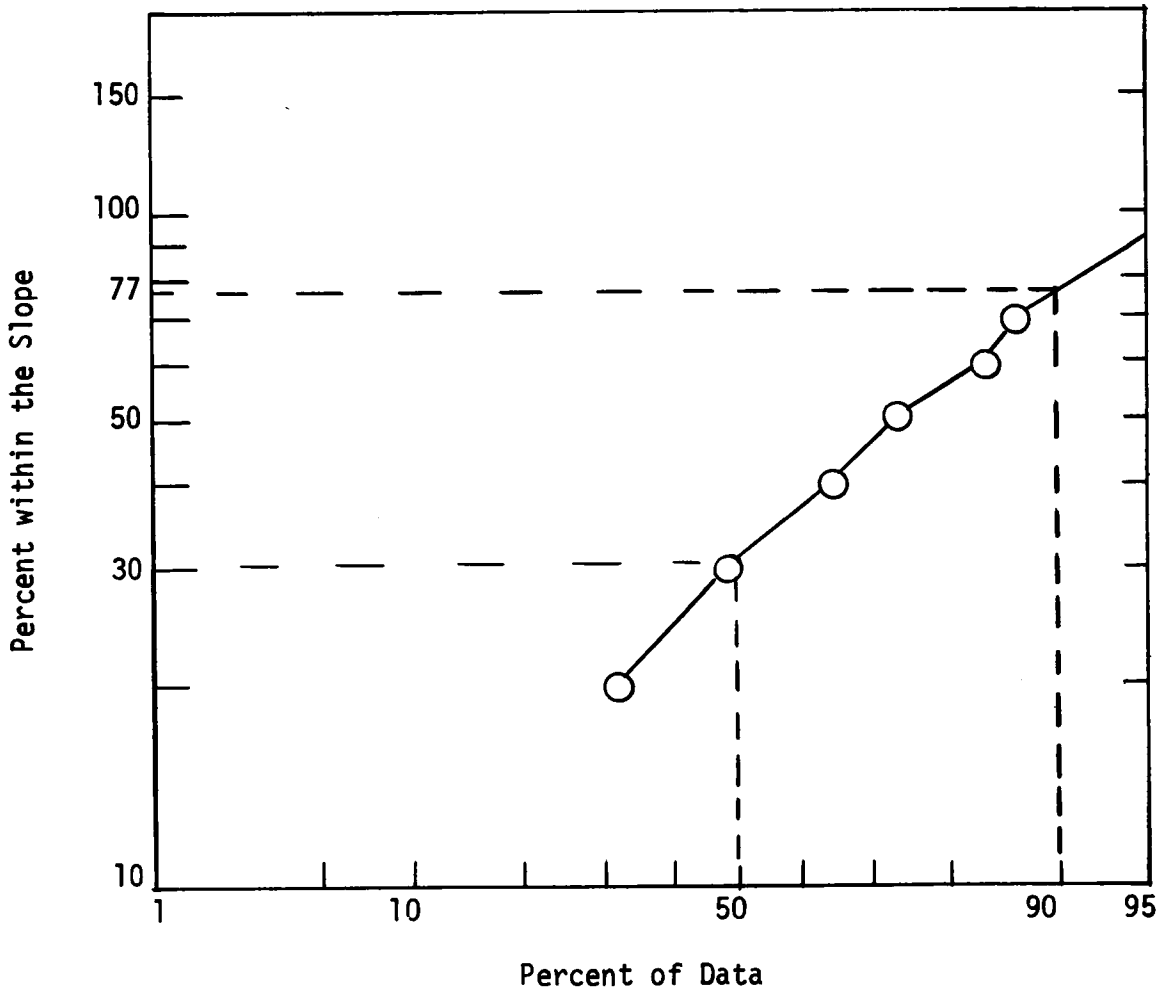

FIGURE 20. UNCALIBRATED SRI MODEL CORRELATION WITH WINDWARD MEASURED DATA

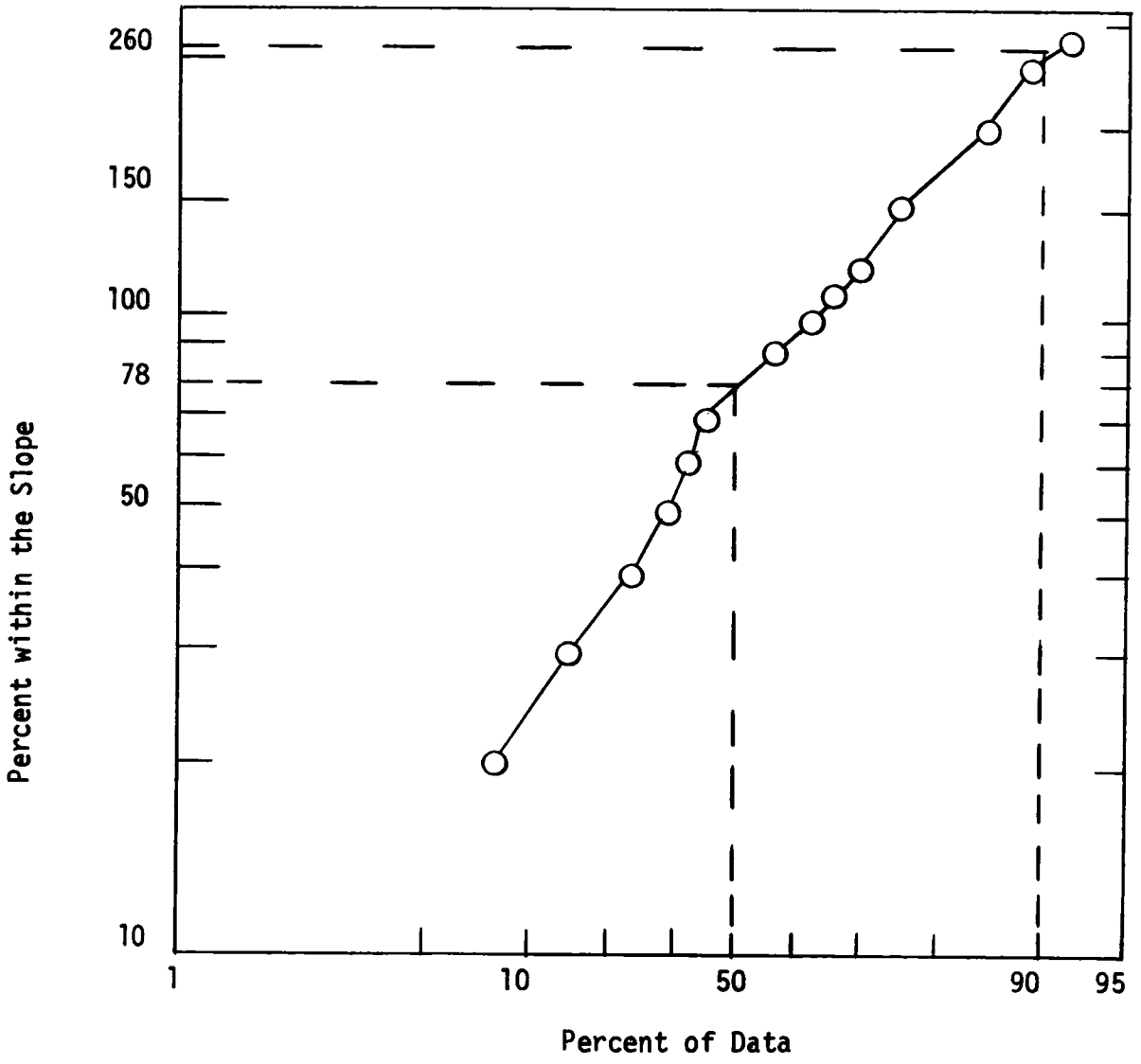

FIGURE 21. UNCALIBRATED SRI MODEL CORRELATION WITH LEEWARD MEASURED DATA

the SRI's model to be used for estimating total nitrogen oxide concentrations within a depressed highway section, the model must at least be calibrated for the leeward side.

V. THE CALIBRATION OF SRI'S MODEL FOR TOTAL NITROGEN OXIDE ESTIMATES WITHIN A DEPRESSED HIGHWAY SECTION

Due to extending SRI's model usage to determining total nitrogen oxide concentrations within a depressed highway section, new calibration coefficients were required for improved data correlations. Because a standard regression analysis gives the best linear fit of one dependent viable to one independent variable, this approach was first investigated for ascertaining a calibration coefficients. Since the field measured data had the greatest degree of accuracy, it was used as the independent variable for this equation. By using this approach, the SRI model's estimates can be calibrated with the field measured data by using the slope of the regression line. However, after analyzing the least squares fit of the SRI model's estimates versus measured data, it was decided that this approach did not give a realistic solution due to an intercept offset. Figure 22 gives the results of the least squares fit for the windward and leeward measured data. The only physical explanation of offsets of 0.017 and 0.089 parts per million would have to be due to negative background levels of these magnitudes. This implied the background concentration measurements were unrealistically high. Since the measured background concentration ranged from 0.01 to 0.01 parts per million and due to the high degree of confidence in the accuracy levels measured, the probability such inaccuracies in background determinations seemed

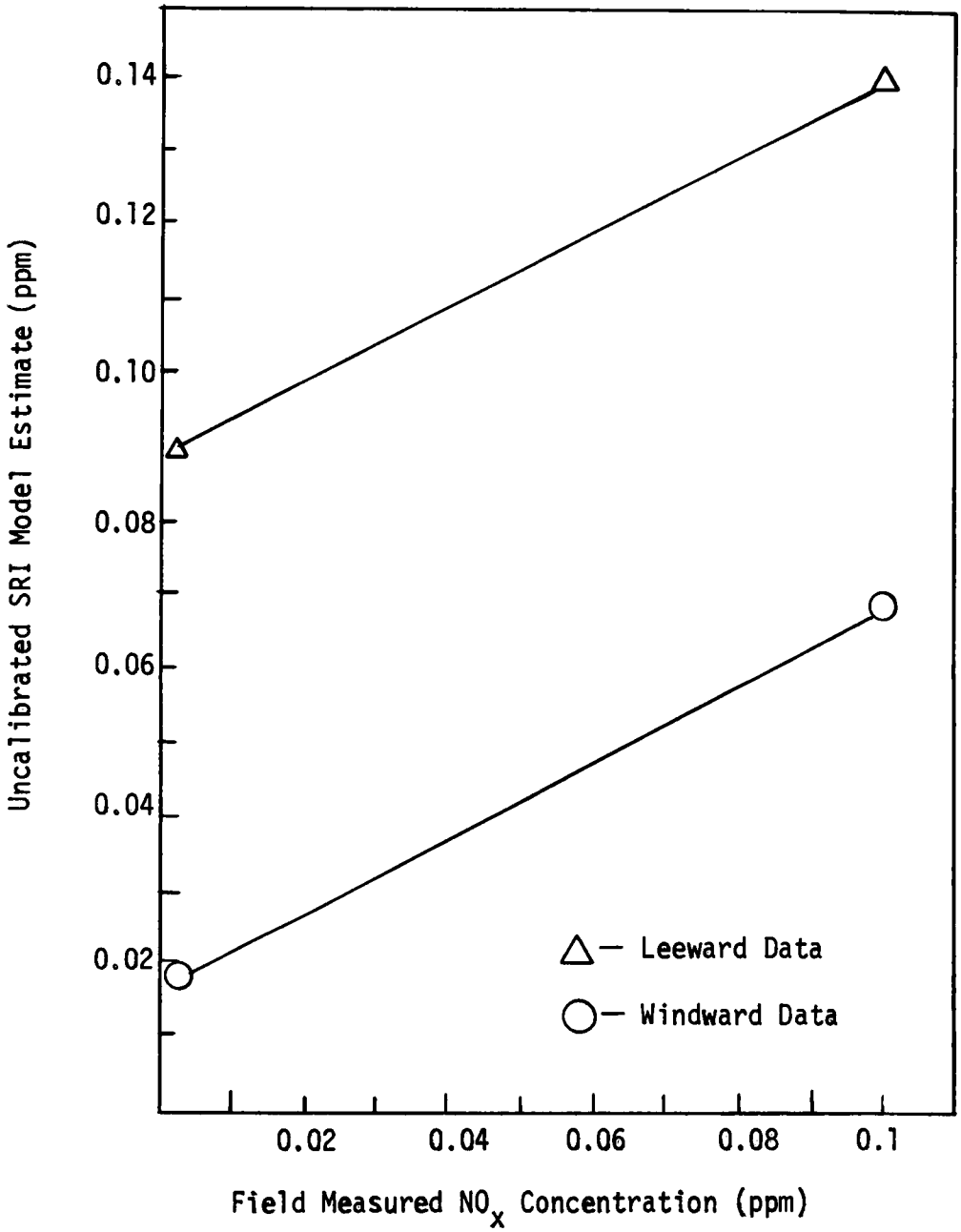

FIGURE 22. LEAST SQUARES FIT OF UNCALIBRATED SRI MODEL

very remote. Because the linear method gave unrealistic results, another approach was investigated for calibrating SRI's model.

The next approach selected for determining the calibration coefficient was a geometric mean K procedure. This procedure determined the geometric mean of the ratio, K, of SRI's predicted concentration to the measured concentration for the total data for each side of the road. The value of this geometric mean K was taken to be the calibration constant for the model. This approach is dependent upon the ratio, K, of ΔC estimated to ΔC measured being lognormally distributed.

In order to examine the distribution of the K values, the cumulative frequency of the K values were plotted on log-probability paper.[31] Due to the linearity of Figures 23 and 24, the distribution was verified as being roughly lognormally distributed. From Figures 23 and 24, the geometric mean K was also determined by taking the intercept of the linear slope and the 50 percentile. This resulted in geometric mean calibration coefficients of nine and four for the windward and leeward data.

After calibration coefficients were determined, the statistical analysis was again utilized to give a correlation of the calibrated SRI's model with the measured windward and leeward data. This resulted in 50 percent of the measured windward data being within $\pm$27 percent of the value calculated using the calibrated model, where K = 9. For the leeward measurements, the data were within $\pm$35 percent of the value obtained using the calibrated model, where K = 4. Using the statistical program for the geometric mean, a calibrated model was obtained that gave improved correlations with measured data. A minor improvement was obtained for the windward side and a substantial improvement for the leeward side.

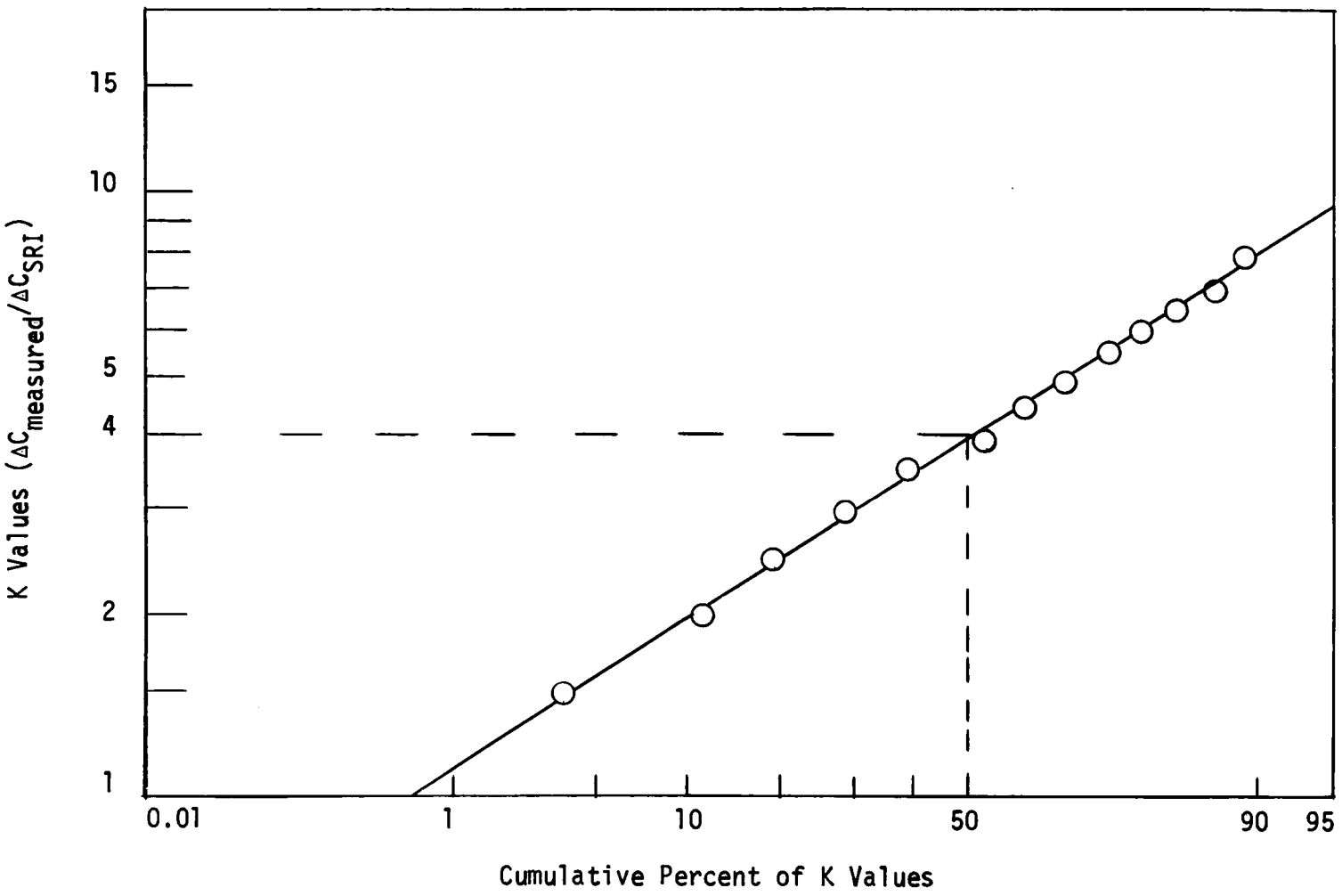

FIGURE 23. CUMULATIVE FREQUENCY OF K VALUES FOR THE LEEWARD DATA

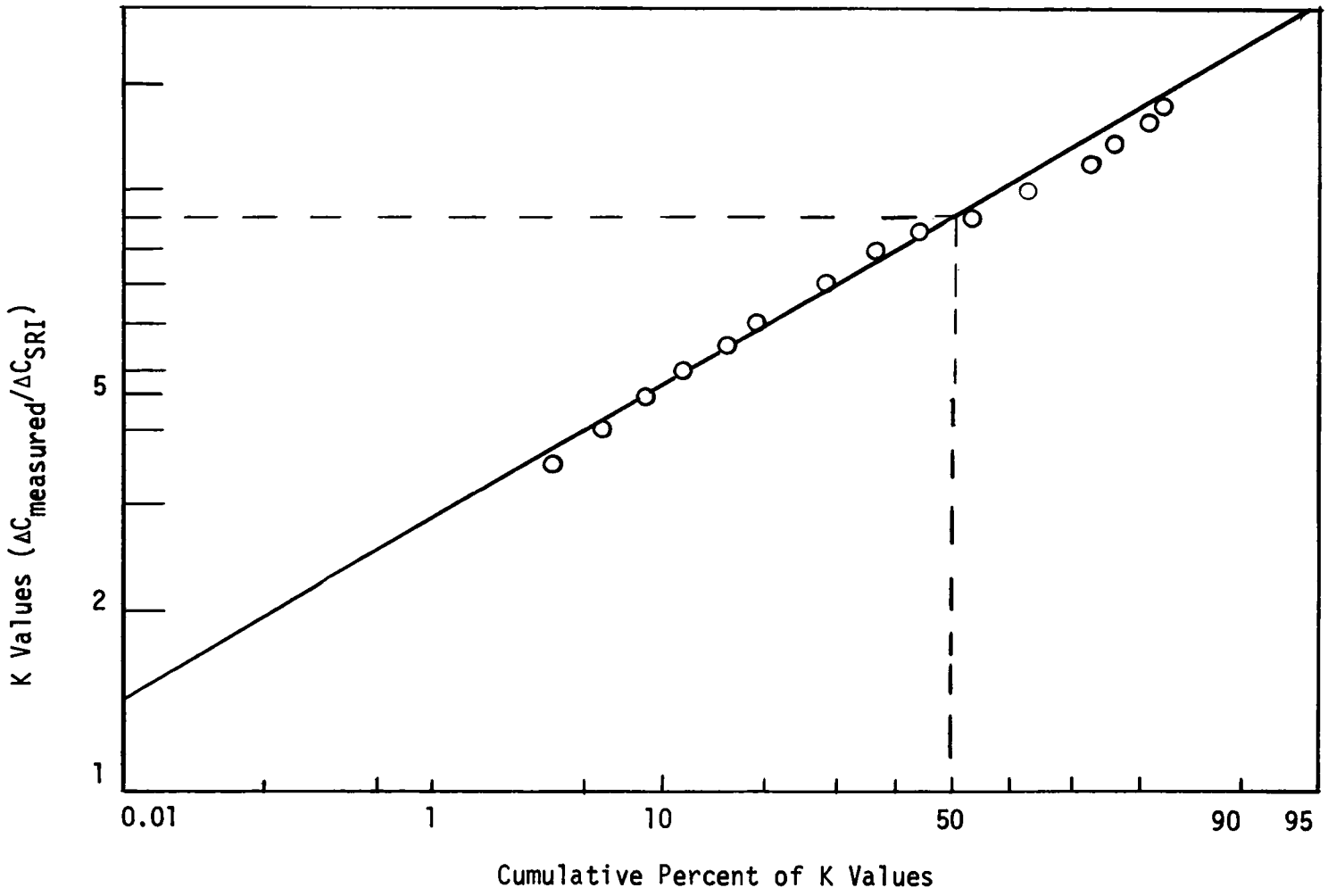

FIGURE 24. CUMULATIVE FREQUENCY OF K VALUES FOR THE WINDWARD DATA

VI. THE CORRELATION OF THE MEASURED TOTAL NITROGEN OXIDE CONCENTRATIONS WITH VARIOUS PARAMETERS

The geometric mean K calibration and the statistical analysis procedures described previously in this chapter can be utilized to determine the significance of different variables upon the variance of the data and the calibration coefficient. These methods were employed to determine if individual or combinations of such parameters as traffic volume, inverse wind speed, and emission factors improve the variance. Tables 7 and 8 give the results of these tests for the leeward and windward data. For the leeward side, all the different combinations improved upon the uncalibrated SRI model. However, only the inverse wind speed gave satisfactory correlation with the monitoring data for the windward side. Although some of these tests improved upon the uncalibrated SRI model, none produced the minimum deviation of data as the calibrated SRI model of four for windward side and of nine for leeward side.

TABLE 7. LEEWARD DATA CORRELATIONS WITH DIFFERENT PARAMETERS.

Case	K	50%	90%
Uncalibrated SRI Model	7	77%	260%
Calibrated SRI Model	4	35%	107%
Traffic Volume	7.7×10^{-5}	42%	116%
Inverse Wind Speed	0.245	37%	110%
Traffic Volume Times Inverse Wind Speed	2.9×10^{-4}	40%	120%
Emission Rate Times Inverse Wind Speed	3.6×10^{-5}	42%	112%

TABLE 8. WINDWARD DATA CORRELATIONS WITH DIFFERENT PARAMETERS.

Case	K	50%	90%
Uncalibrated SRI Model	7	30%	74%
Calibrated SRI Model	9	27%	85%
Traffic Volume	6.7×10^{-5}	56%	120%
Inverse Wind Speed	0.197	30%	95%
Traffic Volume Times Inverse Wind Speed	2.3×10^{-4}	42%	95%
Emission Rate Times Inverse Wind Speed	2.9×10^{-5}	40%	95%

CHAPTER V

A NEW DEPRESSED HIGHWAY MODEL

I. INTRODUCTION

A new depressed highway model for the determination of nitrogen oxide concentration was formulated using the following basic equation.

$$\Delta C_{NO_x} = \frac{K \times Q \times (.533)}{U \times L^{Y}} \qquad (8)$$

Where: ΔC_{NO_x} = the measured nitrogen oxide concentration minus the background concentration (ppm).

U = wind speed at 30 feet above the cut (m/sec.).

L^{Y} = dispersion term, based on the distance from the center of the road to the receptor (m).

Q = emission rate ($\mu g/m$ sec.).

K = the mean K, calibration constant, equal to $1/k_1\ k_2$.

.533 = conversion factor of $\mu g/m^3$ to parts per million.

This equation, a modified form of the existing Stanford Research Institute's (SRI) leeward side crosswind equation, was used for the prediction of both the leeward and windward side, parallel and cross-wind cases. The new model's modifications vary from the SRI model's leeward side crosswind case with respect to the relationship between the wind speed above the cut section and within the cut and to the determination of the dispersion term.

The determination of the dispersion term is most significant variation between the two models. In SRI's model, the dispersion was

assumed to be linearly proportional to the distance traveled from the center of the nearest lane to the receptor. This form for the dispersion term is as follows.

$$D = k_2 (X^2 + Z^2)^{\frac{1}{2}} \quad (9)$$

Where: D = dispersion term.

X = horizontal distance from center of the nearest lane to the receptor (m).

Z = vertical distance from the ground to the receptor (m).

For the new model, the dispersion was assumed as a power function of the distance traveled from the center of the highway to the nearest receptor. This form is given as follows.

$$D = k_2 L^{\gamma} \quad (10)$$

$$L = (X^2 + Z^2)^{\frac{1}{2}} \quad (11)$$

Where: X = horizontal distance from the center of the road to the receptor (m).

γ = exponent in the dispersion term.

This dispersion form is now similar to conventional dispersion functions when expressed in the form $a\ x^{b}$ where x is the downwind distance from the source.[32,33]

The other modification in the SRI's equation form was the relationship of the wind speed within and above the depressed section. This modification was based on experimental data of the relationship between the wind instrument at 30 feet above the cut and at 10 feet within the cut section. This relationship was determined as follows the I-40 East site.

$$U_{\text{In cut section}} = k_1 \times U_{\text{Above cut section}} \quad (12)$$

Where: $k_1 = .27$

Figure 25 gives a graphical representation of the data on which this relationship was based.

II. LEEWARD CASE

The Determination of the Dispersion Term's Exponent

The exponent in the dispersion term was determined from the analysis of the ratio of the probe concentrations within the cut section and the diagonal distances from the center of the road to the probes.

$$R = \Delta C_1/\Delta C_2 = L_2^{\gamma}/L_1^{\gamma} \quad (13)$$

Where: R = ratio -15 foot receptor concentration to -25 foot receptor concentration.

L = diagonal distance from the center of the road to the receptor.

ΔC = measured receptor concentration minus the background concentration.

Upon segregation of the ratios of the concentrations, R, by wind directions (see Figure 26), it was found that the geometric mean concentration ratios for each direction varied significantly. The dispersion of one receptor distance to another receptor was not constant for all wind directions. Therefore, a statistical analysis was performed on the data to determine what relationships best represented this data. Figure 27 illustrates the curve fits of the data that were employed.

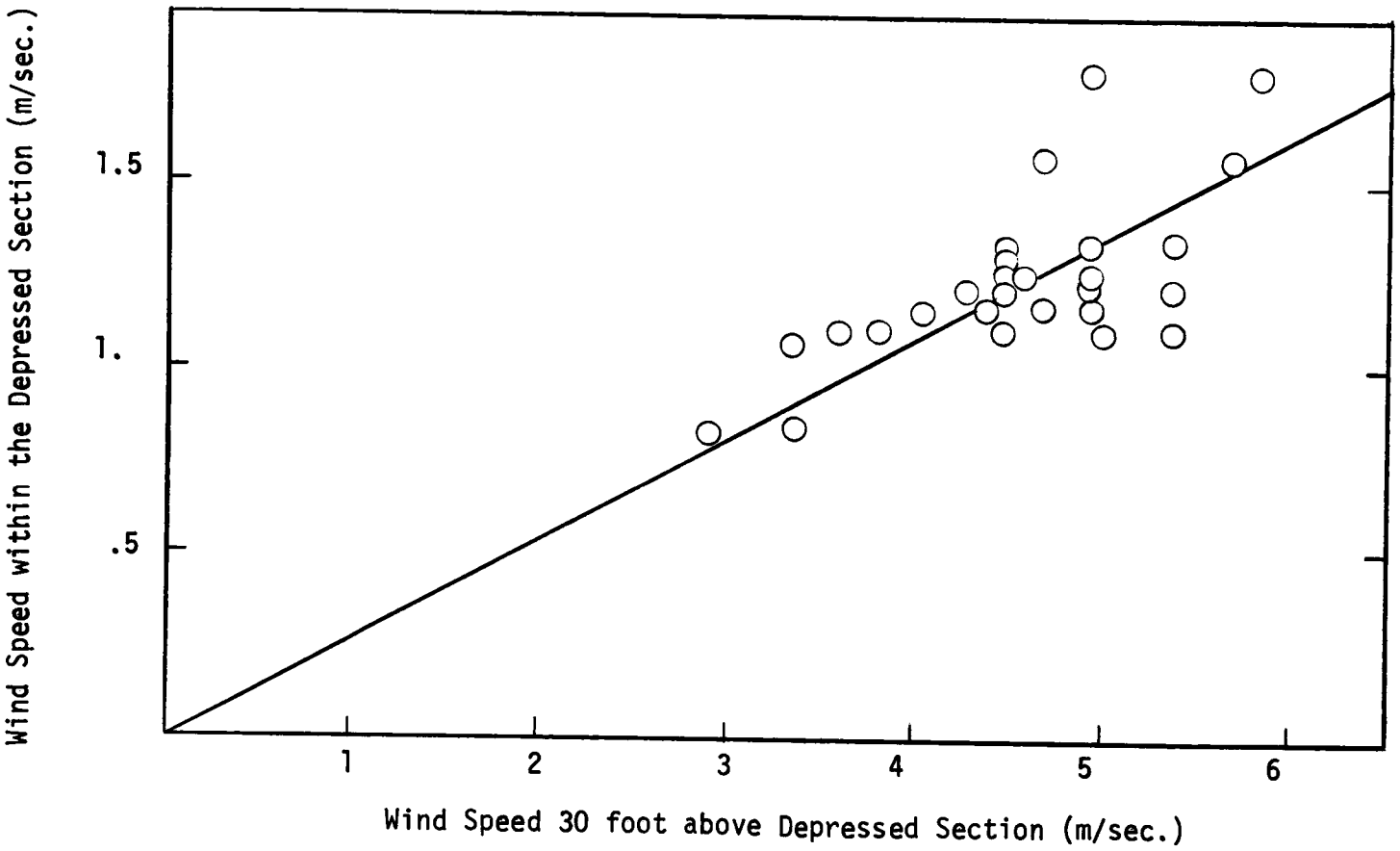

FIGURE 25. COMPARISON OF WIND SPEED ABOVE AND WITHIN THE DEPRESSED SECTION

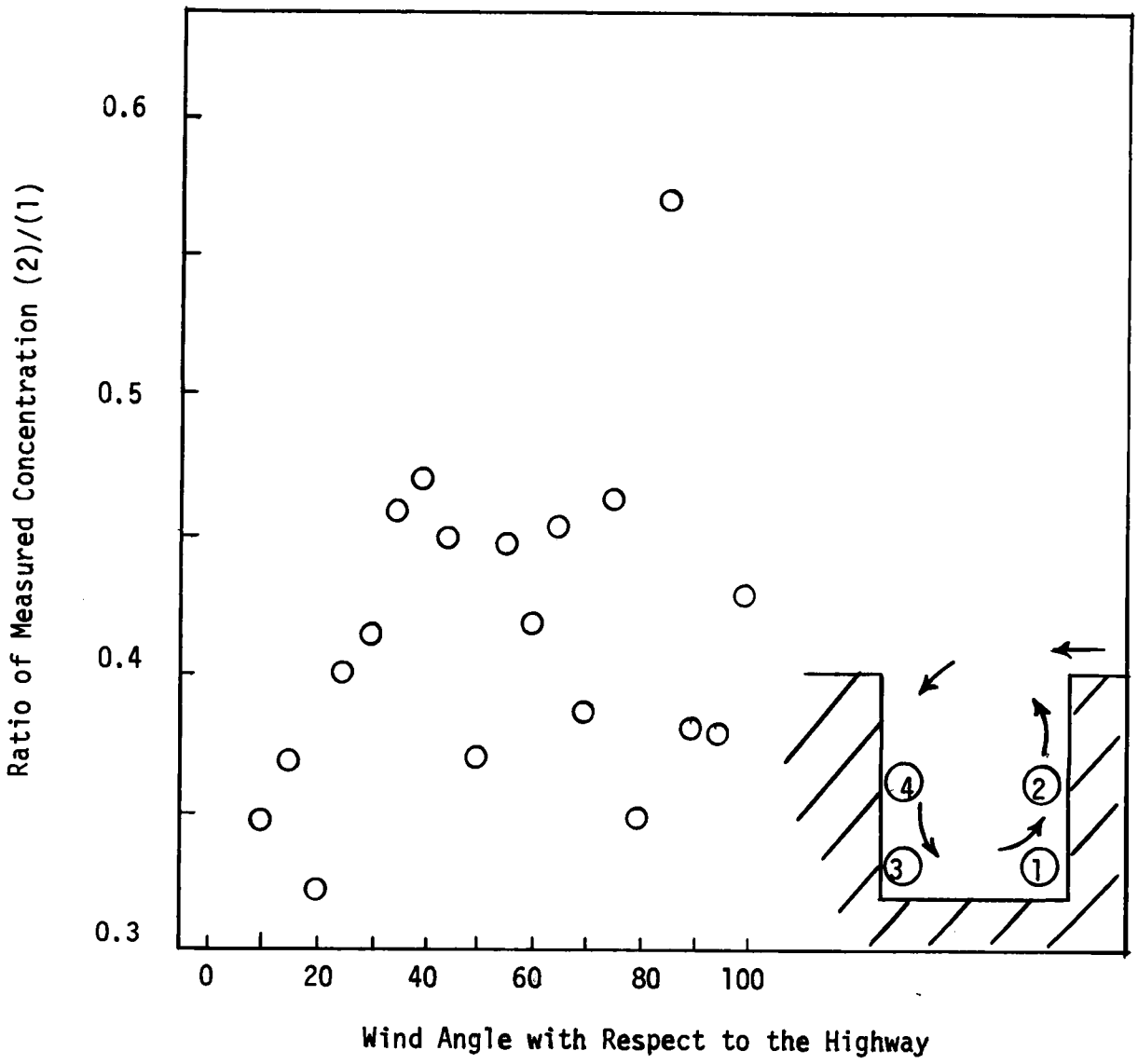

FIGURE 26. WIND ANGLE RELATIONSHIP WITH THE LEEWARD SIDE OF THE -15 FOOT TO -25 FOOT MEASURED CONCENTRATION

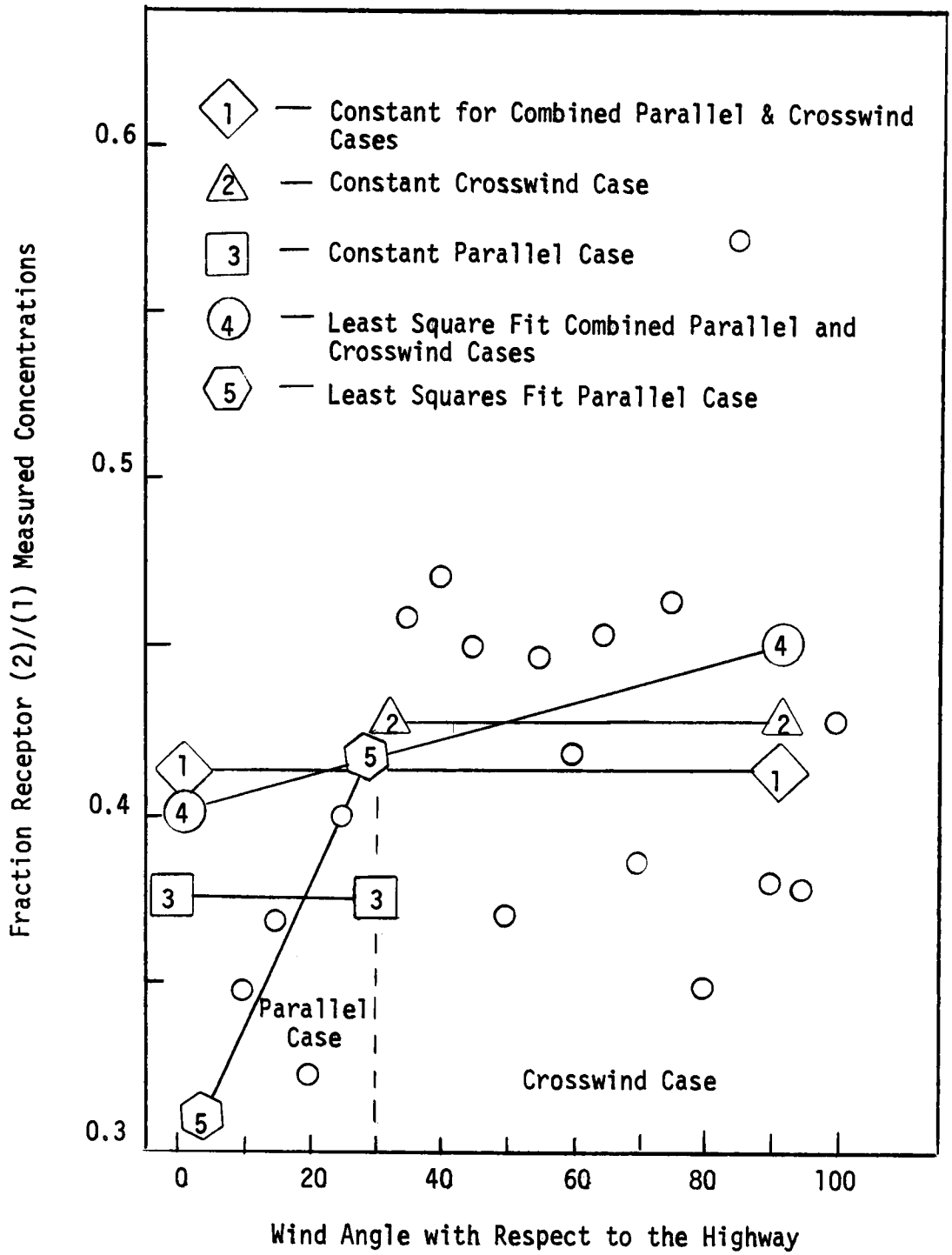

FIGURE 27. VARIOUS FITS OF CONCENTRATION RATIOS WITH RESPECT TO THE LEEWARD WIND ANGLES

Five different equation fits were investigated as follows:

(1) The ratio of the concentration of the -15 foot receptor to the concentration of the -25 foot receptor was assumed constant over the combined crosswind and parallel cases.

(2) The ratio of the concentration was fit to separate constants, one for the crosswind and one for the parallel case.

(3) A least squares fit of the ratio of the concentrations with respect to the wind direction was performed for the combined parallel and leeward case.

(4) A combination of a least squares fit of the concentration ratio with respect to the wind direction was used for the parallel case, and a constant concentration ratio was used for the corsswind case.

(5) A sine function (not shown in Figure 26) was used for the combined parallel and crosswind cases.

Table 9 gives the results of the statistical analysis of these five different approaches. Although 50 percent of the data is within $\pm$13.5% of the geometric mean slope for cases 1, 2, and 4, the cumulative error for 90 percent of the data was different for each of these cases. Based on the 90 percentile, case 4, a least square fit of the parallel case and constant fit of the crosswind case gave the best fit. Because of the logic of case 4 and its superior fit to the data, this case was utilized to calculate the exponential of the dispersion term. This is different from SRI's prediction of the ratio of the -25 foot and -15 foot receptors' concentration, as shown in Figure 28. The SRI model used a step function for the change from the parallel to the crosswind case. In the new model, the parallel case approaches the crosswind case linearly, which seems more realistic than the discontinuous step function change as presented by SRI. SRI's model also underestimated the ratio of the concentrations rate of dispersion by a factor of about two, which accounts for the shift of the two curves in Figure 28.

TABLE 9. THE CORRELATION OF THE VARIOUS APPROACHES WITH THE LEEWARD DATA

	Approach	Parallel	Crosswind	±50%	±90%
1.	One constant for the combined crosswind and parallel cases.	.414	.414	13.5%	37%
2.	Two constants, one for the crosswind and one for the parallel case.	.377	.428	13.5%	36.5%
3.	Least squares fit for the combined crosswind and parallel cases.	$0.4+5.46\times10^{-4}$ x (wind angle)	$0.4+5.46\times10^{-4}$ (wind angle)	15%	36.5%
4.	Least squares fit for the parallel case and a constant fit for the crosswind case.	$.29+4.46\times10^{-3}$x (wind angle)	.428	13.5%	35%
5.	Sin function times a constant for the combined parallel and crosswind cases.	.72xsinx(wind angle)	.72xsinx(wind angle)	20.5%	66%

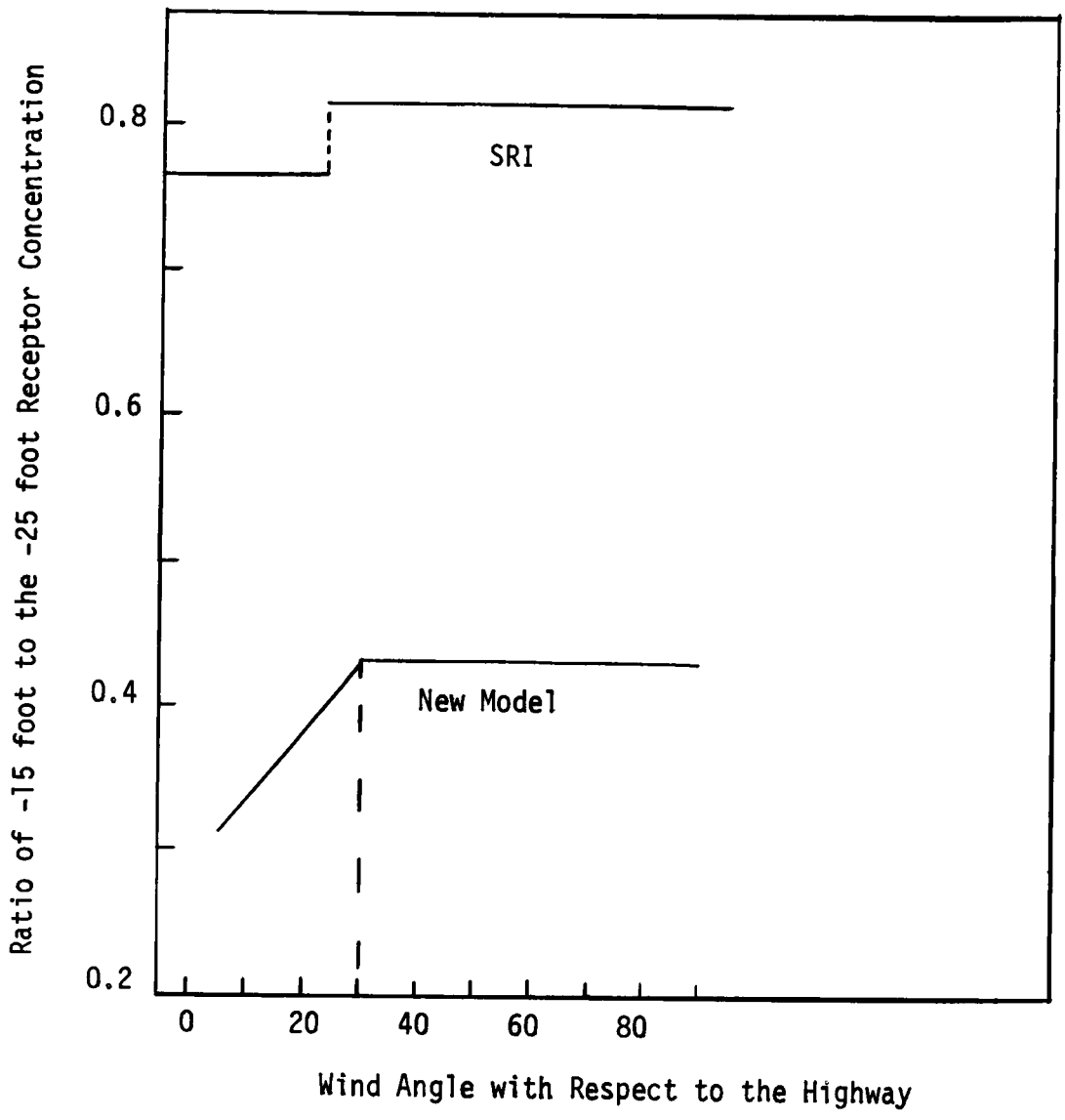

FIGURE 28. A COMPARISON OF THE NEW MODEL'S RATIO OF MEASURED CONCENTRATIONS WITH SRI MODEL'S

The only difference in the calculation of the -25 foot leeward concentration and the -15 foot leeward concentration is due to the additional dispersion occurring over the longer diagonal distance from the source to the receptor. The dispersion factor, γ, can be determined as follows.

Crosswind (wind direction $>30^{o}$ with respect to road)

$$R = \Delta C_{-15}/\Delta C_{-25} = \left(\frac{(X_{-25}^{2} + Z_{-25}^{2})^{\frac{1}{2}}}{(X_{-15}^{2} + Z_{-15}^{2})^{\frac{1}{2}}} \right)^{\gamma} \tag{14}$$

$$.428 = \left(\frac{6.8766}{8.116} \right)^{\gamma} \tag{15}$$

$$\gamma = 5.12 \tag{16}$$

Parallel (wind direction $<30^{o}$ with respect to road)

$$R = \Delta C_{-15}/\Delta C_{-25} = \left(\frac{(X_{-25}^{2} + Z_{-25}^{2})^{\frac{1}{2}}}{(X_{-15}^{2} + Z_{-25}^{2})^{\frac{1}{2}}} \right)^{\gamma} \tag{17}$$

$\Delta C_{-15}/\Delta C_{-25}$ from least square fit

$$.29 + 4.46 \times 10^{-3} \times (\text{wind angle}) = \left(\frac{6.876}{8.116} \right)^{\gamma} \tag{18}$$

$$\gamma = \frac{\ln (.29 + 4.46 \times 10^{-3} \times (\text{wind angle})}{\ln (.8473)} \tag{19}$$

Table 10 gives the values of these dispersion term exponents for the respective wind direction. The final form of this uncalibrated model was as follows.

$$\Delta C = \frac{Q\ (.533)}{U \times L^{\gamma}} \tag{20}$$

TABLE 10. LEEWARD SIDE EXPONENTS OF THE DISPERSION TERM.

Wind Direction	γ
0	7.46
5	7.0
10	6.6
15	6.21
20	5.85
25	5.5
30	5.17
30-90	5.12

The Determination of the Calibration Coefficient

After values for the dispersion term's exponent were known, the only remaining term needed for calibration was the calibration coefficient in Equation (8) of this chapter. The calibration coefficient was determined by dividing the measured concentration by the uncalibrated concentration in Equation (17). By knowing these terms, the calibration constant, K, could be determined for each separate angle for the parallel case and for the entire crosswind direction. Table 11 lists the values of the mean constants determined for the parallel and crosswind case. Similarly, Figure 29 gives a plot of the mean constants and the values as represented by the following.

Crosswind Case:

$$K = 1.14 \times 10^4 \tag{21}$$

Parallel Case:

$$K = 1 \times 10^6 \, e^{-(.145 \times \text{wind angle})} \tag{22}$$

The Comparison of the Models

This equation was then input into the computer statistical program, in order to be able to compare its correlation of the measured leeward data with that of the calibrated Stanford Research Institute's model. Figure 30 gives the results of this analysis for the new model. The correlation of the new model indicates 50 percent of the data within $\pm$24 percent of the slope one, while the calibrated SRI's model describes the data with $\pm$34 percent. Thus, the new model gives a significant improvement over current model's form.

TABLE 11. LEEWARD SIDE CALIBRATION COEFFICIENTS.

Angle	γ	Q/u	$C_{5\ ft.}$	$C_{15\ ft.}$	K Mean
0	7.46	2051.4	.16	.06	1.7×10^{6}
10	6.6	2051.4	.12	.042	2.18×10^{5}
15	6.21	2051.4	.118	.044	1.02×10^{5}
20	5.85	2051.4	.134	.044	5.19×10^{4}
25	5.5	2051.4	.15	.06	3.19×10^{4}
30-90	5.12	1860.2	.0996	.044	1.14×10^{4}

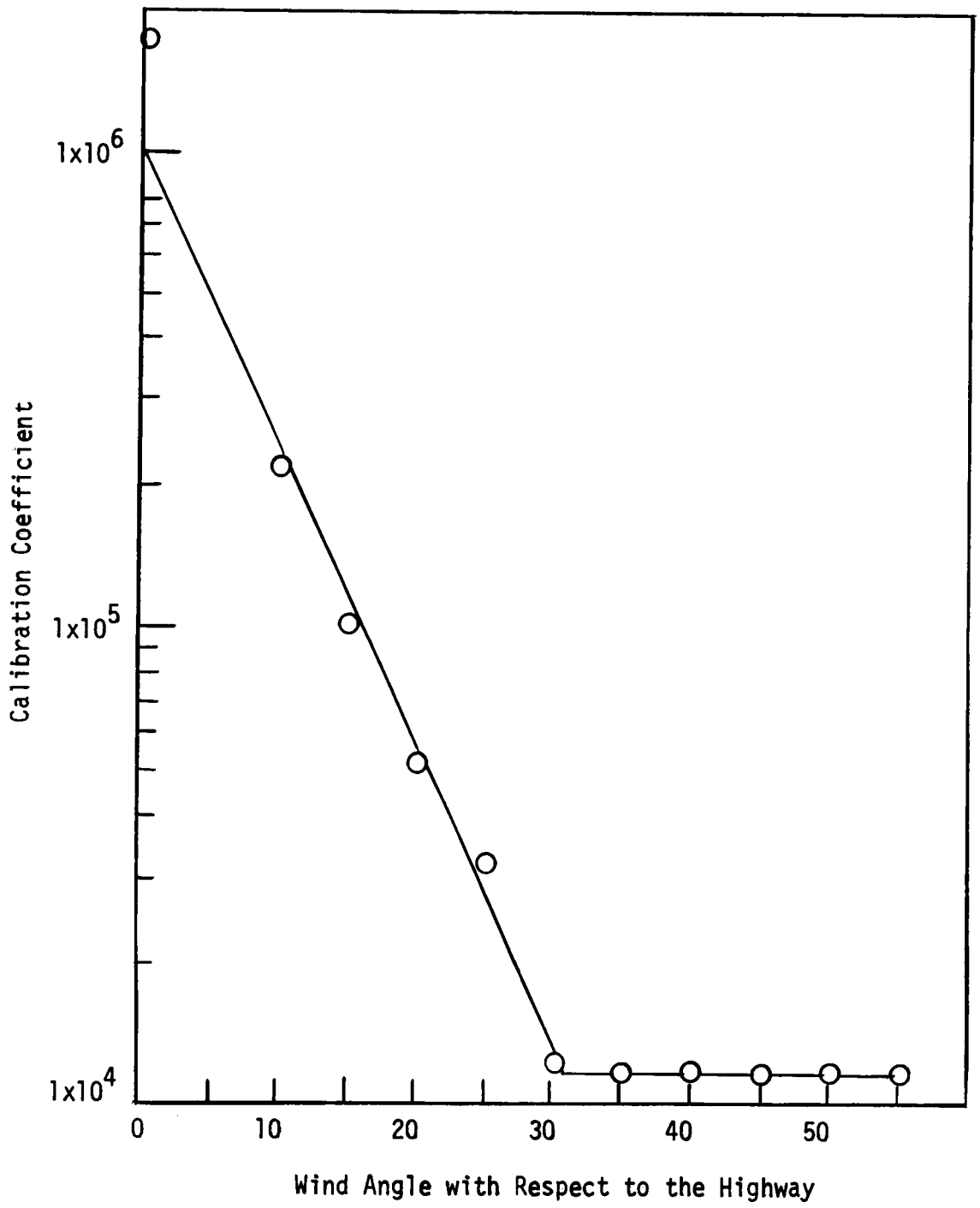

FIGURE 29. LEEWARD SIDE CALIBRATION COEFFICIENTS WITH RESPECT TO THE WIND ANGLE

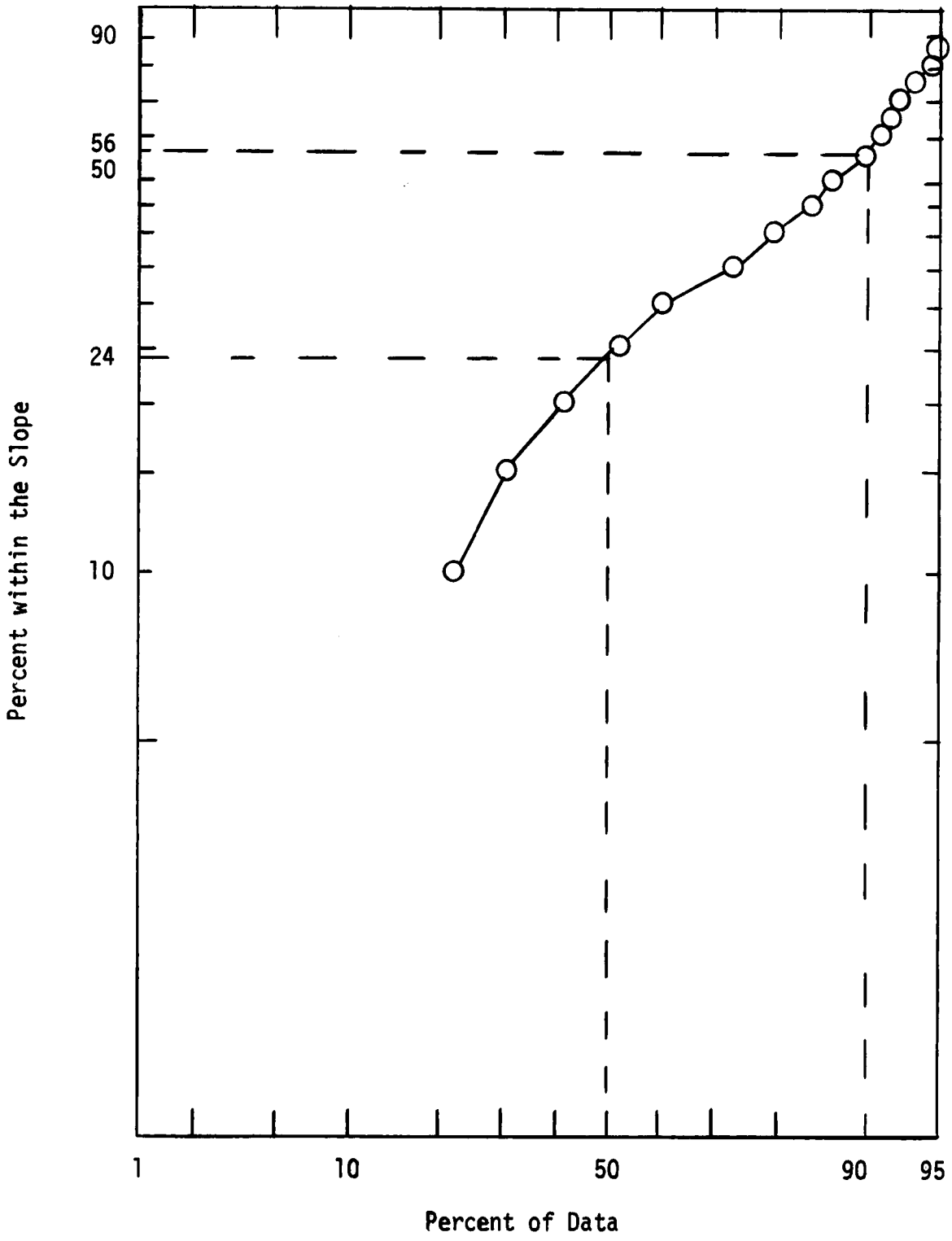

FIGURE 30. THE NEW MODEL'S CORRELATION WITH THE MEASURED LEEWARD DATA

III. WINDWARD CASE

The Determination of the Dispersion Term's Exponent

Although the procedure for determining the exponent was the same previously given for the leeward side, the windward side values were different from the leeward's values. Figure 31 illustrated the various fits of the receptor concentration ratios for parallel and crosswind cases. After establishing the correlation of these various fits with the data, it was determined that one constant for parallel case and one constant for the crosswind case gave slightly better results. These results are listed in Table 12 for each attempted fit. Although both this approach and SRI's model gave a step function change between parallel and crosswind cases, they were the reverse of each other, as shown in Figure 32. The ratio of receptor concentrations decreased in SRI's model, and they increased for the field measured data.

From the constant fits for the parallel and crosswind cases, the exponential was determined as follows.

Crosswind (wind direction >30^{0} with respect to the road)

$$R = \Delta C_{-15}/\Delta C_{-25} = \left(\frac{(X_{-25}^{2} + Z_{-25}^{2})^{\frac{1}{2}}}{(X_{-15}^{2} + Z_{-15}^{2})^{\frac{1}{2}}} \right)^{\gamma} \tag{23}$$

$$0.78 = \left(\frac{6.876}{8.116} \right)^{\gamma} \tag{24}$$

$$\gamma \approx .76 \tag{25}$$

Parallel (wind direction <30^{0} with respect to the road)

$$0.0703 = \left(\frac{6.876}{8.116} \right)^{\gamma} \tag{26}$$

$$\gamma \approx 1 \tag{27}$$

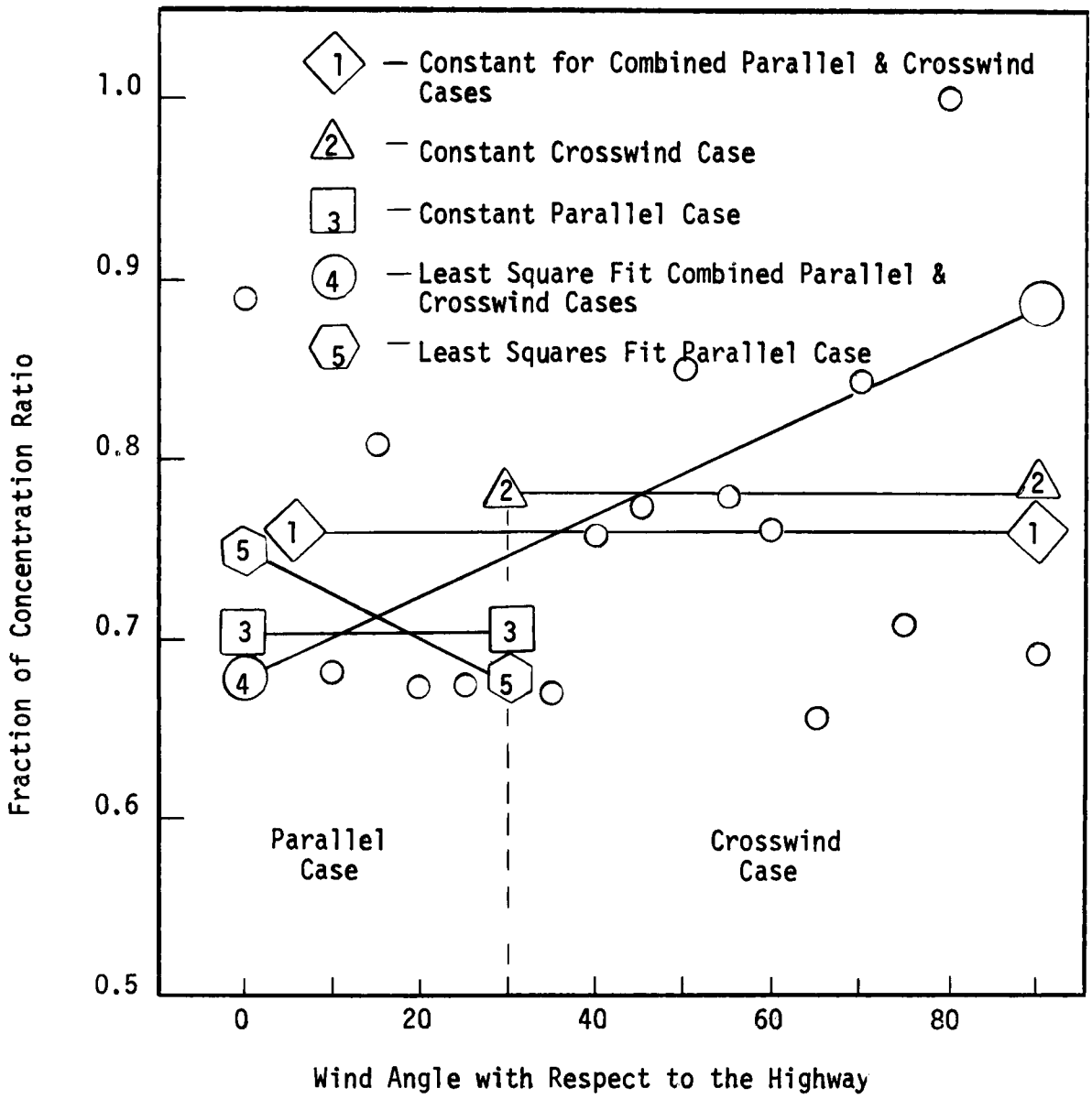

FIGURE 31. VARIOUS FITS OF CONCENTRATION RATIOS WITH RESPECT TO THE WINDWARD WIND ANGLES

TABLE 12. THE CORRELATION OF THE VARIOUS APPROACHES WITH WINDWARD DATA.

	Approach	Parallel	Crosswind	50%	90%
1.	One constant for the combined crosswind and parallel cases.	.76	.76	12.5%	37.5%
2.	Two constants, one for the crosswind and one for the parallel case.	.703	.78	12%	31%
3.	Least squares fit for the combined crosswind and parallel cases.	$.66+2.4\times10^{-3}x$ (wind angle)	$.66+2.49\times10^{-3}x$ (wind angle)	12.5%	31%
4.	Least squares fit for the parallel case and a constant fit for the crosswind case.	$.755-2.19\times10^{-3}x$ (wind angle)	.78	12%	31.5%

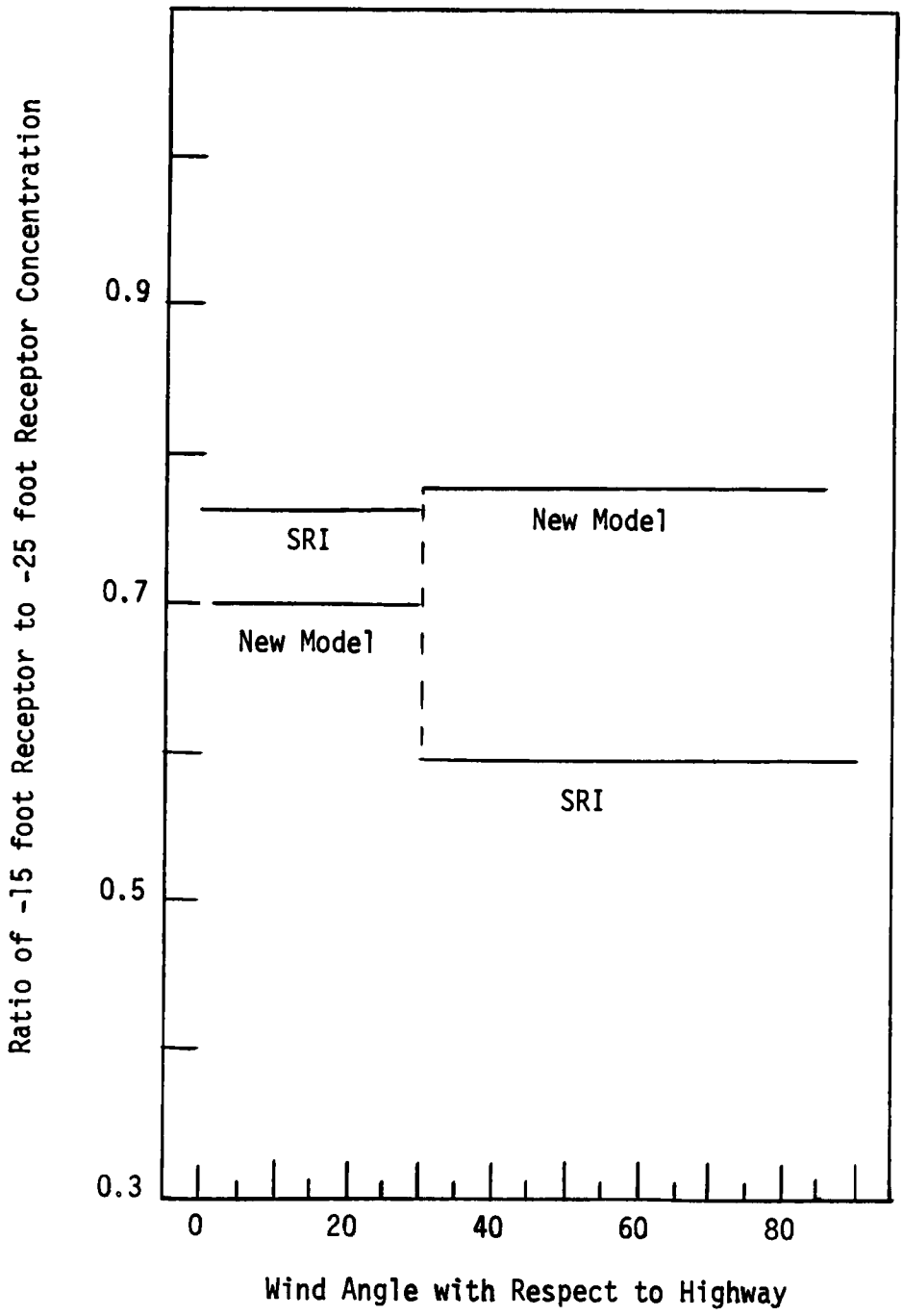

FIGURE 32. COMPARISON OF THE WINDWARD CONCENTRATION RATIO FOR SRI AND THE NEW MODEL

The Determination of the Calibration Coefficient

Since the exponents of the dispersion term did not vary as happened in the leeward parallel case, the geometric mean K approach was used to calibrate the windward model for the parallel and crosswind case. The geometric mean K for the crosswind case was determined to be equal to six. For the windward case, the geometric mean K was equal to 28.

The Comparison of the Models

The statistical analysis program was utilized to determine the correlation of the new model with the experimental windward data. Figure 33 gives the results of this analysis. The new model's determined 50 and 90 percentiles were within $\pm$27 percent and $\pm$79 percent of the slope of one. This was only a slight improvement over the calibrated SRI model which was within $\pm$27 percent and $\pm$85 percent.

The Predicted Nitrogen Oxide Concentrations above the Depressed Highway Section

Since the new model allows the determination of concentrations above the depressed highway section, it was decided to test the model's predictive capabilities for the windward data above the depressed section. Using the previously determined calibration coefficients and dispersion exponents, the model was correlated with the 5, 10, 15, and 20 foot measured concentrations above the depressed highway section. The results of the model predictive capabilities above the depressed highway are listed for each receptor height in Table 13. These results indicated that the new model can be utilized for predicting total nitrogen oxide concentration above the depressed highway section with a reasonable degree of accuracy.

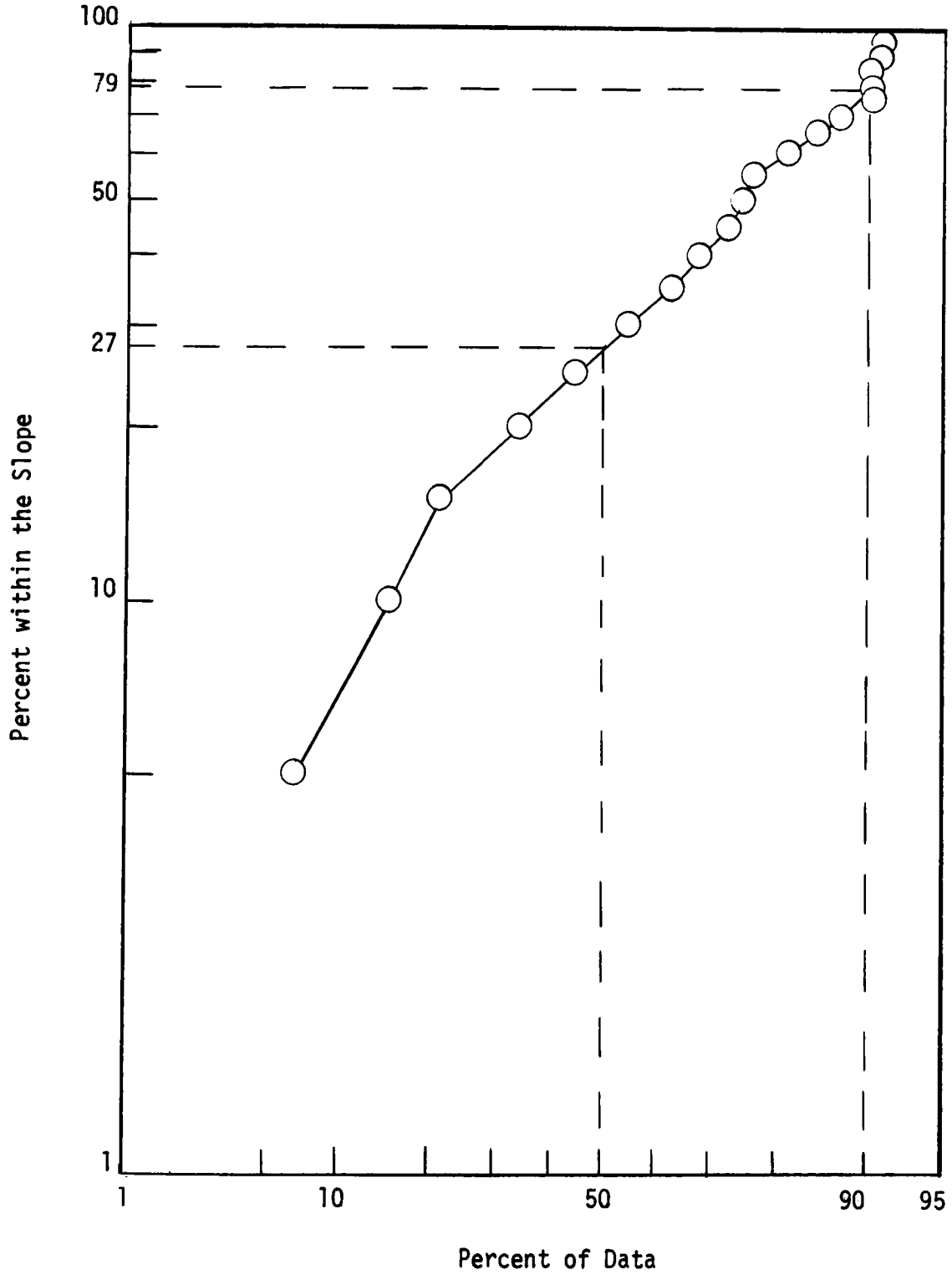

FIGURE 33. CORRELATION OF NEW MODEL WITH WINDWARD DATA

TABLE 13. THE NEW MODEL'S PREDICTIVE CAPABILITIES ABOVE THE DEPRESSED HIGHWAY SECTION.

Receptor Height above the Depressed Highway	50%	90%
5 foot	35%	70%
10 foot	42%	68%
15 foot	40%	80%
20 foot	40%	140%

CHAPTER VI

CONCLUSIONS

The Stanford Research Institute Street Canyon Submodel used in this report was formulated only for the prediction of carbon monoxide dispersion within the canyon effects produced by tall buildings along inner city streets. Since the monitoring site in this investigation was a depressed interstate highway section on the outer edge of urban Nashville, the use of SRI's model was extended far beyond its original purpose. This is further compounded by the fact that total nitrogen oxide concentrations were measured rather than carbon monoxide concentrations. Therefore, the results given in this report cannot be used to verify the SRI's model as it was intended to be used. It does, however, show that a calibrated SRI's model can be used to estimate ambient concentrations within a depressed highway section with reasonable accuracy.

An important result of this investigation was the methodology used to determine the calibration coefficient and exponent of the dispersion terms. Although the results of this study may not be generally applicable for all depressed highway sections, the general Equation (8) is valid. The methodology used to determine the best correlation of a mathematical model to measured concentrations at the I-40 East site can be used to determine useful models for other site locations. This is accomplished by:

(1) Taking field measurements of the vertical profile.

(2) Ascertaining the best least squares of constant fit of the measured concentration ratios at different receptor heights.

(3) Determining the dispersion term by comparing the measured ratios to the ratio of the diagonal source to receptor distance.

(4) Resolving the calibration coefficient using the geometric mean of K.

(5) Checking the correlation of the new model with measured data using the geometric mean K of the new model with measured data using the statistical program.

(6) Testing the new model's prediction capabilities with new monitoring data.

Using this same general methodology, statistical models can also be developed which predict ambient levels for highway terrain configurations which are considerably different from the type of highway section investigated in this report.

The specific values of the dispersion factor and the calibration coefficient formulated from the monitoring data gives an empirical equation for the I-40 East site. These values should not be used as a general equation for estimating total nitrogen oxide dispersion for all depressed highway sections. These results would, however, be expected to give favorable correlations of the nitrogen oxide dispersion for very similar conditions of two lane high speed highway depressed sections.

The magnitude of the dispersion factor and calibration coefficient is dependent upon the assumed location of the highway such as the point of line source reference. If the center of the nearest lane is used, as in SRI's leeward case equation, both the calibration coefficient and the dispersion exponent would be substantially decreased. Although this would provide more realistic dispersion exponent and calibration coefficient numbers, it does not actually improve the accuracy of the model estimate.

Another important result of the study that the new equation allowed for predictions of ambient concentrations above, as well as within, the depressed highway section. A comparison of measured values with model predictions gave quite favorable results. This indicates that the model describes concentrations profiles outside the physical spectrum within which it was developed. This improved confidence in the ability of the model to describe vertical concentration profiles.

Another method that could be utilized that was not investigated in this report would be to use a modification of the general equation for SRI's leeward case determination. Since the measured data indicates that dispersion is greater in the "street canyon" than as indicated by SRI's model, the general model could be calibrated for the center of the nearest lane conditions rather than using the center of the road. This would allow the same windward equation as given in SRI's model based on the width of the dispression, and a similar parallel case equation that would be an average of the new calibrated leeward case equation and the existing windward equation.

LIST OF REFERENCES

LIST OF REFERENCES

1. Patterson, D. J. and N. A. Henein, Emissions from Combustion Engines and Their Control, Ann Arbor Science Publisher Inc., Ann Arbor, Michigan, 1973.

2. Zeldovich, Ya. B., P. Ya Sadovnikov, and D. A. Frank - Kamenetskii, "Oxidation of Nitrogen in Combustion," Academy of Sciences, USSR, 1947.

3. Berhardt, E. A., "Kinetics of Nitric Oxide Formation in Internal Combustion engines," Air Pollution Control in Transport Engines, A Symposium of the Institute of Mechanical Engineers, November 9-11, 1971, p. 279.

4. Lavoie, G. A., J. B. Heywood, and J. C. Keck, "Experimental and Theoretical Study of Nitric Oxide Formation in Internal Combustion Engines," Combustion Science and Technology, Vol. 1, March 1970, p. 313.

5. Federal Register, 35, Part II, 1970, p. 219.

6. Federal Register, 36, Part II, 1971, p. 128.

7. Compilation of Air Pollution Emission Factors, Second Edition, U. S. Environmental Protection Agency, AP-42, Research Triangle Park, North Carolina, April 1973.

8. Benson, J. D. and R. F. Stegar, "Effects of Change Dilution on Nitric Oxide Emissions from a Single Cylinder Engine." Society of Automotive Engineers, Preprint 710008, 1971.

9. Perkins, H. C., Air Pollution, McGraw-Hill Book Company, New York, 1974.

10. Starkman, E. S., Combustion Generated Air Pollution, Plenum Press, New York, 1971.

11. Rossano, A. T., Jr., Air Pollution Control Guidebook for Management, Environmental Science Service Division of E.R.A. Inc., Stamford, Connecticut, 1969.

12. Continuous Air Monitoring Project in Philadelphia 1962-1965, U. S. Department of Health, Education, and Welfare, Public Health Service, Cincinnati, Ohio, 1969.

13. Johnson, W.B., et al., Field Study for Initial Evaluation of an Urban Diffusion Model for Carbon Monoxide, National Technical Information Service No. PB 196003, 1971.

14. Slade, D. H., Meteorology and Atomic Energy 1968, U. S. Atomic Energy Commission Office of Information Services, Springfield, Virginia, 1968.

15. The Oxides of Nitrogen in Air Pollution, State of California Department of Public Health, Berkeley, California, 1966.

16. Stern, A. C., Air Pollution, Vol. II, Academic Press, Second Edition, New York, 1968.

17. Atshuller, A. P. and J. J. Bufalini, "Photochemical Aspects of Air Pollution: A Review," Environmental Science and Technology, Vol. 5, No. 1, January 1971, p. 39.

18. Danielson, J. A., Air Pollution Engineering Manual, U. S. Department of Health, Education, and Welfare, Public Health Service, Cincinnati, Ohio, 1967.

19. Nelson, G. O., Controlled Test Atmospheres Principles and Techniques, Ann Arbor Science Publishers Inc., Ann Arbor, Michigan, 1972.

20. Arnold, B. L., "Highway Air Monitoring for Non-Methane Hydrocarbons," Master's Thesis, The University of Tennessee, March 1974.

21. Pignatato, L. J., Traffic Engineering Theory and Practice, Prentice-Hall Inc., Englewood Cliffs, New Jersey, 1973.

22. Highway Capacity Manual 1965, Highway Research Board Report 87, National Academy of Sciences National Research Council, Publication 1328, Washington, D. C., 1965.

23. Mechanical Weather Station Models 1071-1072 Instruction Manual, Meteorology Research Inc., Altadena, California.

24. Schnelle, K. B., F. G. Ziegler, and P. A. Krenkel, "A Study of the Vertical Distribution of Carbon Monoxide and Temperature above an Urban Intersection," APCA, Paper No. 69-152, 1969.

25. Bendix Model 8101-B Oxides of Nitrogen Analyzer Operation and Service Manual, Second Edition, Bendix Process Instruments Division, Ronceverte, West Virginia.

26. Noll, K. E., J. O. Walling, and B. L. Arnold, Calibration Procedures for Continuous Air Monitoring Instruments, Vol. I, Department of Civil Engineering, The University of Tennessee, September 1973.

27. Johnson, W. B., Field Study for Initial Evaluation of an Urban Diffusion Model for Carbon Monoxide, Stanford Research Institute, Menlo Park, California, NTIS No. PB 203469, 1971.

28. Georgii, H. W., E. Busch, and E. Weber, Investigation of the Temporal and Spatial Distribution of the Immission Concentration of Carbon Monoxide in Frankfurt/Main, Report No. 11 of the Institute of Meteorology and Geophysics of the University of Frankfurt/Main (Translation No. 0477, NAPCA), 1967.

29. Johnson, W. B., "An Urban Diffusion Simulation Model for Carbon Monoxide," APCA, Vol. 23, No. 6, June 1973, p. 490-498.

30. Study of the Emission from Light Duty Vehicles in Six Cities, APTD-1497, U. S. Environmental Protection Agency, Ann Arbor, Michigan, March 1973.

31. Larsen, R. I., A Mathematical Model for Relating Air Quality Measurements to Air Quality Standards, U. S. Environmental Protection Agency, Research Triangle Park, North Carolina, November 1971.

32. Hanna, S. R., "A Simple Method of Calculating Dispersion from Urban Area Sources," APCA, Vol. 21, No. 12, December 1971.

33. Calder, K. L., "A Climatological Model for Multiple Source Urban Area Pollution," Proceedings of the Second Meeting of the Expert Panel on Air Pollution Modeling, NATO Committee on the Challenges of Modern Society, Paris, France, July 26-27, 1971.

VITA

John Otis Walling was born in Robinson, Illinois on June 20, 1946. He attended elementary schools in White County, Illinois and graduated from Carmi Township High School in 1964. The following September, he entered the University of Illinois at Champaign. In 1966, he transferred to The University of Tennessee at Knoxville. He entered the U. S. Army in 1969. After completing his two year obligation, he re-entered The University of Tennessee. He received a Bachelor of Science degree in Chemical Engineering in December 1972.

After graduation, he accepted a teaching assistantship at The University of Tennessee and began study toward a Master's degree. He received a degree in Environmental Engineering in August 1974, He is a member of the Air Pollution Control Association.

He is married to the former Connie Lou Thomas of Carmi, Illinois.